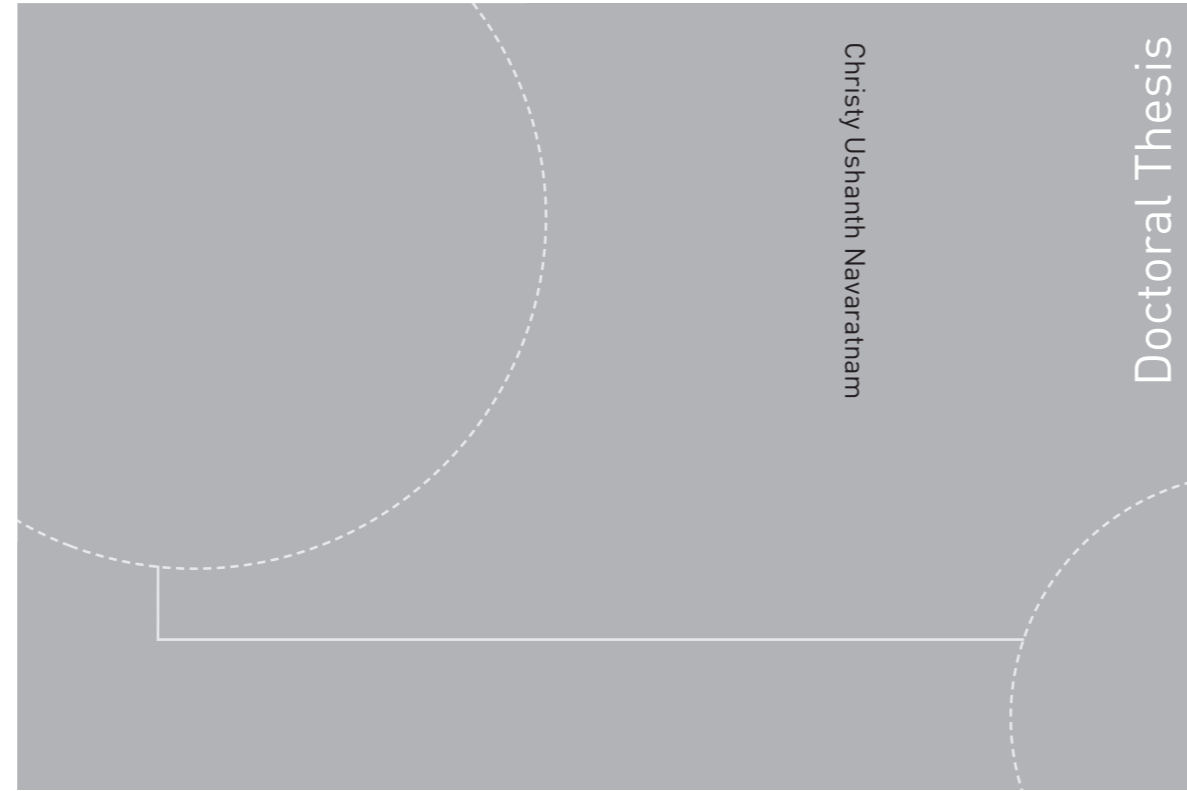


ISBN 978-82-326-3492-7 (printed version)  
ISBN 978-82-326-3493-4 (electronic version)  
ISSN 1503-8181



Doctoral theses at NTNU, 2018:352

Christy Ushanth Navaratnam

**The effect of bed porosity on turbulent  
flow in gravel-bed rivers**

Doctoral theses at NTNU, 2018:352

**NTNU**  
Norwegian University of  
Science and Technology  
Faculty of Engineering  
Department of Civil and Environmental Engineering

 **NTNU**  
Norwegian University of  
Science and Technology

 NTNU

 **NTNU**  
Norwegian University of  
Science and Technology

Christy Ushanth Navaratnam

# The effect of bed porosity on turbulent flow in gravel-bed rivers

Thesis for the degree of Philosophiae Doctor

Trondheim, November 2018

Norwegian University of Science and Technology  
Faculty of Engineering  
Department of Civil and Environmental Engineering



Norwegian University of  
Science and Technology



**NTNU**

Norwegian University of Science and Technology

Thesis for the degree of Philosophiae Doctor

Faculty of Engineering

Department of Civil and Environmental Engineering

© Christy Ushanth Navaratnam

ISBN 978-82-326-3492-7 (printed version)

ISBN 978-82-326-3493-4 (electronic version)

ISSN 1503-8181

Doctoral theses at NTNU, 2018:352



Printed by Skipnes Kommunikasjon as

## Abstract

This thesis presents the main findings from laboratory experiments that were specially designed to study the effect of gravel bed porosity on the surface flow characteristics. The thesis also contains five primary and two secondary research papers in which the results are discussed in detail.

In order to study the effect of porosity on flow resistance and near-bed turbulence, a non-porous counterpart of a water-worked gravel-bed surface was produced using a casting technique. The casting technique was also used to study the influence of gravel grain orientation on bulk flow resistance. The accuracy of the casting technique was evaluated, and the results indicated that the cast replicated the original surface accurately. The vertical distribution of porosity in the water-worked gravel-bed was also investigated. Hydraulic measurements were performed over three different bed types: water-worked gravel-bed, cast-bed and rotated cast-bed (cast tiles were rotated 180 degrees). The rotated cast-bed imposed larger flow resistance on the flow, thus the grain orientation played an important role determining the flow resistance. Moreover, differences in flow resistance and turbulence characteristics between porous water-worked gravel-bed and non-porous cast-bed are discussed. The porous water-worked gravel-bed imposed slightly larger resistance on the flow than the non-porous cast-bed. The analysis of turbulence flow characteristics between water-worked gravel-bed and cast-bed revealed that a higher momentum flux occurred over the water-worked gravel-bed. Moreover, the form-induced stresses were higher over the cast-bed than over the gravel-bed. This was associated with a strong recirculation of the fluid over the cast-bed as fluid cannot infiltrate. In contrast, fluid can infiltrate into the subsurface of the water-worked gravel-bed, causing less recirculation in the water-sediment interface.



## Preface

This thesis is submitted to the Norwegian University of Science and Technology (NTNU) in Trondheim for partial fulfilment of the requirements for the degree of 'Philosophiae Doctor (PhD)'.

This work is a result of a four-year PhD programme, which was conducted at the Department of Civil and Environmental Engineering. The research has been supervised by Professor Jochen Aberle and Associate Professor Nils Rüther. The PhD position was allocated to 75% research and 25% teaching. The teaching has included supervising master students, laboratory demonstrations and teaching partly the course TVM 5125 Hydraulic Design.

In accordance with the guidelines of the Faculty of Engineering, this thesis comprises an introduction to the research that has resulted in five scientific papers.



## Acknowledgements

I wish to thank various people for their contribution to this research work. First of all, I would like to express my deep gratitude to my supervisor Prof. Jochen Aberle for guiding me with his valuable and constructive suggestions during the planning and development of this research work. He has been very supportive and available whenever I needed to discuss something. His great passion and enthusiasm for the academia is a real inspiration. I have learnt a lot regarding scientific writing from him. I could not have asked for a better mentor. I would also like to extend my thanks to my co-supervisor Dr. Nils R  ther for the encouragement and motivation that he provided throughout these past few years.

A very special gratitude goes out to Jie, Pierre-Yves, Paride and Stephan who have been closely involved in my research work. I owe a big thanks for all your help in different ways. I wish to thank our technical people in the hydraulics lab, Geir, Gustav, Kristian and Endre for their enormous support in the experimental work. Of course, this huge experimental work would not be possible without the help from my colleagues and master students (it is a long list indeed) who have been helping specially in the casting work. Many thanks to all of you.

I am grateful to Martin, Dan and Amine from TSI. They have been helping me with the issues related to PIV.

I should also mention that the valuable contacts that I made through the HYTECH summer schools. Thanks to all the mentors and friends in HYTECH for the nice time with useful discussions. Thanks again to Jochen for encouraging me to attend these summer schools.

I would also like extend my gratitude to the administrative staff at the department.

My special thanks to my family for their patience and moral support over the years.

Last but not least, I would like to thank my loving wife Portia and beloved son Jevon for their patience and support especially in the last year.



# Contents

|   |      |
|---|------|
| Abstract.....   | i    |
| Preface.....  | iii  |
| Acknowledgements.....                                     | v    |
| List of Papers.....                                       | ix   |
| List of Figures.....                                      | xi   |
| List of Tables.....                                       | xiii |
| List of Abbreviations.....                                | xv   |
| 1. Introduction.....                                      | 1    |
| 1.1 Scope and Aim.....                                    | 3    |
| 1.2 Thesis outline.....                                   | 4    |
| 2. Theoretical Background.....                            | 5    |
| 2.1 Rough bed flows.....                                  | 5    |
| 2.2 The effect of bed porosity on the surface flow.....   | 7    |
| 3. Research Methodology.....                              | 9    |
| 3.1 Porosity measurements.....                            | 11   |
| 3.2 Cast bed production.....                              | 11   |
| 3.3 Scanning of the bed.....                              | 14   |
| 3.4 Hydraulic Measurements.....                           | 16   |
| 3.4.1 Particle Image Velocimetry (PIV) measurements.....  | 18   |
| 3.4.1.1 Stereo PIV.....                                   | 18   |
| 3.4.1.2 Volumetric 3-Component Velocimetry (V3V).....     | 19   |
| 3.5 Double-Averaging Methodology (DAM).....               | 20   |
| 4. Results and Discussions.....                           | 23   |
| 4.1 Porosity distribution of water-worked gravel-bed..... | 23   |
| 4.2 Accuracy of the casting technique.....                | 25   |
| 4.3 Flow resistance.....                                  | 26   |
| 4.4 Turbulence Characteristics.....                       | 29   |
| 5. Conclusions and Recommendations.....                   | 35   |
| References.....   | 39   |
| Research Articles.....                                    | 43   |





## List of Papers

### Primary Papers

**Paper I: The effect of bed porosity on near-bed turbulent flow characteristics in gravel-bed rivers**

Christy Ushanth Navaratnam, Jochen Aberle  
*VANN, 2017, 52*

**Paper II: An Experimental Investigation on Porosity in Gravel Beds**

Christy Ushanth Navaratnam, Jochen Aberle, Jana Daxnerová  
*Free Surface Flows and Transport Processes, 2018*

**Paper III: Evaluation of the accuracy of a bed casting technique**

Christy Ushanth Navaratnam, Jochen Aberle, Stephan Spiller  
*River Flow 2016 – International Conference on Fluvial Hydraulics*  
*St. Louis, Missouri, USA*

**Paper IV: Influence of Gravel-Bed Porosity and Grain Orientation on Bulk Flow Resistance**

Christy Ushanth Navaratnam, Jochen Aberle, Jie Qin, Pierre-Yves Henry  
*Water, 2018, 10, 561*

**Paper V: An experimental investigation on the flow resistance over a porous gravel bed surface and its non-porous counterpart**

Christy Ushanth Navaratnam, Jochen Aberle, Jie Qin, Pierre-Yves Henry  
*Accepted manuscript for River Flow 2018 – International Conference on Fluvial Hydraulics*  
*Lyon, France.*

### Secondary Papers

**SP I: Experimental hydraulics on fish-friendly trash-racks: an ecological approach**

Marcell Szabo-Meszaros, Christy Ushanth Navaratnam, Jochen Aberle, Ana T. Silva, Torbjørn Forseth, Olle Calles, Hans-Petter Fjeldstad, Knut Alfredsen  
*Ecological Engineering, 2018, 113*

**SP II: Geometric and hydraulic assessment of the accuracy of a bed moulding technique**

Christy Ushanth Navaratnam, Jochen Aberle, Stephan Spiller  
*IAHR World Congress 2015*  
*The Hague, The Netherlands*



## List of Figures

|  |    |
|--|----|
| Figure 1: Colmation (external) and decolmation in gravel-bed rivers. ....  | 2  |
| Figure 2: Flow layers and flow type classification over rough permeable beds<br>(adapted from Nikora et al., 2007b) .....  | 6  |
| Figure 3: Isometric view of the 3D drawing of the recirculating flume (the<br>pumps, which are located below the inlet tank, are not shown). All units<br>are in [mm] .....  | 10 |
| Figure 4: Sketch of the experimental set-up for WDM. ....  | 11 |
| Figure 5: (a) Silicon moulding in the flume; (b) silicon mould in the form work<br>for the casting; (c) resin poured over the mould, (d) a piece of cast, (e)<br>cast installation in the flume; (f) flume with cast-bed installed. © C. U.<br>Navaratnam..... | 12 |
| Figure 6: Visual comparison between (a) water-worked gravel-bed surface and<br>(b) its non-porous facsimile.....   | 13 |
| Figure 7: (a) Acuity AP820-120; (b) Acuity AR200-100 laser scanners. ....  | 15 |
| Figure 8: The set-up of the laser scanning .....   | 15 |
| Figure 9: (a) Camera arrangement in the stereo PIV, (b) Picture of the<br>illuminated particles in the laser sheet.....  | 19 |
| Figure 10: Single body camera mount for V3V .....  | 20 |
| Figure 11: Porosity distribution of different bed types; $H$ is the total height of<br>the bed.....  | 24 |
| Figure 12: $(8/f)^{0.5}$ as function of relative submergence $(h/k)$ .....   | 27 |
| Figure 13: The variation of bulk friction factors with $Re$ for the tested bed<br>surfaces.....  | 28 |
| Figure 14: The double-averaged streamwise velocity profiles. ....  | 29 |
| Figure 15: (a) Streamwise turbulent intensity, (b) Vertical turbulent intensity, (c)<br>Reynolds stress distribution, (d) Turbulence coefficient .....   | 31 |
| Figure 16: (a) Streamwise form-induced intensity, (b) Vertical form-induced<br>intensity, (c) Form-induced stress.....   | 32 |



## List of Tables

|   |    |
|---|----|
| Table 1: Hydraulic boundary conditions for the measurements over three different beds; (a) water-worked gravel bed; (b) Cast-bed; and (c) rotated cast-bed. The bulk flow velocity was determined from the equation of continuity $U = Q/A$ where $A = hb$ denotes the cross-sectional area with $b$ = flume width (1 m)..... | 17 |
| Table 2: Different turbulence parameters .....  | 22 |
| Table 3: Flow statistics at the roughness crest.....  | 33 |



## List of Abbreviations

|       |                                     |
|-------|-------------------------------------|
| WDM   | Water Displacement Method           |
| PIV   | Particle Image Velocimetry          |
| PVC   | Polyvinyl Chloride                  |
| CCD   | Charge-Coupled Device               |
| DEM   | Digital Elevation Models            |
| SPIV  | Stereo Particle Image Velocimetry   |
| DPDS  | Dual Plane Dual Side                |
| V3V   | Volumetric 3-Component Velocimetry  |
| DAM   | Double-Averaging Methodology        |
| 2DSSF | 2D-Second order Structure Functions |
| SP    | Secondary Papers                    |





# 1

## Introduction

Gravel-bed rivers are an important stream type in mountainous environments. They are characterized by large to small scale morphological features such as step-pool and riffle-pool systems, bars, as well as static and mobile armour layers (Church, 2006, Hendrick et al., 2010). The morphological features of gravel bed rivers are directly related to sediment transport processes which in turn are governed by hydrological and geological boundary conditions, anthropogenic influences, near-bed hydraulics, slope and sediment size and composition. Gravel-bed rivers also provide habitat for flora and fauna (Beschta and Ripple, 2012; Boano et al., 2014; Marion et al., 2014; Forseth and Harby, 2014). Because of their significance for engineering and ecological applications, gravel-bed rivers have been in focus of research for a long time. For instance, hydropower production controls the dynamics of the hydrological regime of rivers (e.g. load fluctuations or hydro peaking etc.) and subsequently affects the exchange process between surface and sub-surface flows- the so-called 'hyporheic exchange' which is governed by hydrodynamic processes acting over different spatial and temporal scales of (e.g. Tonina and Buffington, 2007; Marion et al., 2014; Boano et al., 2014). An example of such exchange processes in gravel-bed rivers is 'colmation' or 'decolmation', i.e. the retention of fine particles clogging the pores in the armoured layer during low flow conditions (see Figure 1) or re-suspension of settled particles due to turbulence (Brunke, 1999; Francisco et al., 2016), respectively. Colmation reduces the porosity and subsequently affects the spawning areas for salmon and other organisms in the hyporheic zone (Sternecker et al., 2014).

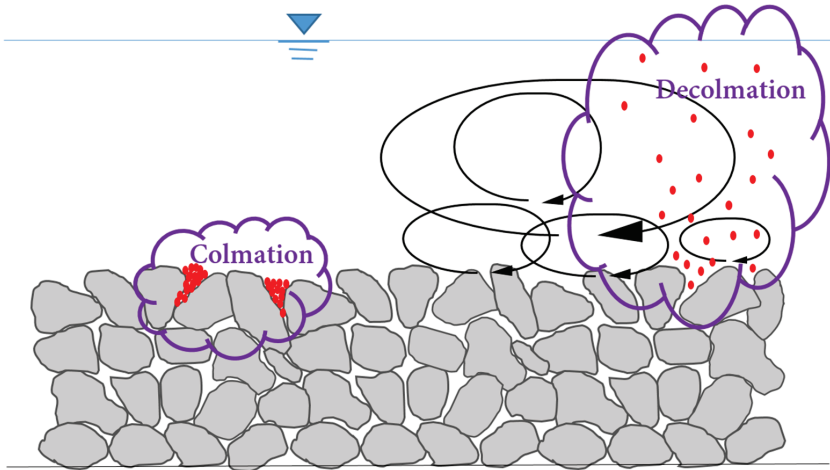


Figure 1: Colmation (external) and decolmation in gravel-bed rivers.

Despite the significance of gravel-bed rivers for engineering and ecological applications, there is still a lack of knowledge regarding the near-bed flow structure over porous gravel-beds in general, and the exchange processes between surface and sub-surface flows in particular. In fact, it is not clear how the gravel-bed porosity influences the surface flow characteristics such as turbulence and flow resistance, which in turn govern the transport mechanism across the sediment-water interface. The lack of knowledge in this topic is partly associated with the fact that many studies have focused only on the roughness characteristics or turbulent flow over rough impermeable walls or classical porous media flows (Pokrajac and Manes, 2009). Many studies have considered only the bed surface characteristics to study flow resistance thereby ignoring the sub-surface characteristics, i.e. beds were assumed to be non-porous. In fact, only few studies have addressed the effect of porosity on the surface flow. In these studies, multiple or single layers of identical elements like spheres were used to simulate the porous and non-porous bed, respectively (e.g. Zagni and Smith, 1979; Manes et al., 2009; etc). These studies revealed that the near bed surface flow characteristics over porous and non-porous beds are different and that a porous bed is characterized by larger flow resistance than its non-porous counterpart.

The use of artificial elements in these studies was associated with the fact that specific experimental techniques are needed to accurately reproduce the complex surface

texture of natural gravel-beds to create an impermeable facsimile of a natural bed. In fact, this has been difficult for a long time, but novel techniques such as the casting technique described in Spiller and R  ther (2012) can nowadays be used to accurately reproduce natural bed structures. In addition, cast-beds offer the opportunity to investigate the influence of gravel-grain orientation on the flow resistance as well as turbulence characteristics, as will be described later in this thesis.

In order to assess the importance of the porosity of water worked gravel-beds, the knowledge of its distribution over the depth of the sediment layer is a prerequisite. Aberle (2007) investigated the vertical porosity distribution of a water-worked gravel-bed using the water displacement method (WDM), and this method has also been used by others to determine the porosity profile for uniform gravel-beds (e.g., Dey and Das, 2012). Aberle (2007) found an absolute minimum porosity value at the level of roughness trough of a water-worked gravel-bed and speculated that the sediment transport processes and mixing of sediments in the active layer during armouring (water working the bed) caused this absolute minimum porosity. Aberle (2007) also pointed out that the absolute minimum porosity could be even smaller in armour layers in the field as finer sediments can typically be found in nature (e.g. wash-load) than in his laboratory experiments, in which the smallest particle size was 0.63 mm. Therefore, flow over gravel-beds is responsible for complex hydrodynamic processes that raise open questions with regard to the exchange of mass and momentum across the sediment-water interface.

## 1.1 Scope and Aim

The overall objective of this study is the quantification of the effect of bed-porosity on the near-bed hydraulics, surface flow characteristics, and hence flow resistance. In order to achieve this objective, the knowledge of the porosity distribution in gravel bed, as well as the accuracy of the casting technique is a prerequisite. Therefore, the objectives can be specifically defined as follows:

- Quantification of the porosity distribution of a water-worked gravel-bed to verify results from the literature (e.g. Aberle, 2007) and to study the reason for the absolute minimum porosity at the roughness trough;

- Assessment of the accuracy of the casting technique in order to evaluate how accurate the cast surface replicates the original surface;
- Quantification of the effect of the gravel-bed porosity on the flow resistance and near-bed turbulence characteristics;
- Experimental quantification of the influence of grain orientation on the flow resistance in water-worked gravel-beds.

## 1.2 Thesis outline

This thesis is composed of five main chapters. The present chapter introduces the topic and describes the need and objective of the study. Chapter 2 presents the theoretical background of rough-bed flows and a literature review on the effect of porosity on the surface flow (also refer to Paper I). Chapter 3 describes the research methodology and gives an overview of the experimental work that is presented in the papers. In addition to the papers, Chapter 3 contains a description of the Particle Image Velocimetry (PIV) system used in the experiments along with the double-averaging methodology for the analysis of the velocity data. Chapter 4 summarises and discusses the results from the papers, specifically, the porosity distribution in the water-worked gravel, the accuracy of the casting technique and the effect of gravel-bed porosity on flow resistance. Subsequently, the influence of porosity on turbulence characteristics (not published at time of writing) is highlighted at the end of Chapter 4. Chapter 5 summarizes the findings of this study and outlines some suggestions for further research.

# 2

## Theoretical Background

*This chapter briefly reflects Paper I with an overview of rough-bed flows with definitions of different flow layers and flow types. A brief review on the literature is then presented within the context of porosity effect on surface flow.*

### 2.1 Rough bed flows

The flow over rough gravel-beds can be split into three distinct regions, (i) surface flow region, (ii) sub-surface flow region and (iii) interface region where the surface flow interacts with the sub-surface flow (e.g. Nikora et al., 2001; Manes et al., 2009). These three main regions can further be classified into sub-layers. The region above the roughness crest can be split into three layers: outer layer, logarithmic layer and form-induced sublayer (as shown in Figure 2; Nikora et al., 2007b). The interfacial sublayer is defined as the region where the roughness geometry function/porosity  $\phi$ , varies from 1 (at the roughness crest,  $Z_c$ ) to an approximately constant value (from the level of the roughness trough,  $Z_t$  and below). The porosity/roughness geometry function  $\phi$ , is defined as

$$\phi = \frac{V_f}{V_t} \quad (2.1)$$

where  $V_f$  is the volume of fluid within the total volume  $V_t$ .

The form-induced sublayer is the region just above the roughness crest, where the flow is highly three dimensional and affected by the form drag of the gravel grains, i.e. by form-induced stress due to flow separation from the gravel grains (Nikora et al., 2001). Together with the interfacial sublayer, the form-induced sublayer is defined as the 'roughness layer'.

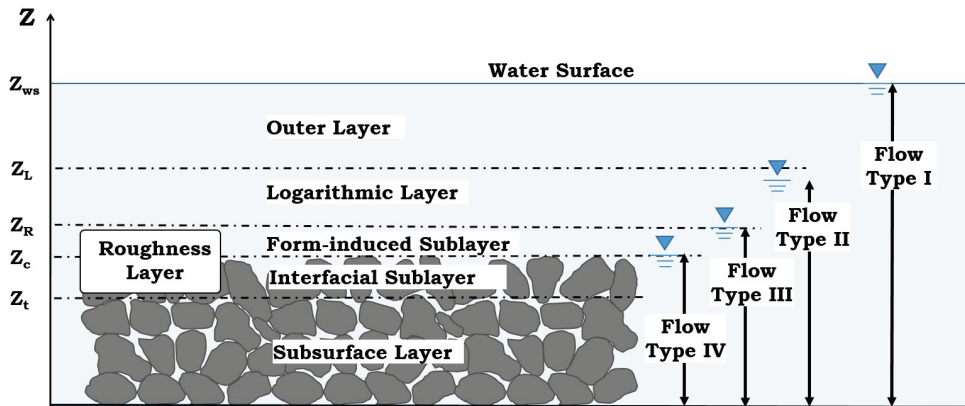


Figure 2: Flow layers and flow type classification over rough permeable beds (adapted from Nikora et al., 2007b)

The flow velocities in the logarithmic layer can be described by the logarithmic formula, i.e. the ‘law of the wall’. The log-layer extends from the upper boundary of the roughness layer ( $z_R$ ) to the lower boundary of the outer layer ( $z_L$ ). The law of the wall is valid up to approximately 20% of the water depth (Nezu and Nakagawa, 1993; Jiménez, 2004) and the flow is less spatially heterogeneous in this region compared to the roughness layer.

The outer layer is defined above the logarithmic layer in which the time-averaged flow velocities are basically equal to the spatially-averaged flow velocities as the bed roughness (and hence form-induced stresses) has almost no influence.

The existence of the different flow layers over rough beds depends on the relative submergence (ratio between the flow depth,  $h$  and the roughness height,  $k$ ). Based on the relative submergence, as shown in Figure 2 (Nikora et al., 2007b), different flow types can be defined. Flow type I corresponds to flows with large relative submergences and is, for porous beds, characterized by the existence of all five aforementioned flow layers. In case of a non-porous bed the subsurface layer will disappear, but the other four layers will still exist for flow type I. Flow type II corresponds to flows with intermediate relative submergence,  $h/k$  (e.g.  $h/k < 10$ ) and is characterized by the existence of the subsurface layer, the roughness layer and the logarithmic layer. It needs to be highlighted that the log-profile does not necessarily develop for flow type II; however the velocity distribution in this sublayer has often been parametrized using the logarithmic function (e.g. Koll, 2006) or through the

mixing layer theory (e.g. Katul et al., 2002). Flow type III is characterized by small relative submergences where the free surface corresponds to the upper boundary of the roughness layer. The shape of the velocity profile is similar to that for flow type II up to the upper boundary of the roughness layer, i.e. in the region with large spatial flow heterogeneity. Flow type IV is characterized by relative submergences  $h/k < 1$ , i.e. the roughness elements are partially submerged, and the water level defines the upper boundary of the interfacial sublayer. The velocity profile for flow type IV depends on the roughness characteristics and its shape can be derived based on the vertical distribution of the roughness elevations (Nikora et al., 2004), i.e. the velocity distribution within the interfacial sublayer is linear for gravel-beds

## 2.2 The effect of bed porosity on the surface flow

While the surface flow characteristics over gravel-beds have been investigated in many studies (e.g. Mohajeri et al., 2016, Stewart, 2014, Sarkar and Dey, 2010, Aberle et al., 2008, Kironoto et al., 1994 etc.), only few studies have focused on the effect of bed porosity on surface flow characteristics (e.g. Zagni and Smith, 1979; Zippe and Graf, 1983; Jiménez et al., 2001; Manes et al., 2009; Manes et al., 2011a; Cooper et al., 2018; Fang et al., 2018). In order to study and quantify the effect of porosity on the surface flow characteristics, an identical surface roughness texture is required for a porous bed and its non-porous counterpart. Therefore, in most of the aforementioned studies, rough beds were composed of identical elements such as spheres (e.g. Zagni and Smith, 1979; Breugem et al., 2006; Manes et al., 2009; Fang et al., 2018). These studies revealed that porous beds impose higher flow resistance than non-porous beds and that flow resistance depends on the Reynolds number,  $Re = Uh/\nu$  (Zippe and Graf, 1983; Kuwata and Suga, 2017), where  $U$  and  $\nu$  denote the bulk velocity and the kinematic viscosity of the fluid, respectively. The larger flow resistance over the porous bed was also found to be dependent on the relative thickness of the porous layer (Manes et al., 2011b). The increase of flow resistance with  $Re$  was associated with the shear penetration (Manes et al., 2009, Manes et al., 2011a, Manes et al., 2011b) and momentum exchange between the surface and subsurface flow which increases the Reynolds shear stress in the near-bed region, hence the flow resistance (Breugem et al., 2006; Manes et al., 2011a; Kuwata and Suga, 2017). The momentum exchange was



associated with (i) pressure differences in the pore space in the interfacial sublayer, causing upward and downward movement of fluid and (ii) energetic sweeps penetrating into the pores (Pokrajac and Manes, 2009). Detailed studies to determine the porosity-effect of natural beds (like gravel-beds) on surface flow characteristics are rare, because reproducing a gravel-bed surface requires special experimental techniques. Recently, Cooper et al. (2018) reproduced a gravel-bed surface to study the effect of porosity on near-bed flow turbulence and concluded that the bulk flow resistance is lower over the porous water-worked gravel-bed than over its non-porous counterpart. This finding was contrary to previous findings and possible reasons for this discrepancy are explained in Paper IV. Moreover, Cooper et al. (2018) showed that the turbulence over the water-worked gravel-bed was more organised and less intense compared to the turbulence over the non-porous counterpart. It should be noted that the study of Cooper et al. (2018) was published while the experiments of the present study were in progress. However, both the scale of cast production and implementation of the casting technique in Cooper et al. (2018) differed from the present study, which is described in Paper IV.

# 3

## Research Methodology

*This study was based primarily on a wider experimental program at the hydraulics laboratory at the Norwegian University of Science and Technology (NTNU) in Trondheim. This chapter presents a brief overview of all key experimental techniques involved in the program (see listed papers for details) and provides additional information that is not explicitly given in the papers.*

The experiments were carried out in a 12.5 m long, 1 m wide and 1 m deep glass-sided recirculating flume (Figure 3). The flume was equipped with two centrifugal pumps that can supply a discharge up to 0.45 m<sup>3</sup>/s (capacity of each pump was 0.225 m<sup>3</sup>/s), and an electrical jacking system for tilting. For the experiments, the inlet tank of the flume was modified to condition the flow by installing an array of vertical PVC (polyvinyl chloride) rods of 20 mm diameter, followed by a honeycomb panel that served as flow straightener. A 2.19 m long bed section after the honeycomb panel was manually paved by coarse gravel particles and stones to prevent scouring at the inlet (Figure 3).

The porous bed consisted of a well-mixed gravel mixture ( $0.64 \text{ mm} < d < 64 \text{ mm}$ ) which was surface compacted to a height of 0.20 m and screeded at a length of 10.31 m to ensure that the bed surface was parallel to the flume bottom. After installation of the initial bed, the flume was tilted to a slope of  $S = 0.0027$  and the gravel was water worked with a discharge of 0.20 m<sup>3</sup>/s and a water depth of 0.24 m. The water working was done to create a static armour layer of the gravel-bed. The flow rate was measured by Euromag MUT1000 EL inductive flow meters mounted in the recirculating pipes (accuracy of 0.1% of the measured value). The water depth was adjusted by both a weir installed at the downstream end of the flume and by adding or draining the water from the flume using drain valves. The water levels were measured using four pressure taps located at the bottom of the flume or, dependent on the experiment, eight ultrasonic sensors. The first pressure tap was located 6.875 m from the start of the

working section and the spacing between the pressure taps was 1.25 m. The eight ultrasonic sensors were located within the same stretch and the spacing between them varied from 0.4 – 0.7 m.

For the tests with the water-worked gravel-bed, the water level/surface slopes were determined using the aforementioned pressure taps. For the tests with the cast-bed, the solid cast bottom prevented such pressure measurements and the water surface slopes were determined from water level readings using the ultrasonic sensors. Additional measurements were performed to compare the two different methods for determining the water level/surface slope. In these measurements, a water surface slope was recorded 10 times using both techniques. The mean slopes measured by the pressure tubes and acoustic sensors were 0.041 % and 0.042 % respectively, whereas the standard deviations of the measured values were 0.0021 % and 0.0024 % respectively. The standard deviation corresponded to approximately the same deviation from the mean i.e. 5.1 % and 5.3 % for the pressure tubes and acoustic sensors, respectively. Thus, both systems gave the same water surface slope with the same order of magnitude of deviation from the mean. Moreover, the means of the water depth measured from both systems were comparable.

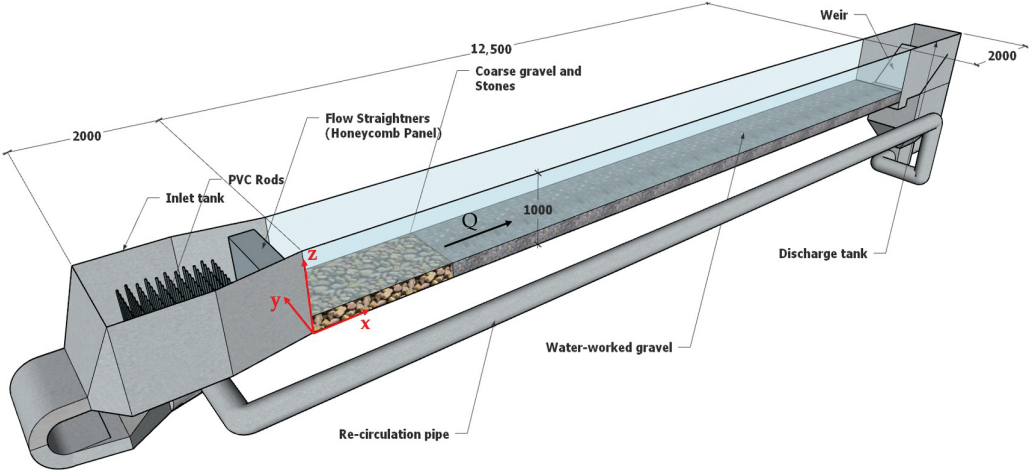


Figure 3: Isometric view of the 3D drawing of the recirculating flume (the pumps, which are located below the inlet tank, are not shown). All units are in [mm]

### 3.1 Porosity measurements

The water displacement method (WDM) was used to determine the vertical porosity distribution of the gravel bed. This method is based on a stepwise addition of water in the gravel-bed and measurement of the corresponding increases in the water level in upstream and downstream basins of known dimensions (Figure 4). A detailed description of the test is reported in Paper II. The porosity measurements were carried out before and after water-working the gravel-bed.

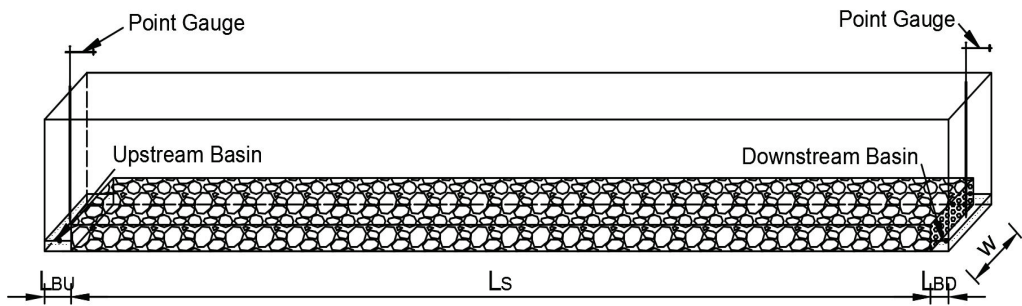


Figure 4: Sketch of the experimental set-up for WDM.

### 3.2 Cast bed production

As mentioned in Chapter 1, to isolate the influence of porosity on the near-bed turbulence, reproducing the same surface structure of the water-worked gravel-bed in an impermeable form was a prerequisite. Therefore a large portion of the water-worked gravel-bed was artificially reproduced using the casting technique described in Spiller and R  ther (2012). The artificial reproduction of the water-worked gravel-bed involved two main processes; (i) making the silicon mould (negative imprint of the surface) and (ii) casting of the bed using polyurethane. The details of the cast-tile production and their placement in the flume are described in Paper IV. Figure 5 (a-f) shows some additional images taken during the casting production, whereas Figure 6 shows a close visual comparison of the water-worked gravel surface and its non-porous facsimile.

In addition to large-scale production of the cast-bed (non-porous counterpart of the water-worked gravel-bed), small-scale cast surfaces were produced to assess the accuracy of the casting technique. The small-scale casting included a small piece of sand paper (grade P60; average sand grain diameter of 269 microns) and a small area of a golf ball bed (0.2 m x 0.5 m section; golf ball diameter = 42 mm). The details of the casting and the accuracy assessments are presented in Paper III.

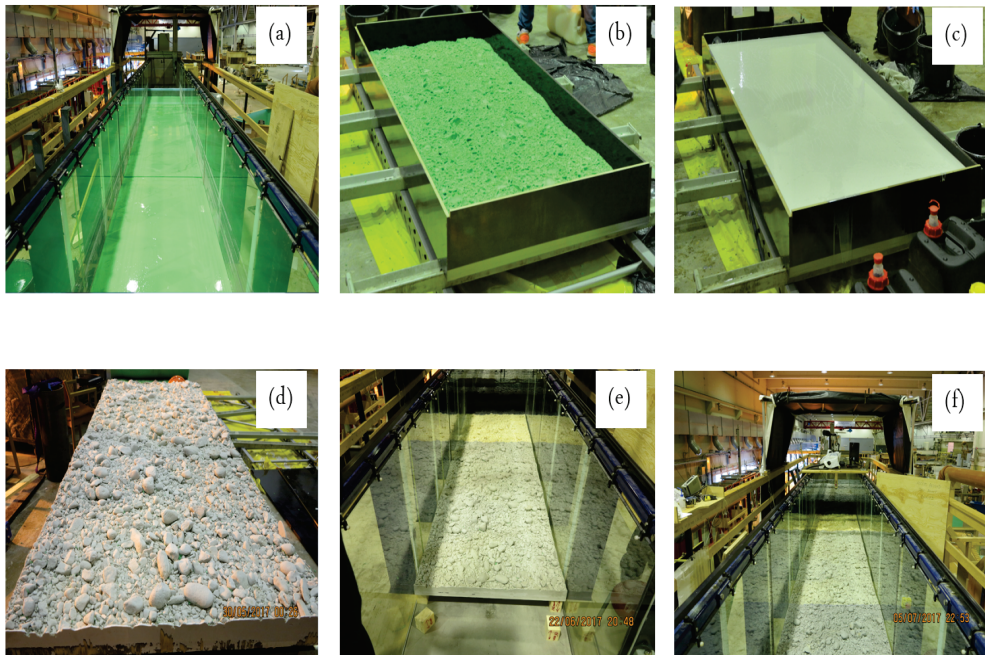


Figure 5: (a) Silicon moulding in the flume; (b) silicon mould in the form work for the casting; (c) resin poured over the mould, (d) a piece of cast, (e) cast installation in the flume; (f) flume with cast-bed installed. © C. U. Navaratnam





Figure 6: Visual comparison between (a) water-worked gravel-bed surface and (b) its non-porous facsimile.

### 3.3 Scanning of the bed

The water-worked gravel-bed and cast-beds were scanned to determine the roughness characteristics and subsequently to study the accuracy of the casting technique. Two different laser scanners, Acuity AP820-120 (Figure 7a) and Acuity AR200-100 (Figure 7b), were used in the tests. The former is a two-dimensional (2D) laser scanner that projects a laser sheet vertically downwards, which forms a red line that contains 290 individual dots, on the surface. A CCD (Charge-Coupled Device) sensor in the laser scanner detects the dots in the line in a perspective angle and measures the distance of each dots from the sensor. The accuracy of this device was  $\pm 72 \mu\text{m}$ . The main disadvantage of this sensor was that the surface behind larger roughness elements could not be measured because of the perspective arrangement of the CCD-sensor. Therefore, this scanner was used only for small rough surfaces (e.g. sand paper) that were used to investigate the accuracy of the casting technique.

In order to scan the water-worked gravel-bed and cast-bed, the Acuity AR200-100 sensor was used. This sensor emits a single laser beam which makes a small dot on the surface (the size of the laser dot varied from 55 to 250  $\mu\text{m}$  depending on the distance of the transmitter to the bed). The accuracy of the distance measurement with this sensor was 30.5  $\mu\text{m}$ . Unlike in the 2D scanner, the CCD sensor in the 1D scanner was located closer to the laser transmitter enabling also distance measurements behind large roughness elements. The laser sensor was attached to an automated traversing system that could move along the flume through given coordinates. Metal bars spanning the flume width were placed at both ends of the laser scanning section as additional reference for the scanning (Figure 8). The laser scanning data were used to produce the digital elevation models (DEMs) of the surfaces, which were subsequently used to compare the surfaces (see Paper III and Paper IV).



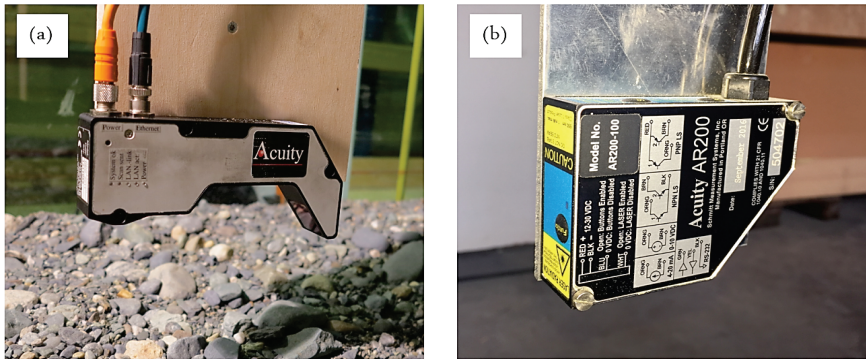


Figure 7: (a) Acuity AP820-120; (b) Acuity AR200-100 laser scanners.

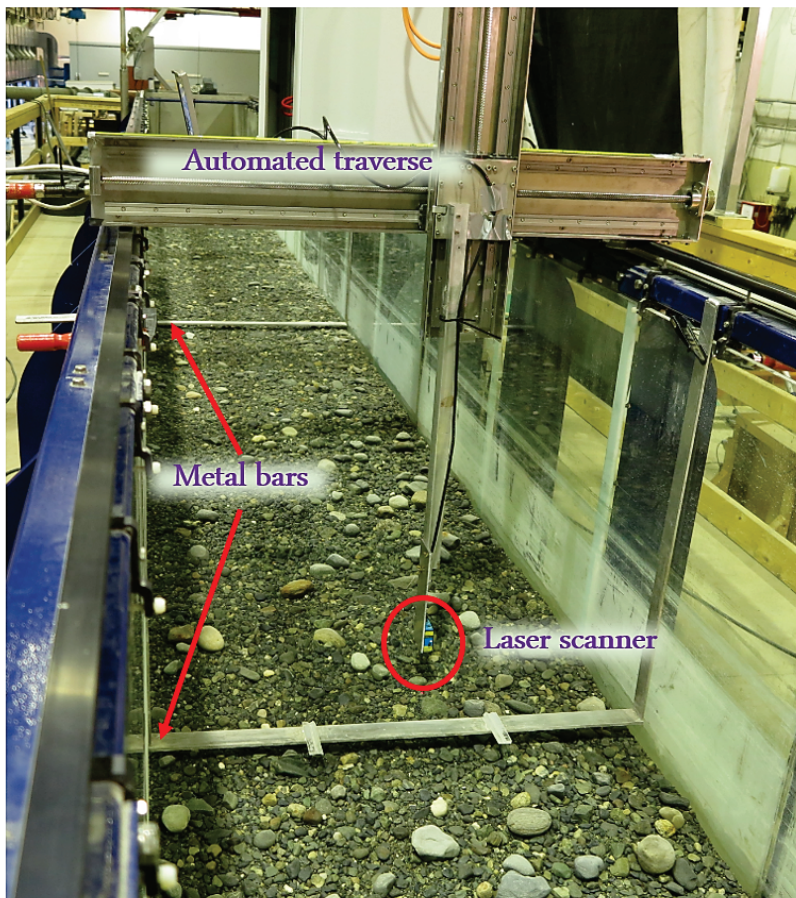


Figure 8: The set-up of the laser scanning



### 3.4 Hydraulic Measurements

The hydraulic measurements were taken over three different bed types,

- (i) water-worked gravel-bed
- (ii) cast-bed (non-porous counterpart of the water-worked gravel-bed)
- (iii) rotated cast-bed (cast tiles were rotated through 180 degrees, see Paper IV for details)

The experiments with bed types (i) and (ii) were designed to isolate the effect of the gravel-bed porosity on flow resistance and near-bed turbulence. The experiments with bed type (iii), i.e. the rotated cast, were designed to study the effect of grain orientation on flow resistance. The hydraulic boundary conditions for the tests are summarised in Table 1. In general, the relative submergences,  $h/k$  varied from 3.4 to 9.3, and the flows were classified as ‘intermediate relative submergence’ and corresponded to flow type II as described in section 2.1. It should be noted that the roughness height,  $k$  was defined as the distance between the roughness crest and trough. The roughness height was determined through the laser scan data as the difference between  $Z_{99}$  and  $Z_{01}$ , i.e.  $k = Z_{99} - Z_{01}$ , where  $Z_{99}$  and  $Z_{01}$  are the 99<sup>th</sup> and 1<sup>st</sup> percentiles of bed elevations respectively.

In total, seven different boundary conditions (BC1-BC7) were established for all the bed types. In order to compare the hydrodynamics, the relative submergence  $h/k$  should be kept constant (Cooper et al., 2013, Cooper et al., 2018) and uniform flow conditions should prevail. Despite the efforts made to obtain uniform flow conditions for a pre-defined  $h/k$ , it was difficult to match the water surface slope exactly with the bed slopes as they were very small slopes. Therefore, the shear velocity was derived from the St.Venant equation (equation 3.1) for non-uniform flow (Graf and Song, 1995).

$$u_* = \left[ ghS_b - gh(S_b - S_w)(1 - Fr^2) \right]^{0.5} \quad (3.1)$$

where,  $u_*$  is the shear velocity,  $h$  the water depth,  $S_b$  the bed slope,  $S_w$  the water surface slope, and  $Fr$  the Froude number that is defined as  $Fr = U / \sqrt{gh}$ .

Table 1: Hydraulic boundary conditions for the measurements over three different beds; (a) water-worked gravel bed; (b) Cast-bed; and (c) rotated cast-bed. The bulk flow velocity was determined from the equation of continuity  $U = Q/A$  where  $A = hb$  denotes the cross-sectional area with  $b =$  flume width (1 m).

| Test                        | $S_b$  | $S_w$   | $h$<br>[m] | $h/k$<br>[-] | $Q$<br>[m <sup>3</sup> /s] | $U$<br>[m/s] | $Fr$ | $Re$   | $u_*$<br>[m/s] |
|-----------------------------|--------|---------|------------|--------------|----------------------------|--------------|------|--------|----------------|
| (a) Water-worked gravel-bed |        |         |            |              |                            |              |      |        |                |
| BC1                         | 0.0018 | 0.00134 | 0.137      | 3.6          | 0.056                      | 0.41         | 0.35 | 55890  | 0.043          |
| BC2                         | 0.0015 | 0.00103 | 0.178      | 4.7          | 0.076                      | 0.43         | 0.32 | 76270  | 0.043          |
| BC3                         | 0.0015 | 0.00103 | 0.236      | 6.2          | 0.121                      | 0.51         | 0.34 | 120787 | 0.050          |
| BC4                         | 0.0020 | 0.00159 | 0.215      | 5.7          | 0.124                      | 0.58         | 0.40 | 124107 | 0.059          |
| BC5                         | 0.0013 | 0.00083 | 0.293      | 7.7          | 0.156                      | 0.53         | 0.31 | 156412 | 0.050          |
| BC6                         | 0.0010 | 0.00051 | 0.353      | 9.3          | 0.168                      | 0.48         | 0.25 | 167987 | 0.043          |
| BC7                         | 0.0015 | 0.00098 | 0.319      | 8.4          | 0.200                      | 0.63         | 0.35 | 199883 | 0.057          |
| (b) Cast-bed                |        |         |            |              |                            |              |      |        |                |
| BC1                         | 0.0018 | 0.00135 | 0.139      | 3.6          | 0.056                      | 0.40         | 0.35 | 56060  | 0.044          |
| BC2                         | 0.0015 | 0.00103 | 0.179      | 4.6          | 0.074                      | 0.41         | 0.31 | 73520  | 0.043          |
| BC3                         | 0.0015 | 0.00099 | 0.239      | 6.2          | 0.121                      | 0.51         | 0.33 | 121120 | 0.049          |
| BC4                         | 0.0020 | 0.00147 | 0.215      | 5.6          | 0.125                      | 0.58         | 0.40 | 124988 | 0.057          |
| BC5                         | 0.0013 | 0.00079 | 0.293      | 7.6          | 0.162                      | 0.55         | 0.33 | 162370 | 0.049          |
| BC6                         | 0.0010 | 0.00051 | 0.353      | 9.1          | 0.172                      | 0.49         | 0.26 | 172170 | 0.043          |
| BC7                         | 0.0015 | 0.00105 | 0.319      | 8.3          | 0.207                      | 0.65         | 0.37 | 207080 | 0.059          |
| (c) Rotated cast-bed        |        |         |            |              |                            |              |      |        |                |
| BC1                         | 0.0017 | 0.00138 | 0.138      | 3.4          | 0.053                      | 0.38         | 0.33 | 53162  | 0.044          |
| BC2                         | 0.0014 | 0.00105 | 0.179      | 4.4          | 0.071                      | 0.40         | 0.30 | 70886  | 0.044          |
| BC3                         | 0.0014 | 0.00103 | 0.239      | 5.9          | 0.115                      | 0.48         | 0.32 | 115267 | 0.050          |
| BC4                         | 0.0019 | 0.00162 | 0.216      | 5.3          | 0.118                      | 0.55         | 0.38 | 118303 | 0.059          |
| BC5                         | 0.0012 | 0.00089 | 0.293      | 7.2          | 0.158                      | 0.54         | 0.32 | 157601 | 0.052          |
| BC6                         | 0.0009 | 0.00053 | 0.353      | 8.7          | 0.170                      | 0.48         | 0.26 | 170468 | 0.044          |
| BC7                         | 0.0014 | 0.00103 | 0.321      | 7.9          | 0.195                      | 0.61         | 0.34 | 195140 | 0.058          |

### 3.4.1 Particle Image Velocimetry (PIV) measurements

#### 3.4.1.1 Stereo PIV

Particle image velocimetry is an image-based velocity measurement technique commonly used to study the turbulent flow field with high spatial resolution. For PIV measurements, the water is seeded with tracer particles having almost the same density as the water. The tracer particles are illuminated by the laser and subsequently, particle images are captured using high speed cameras. The PIV system used in the present study was from TSI and it could be configured as (i) classical two-dimensional (2D) PIV with single camera, (ii) stereo PIV with two camera and (iii) volumetric three component velocimetry (V3V) with three cameras (Adrian and Westerweel, 2011).

The velocity measurements over the water-worked gravel-bed and its impermeable counterpart (cast-bed) were carried out using stereo PIV. In Stereo PIV (SPIV), two cameras view the same plane at different angles meeting the Scheimpflug condition to get the third velocity component (Figure 9). The Scheimpflug condition occurs when the cameras' lens plane, object plane and image plane intersect in a single point. This was achieved by adjusting the camera body with respect to the lens to ensure that the particles within the camera field of view were in focus. The SPIV system consisted of, a double pulsed Nd:YAG (neodymium-doped yttrium aluminium garnet) laser that can fire up to 50Hz, two POWERVIEW cameras (4 mega pixel) that can capture up to 180 frames per second, a synchronizer to control the timing of the captures and computer that controls all the components through the '*Insight 4G*' software from TSI. Polyamid particles of 55  $\mu\text{m}$  diameter were used as seeding/tracing particles. These particles were mixed with a small amount of soap to minimize the sticking effect of particles due to surface tension. A dual plane dual side (DPDS) calibration target gridded with white dots, was used to relate the spatial scale to the image pixels. A special advantage of the DPDS calibration target was that the traversing of the target was not necessary as the white dots on both planes of DPDS give information on the distance normal to the target plane (transverse direction in the present case). An automapping built in tool in *Insight 4G* corrected any misalignment of the calibration target and the laser sheet. In all the tests, images were sampled at a frequency of 20 Hz for a sampling period of 150 seconds resulting 3000 image pairs in each camera. Particle images were processed using *Insight 4G* in three steps; pre-processing, processing, and post-processing. Pre-processing was performed to improve the

particle raw images in terms of the particle clarity. The processing is an important step where many parameters are defined i.e. size of the interrogation window, percent of overlapping of interrogation windows etc. Instantaneous velocity fields were obtained through the statistical cross correlation between the images taken at very short time interval, 'delta t ( $\Delta t$ )'. Finally, the post-processing was performed to polish the vector field by replacing the bad vectors (poorly-correlated particles) with interpolated vectors that are produced using neighbouring good vectors.

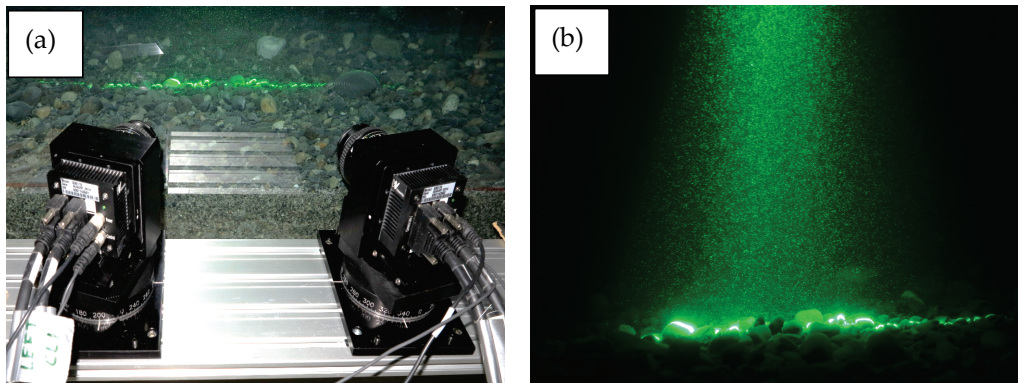


Figure 9: (a) Camera arrangement in the stereo PIV, (b) Picture of the illuminated particles in the laser sheet

#### 3.4.1.2 Volumetric 3-Component Velocimetry (V3V)

The V3V is a three-dimensional three component (3D-3C) velocity measurement technique from TSI. For this setup, three cameras are mounted in triangular pattern on a single body that is specially designed for V3V (Figure 10). A special calibration procedure is followed prior to the measurements. A calibration target with a high precision grid of dots is traversed in steps through the entire measurement volume and cameras take images of the dots in each step (plane). Subsequently, the calibration images are processed with the '*Insight V3V 4G*' software. This process produces a series of triangles corresponding to each calibration plane and vertices of triangle represent the centre of the calibration target seen from each camera. The size and shape of the triangles determine the particle position and alignment of the cameras respectively. The cameras capture the particles illuminated by the laser that is in the form of a cone unlike laser sheet in the SPIV. One capture of V3V consisted of 6 images (3 image pairs). Particle images were processed using *Insight V3V 4G* and processing involved

four main steps; (i) 2D particle identification based on the particle intensity in the images; (ii) 3D particle identification or triplet search using the volumetric calibration as described above; (iii) 3D particle velocity vectors obtained from the 3D particle tracking of successive image pairs, and (iv) obtained particle velocity vectors were interpolated in a grid (Pothos et al., 2009). The V3V system can produce a velocity field in a volume up to 140 mm x 140 mm x 100 mm (streamwise x vertical x spanwise). The V3V technique was used in the tests described in Paper III and SP I.

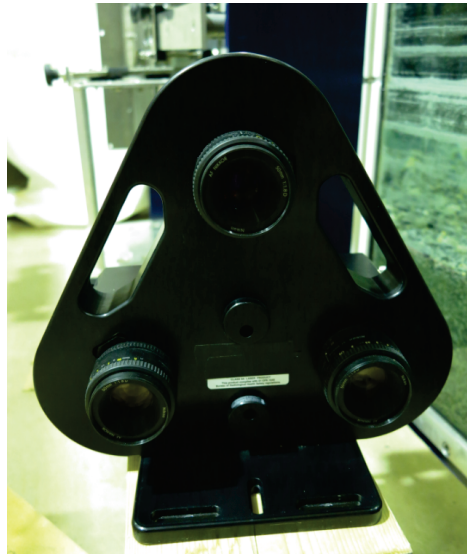


Figure 10: Single body camera mount for V3V

### 3.5 Double-Averaging Methodology (DAM)

The obtained velocity data from the PIV were analysed on the basis of double-averaging methodology. As mentioned in section 2.1, the time-averaged flow in the near-bed region of a rough bed is highly spatially heterogeneous, and spatially heterogeneous flows can be described by DAM (Nikora et al., 2007a). Within the double averaging methodology, the Reynolds Averaged Navier-Stokes (RANS) equations are averaged in space (areal or volume averaging over spatial domain parallel to the bed) to obtain Double-Averaged Navier-Stokes (DANS) equations as shown in equation 3.2. In the present study, double-averaged variables were obtained

by spatially averaging time-averaged quantities within layers parallel to the mean bed elevation.

$$\begin{aligned}
\underbrace{\frac{\partial \langle \bar{u}_i \rangle}{\partial t}}_{\text{Local fluid acceleration}} + \underbrace{\langle \bar{u}_j \rangle \frac{\partial \langle \bar{u}_i \rangle}{\partial x_j}}_{\text{Convective fluid acceleration}} = & \underbrace{g_i}_{\text{Gravity acceleration}} - \underbrace{\frac{1}{\phi \rho} \frac{\partial \phi \langle \bar{p} \rangle}{\partial x_i}}_{\text{Pressure term}} - \underbrace{\frac{1}{\phi} \frac{\partial \phi \langle \overline{u'_i u'_j} \rangle}{\partial x_j}}_{\text{Turbulent stress term}} + \underbrace{\frac{1}{\phi} \frac{\partial}{\partial x_j} \left\langle v \frac{\partial \bar{u}_i}{\partial x_j} \right\rangle}_{\text{Viscous stress term}} \\
& - \underbrace{\frac{1}{\phi} \frac{\partial \phi \langle \tilde{u}_i \tilde{u}_j \rangle}{\partial x_j}}_{\text{Form-induced stress term}} + \underbrace{\frac{1}{\rho \phi} \frac{1}{V_o} \iint_{S_{\text{int}}} p n_i dS}_{\text{Form drag term}} - \underbrace{\frac{1}{\phi} \frac{1}{V_o} \iint_{S_{\text{int}}} \left( v \frac{\partial u_i}{\partial x_j} \right) n_j dS}_{\text{Viscous drag term}}
\end{aligned} \tag{3.2}$$

where,  $u_i$  is the velocity component,  $g_i$  the gravitational acceleration,  $x_i$  the coordinate in  $i$  direction,  $t$  the time,  $\rho$  the density of fluid,  $p$  the pressure,  $V_o$  the total volume of the averaging domain,  $n_i$  the unit vector normal to the bed,  $S_{\text{int}}$  the extent of interfacial region bounded by the averaging domain and  $u'$  is the velocity fluctuation in  $i$  direction obtained from Reynolds decomposition of the instantaneous velocity as shown in equation 3.3.

$$u'(t) = u(t) - \bar{u} \tag{3.3}$$

In the above equations, overbar and angular bracket denote the time-averaged and spatially averaged variables respectively and overbar with 's' denotes the superficial time averaging. The superficial time averaging accounts for mobile bed and for fixed beds this becomes normal time averaging (intrinsic time averaging). Moreover, the wavy overbar (tilde) denotes the form-induced variable which is the spatial variation of the time-averaged variables. The form-induced variables are derived in similar to the Reynolds decomposition for turbulent fluctuations:

$$\tilde{u} = \bar{u} - \langle \bar{u} \rangle \tag{3.4}$$

For steady, uniform and two-dimensional flow, the total fluid stresses above the roughness crest can be derived from equation 3.2 as follows,

$$\tau_f(z) = \rho \left\{ \underbrace{-\langle \overline{u'w'} \rangle}_{\text{Reynolds stress}} - \underbrace{\langle \tilde{u}\tilde{w} \rangle}_{\text{Form-induced stress}} + \underbrace{\left\langle v \frac{\partial u}{\partial z} \right\rangle}_{\text{Viscous stress}} \right\} \tag{3.5}$$

where,  $\tau$  is the total fluid stress and  $z$  the vertical coordinate. Equation 3.5 shows that the total fluid shear stress is the sum of Reynolds, form-induced and viscous shear stresses. Table 2 summarizes the turbulence parameters that are used in this thesis for the analysis of turbulent characteristics above different bed types.

Table 2: Different turbulence parameters

| Parameter                          | Equation   |
|------------------------------------|--|
| Turbulent intensity                | $\sigma_u = \langle u'^2 \rangle^{0.5}$  |
| Reynolds shear stress              | $\tau_{uw} = -\langle u'w' \rangle$  |
| Turbulent kinetic energy (TKE)     | $K = \frac{1}{2}(\sigma_u^2 + \sigma_v^2 + \sigma_w^2)$  |
| Form-induced intensity             | $\sigma_{f,u} = \langle \tilde{u}^2 \rangle$   |
| Form-induced stress                | $\tau_f = \langle \tilde{u}\tilde{w} \rangle$  |
| Turbulence correlation coefficient | $r_{uw} = \frac{-\langle u'w' \rangle}{\langle u'^2 \rangle^{0.5} \langle w'^2 \rangle^{0.5}}$ |

# 4

## Results and Discussions

*In the following sections, the main findings of the research study are discussed. The sections are divided by main outcomes of this research study and the published papers corresponding to each outcome are identified below each heading.*

### 4.1 Porosity distribution of water-worked gravel-bed

[Paper II]

Paper II has its distinctive focus on the porosity distribution of the water-worked gravel-bed. The main objective of this paper was to verify the results from Aberle (2007) and investigate further about the absolute minimum of porosity found just above the roughness trough in the study of Aberle (2007). Figure 11 shows the vertical distribution of the gravel-bed porosity for the present study (before and after water-working) using WDM along with the porosity distributions obtained through the analysis of the laser scans for all three bed types. The porosities obtained from WDM vary from  $\phi=1$  at the roughness crest to an absolute minimum at the level of roughness trough. Below the roughness trough, the porosities reach an approximately constant value and increase to  $\phi \approx 0.75$  just above the flume plastic bottom. In Paper II, it was shown that the absolute minimum just above the roughness trough was associated partly with the capillary action as well as the settlements of small particles which produce a 'sealing' effect during water working. Small-scale tests were also carried out using different bed materials and beds prepared in different ways, i.e. surface compacted, layer compacted etc., in order to study the cause for the absolute minimum. The results of the small-scale tests also showed an absolute minimum porosity close to the surface. This revealed that the settlement of small particles (as hypothesised in Aberle, 2007) was not exclusively causing the absolute minimum



porosity. Thus, it was concluded that the absolute minimum porosity was associated with the combined effect of capillary action and the small particle settlement in the active layer during water working despite the individual contributions of these effects were not quantified.

Larger porosities observed close to the plastic bottom of the flume were associated with the combined effect of capillary action and poor sorting of gravel at the bottom (Figure 11). Paper II concludes that the capillary action in the WDM can influence the porosity close to the gravel-bed surface and the bottom and the porosities determined through WDM, may be under or over estimated. Moreover, the porosities obtained through WDM and laser scan data are in good agreement between the roughness crest and trough (Figure 11). Porosity obtained from laser scan at the roughness trough is zero, because laser can only measure the elevation between roughness crest and trough. Thus, the information below the gravel grains could not be captured by the scan.

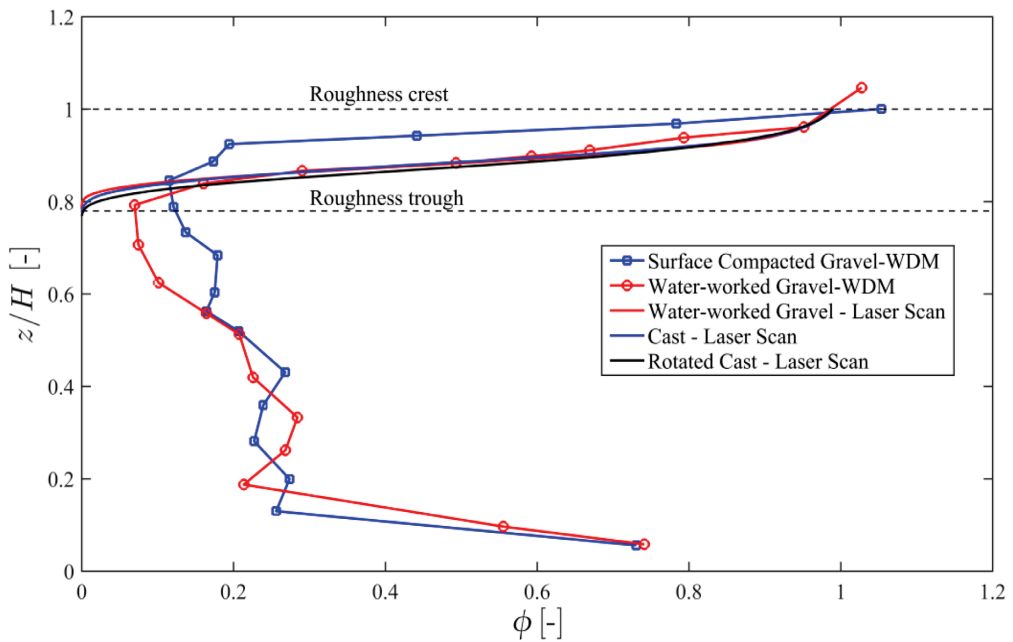


Figure 11: Porosity distribution of different bed types;  $H$  is the total height of the bed

## 4.2 Accuracy of the casting technique

[Paper III, IV and SP II]

The accuracy of the casting technique was thoroughly tested as it was a key prerequisite for the present study. The accuracy has been evaluated for small scale production (Paper III) to large scale production (Paper IV). For small scale production, two different surfaces were tested; (i) a small area (20 cm wide x 50 cm long) of a bed composed of golf balls of diameter 42 mm, and (ii) a piece of sand paper of grade P60 (mean sand grain diameter of 269 microns). The accuracy of the casting technique was assessed geometrically and hydraulically. For the geometrical assessment, DEMs derived from the laser scanning data were compared and the results showed a very good agreement between the original and the cast surface. In fact, the first four statistical moments (mean, standard deviation, skewness, and kurtosis) of the elevations of the original and cast surface were comparable, whereas minor differences were found in the first four statistical moments of the elevations of the original and cast golf ball surface. Slight differences were associated with the uncertainty in the laser scanning (for example 'shadow effect' as described in Section 3.3). For the assessment of the hydraulics over the original and reproduced golf ball bed, the velocity measurements obtained over the original and reproduced golf ball bed using V3V, were compared. The results revealed that there was no significant difference in the mean velocities and the turbulence characteristics between the original and reproduced golf ball bed. However, minor differences in the turbulence characteristics were observed near the bed. These differences were attributed to the uncertainty in the velocity measurement near the bed. Moreover, the minor differences in the surface flow characteristics may partly be associated with the solid bottom of the cast surface. This may slightly change the porosity of the reproduced golf ball bed causing a slightly different porosity than the original golf ball bed.

The accuracy of the large-scale cast production is reported in Paper IV. For the evaluation of the accuracy of the large-scale cast production, 4.65 m long DEMs of water-worked gravel-bed and cast-bed obtained from laser scanning were compared. The results showed that the cast-bed replicated the water-worked gravel-bed with an accuracy of  $\pm 5$  mm. Moreover, the first four statistical moments were directly comparable and fell into the typical range for armoured gravel-bed surfaces as defined by Coleman et al. (2011). The accuracy of the cast production was also verified in terms

of the roughness geometry function/porosity,  $\phi$  (Figure 11). Figure 11 shows a very good agreement of  $\phi$  between the water-worked gravel-bed and cast-bed. The beds were also compared based on 2D-second order structure functions (2DSSF) as reported in Qin et al. (2018). The spatial correlation maps produced from 2DSSF showed in Figure 7 in Paper IV also confirmed that the cast-bed reproduced the water-worked gravel-bed accurately.

### 4.3 Flow resistance

[Paper IV and V]

In addition to the geometrical comparison of the beds, the analysis of the effect of porosity on the bulk flow resistance is reported in Papers IV and V. The casting technique also allowed the investigation of the effect of grain orientation on the flow resistance. Cast tiles were rotated through 180 degrees to study the effect of grain orientation on the bulk flow resistance (see Paper IV for details). The bulk flow resistance was calculated based on the Darcy-Weisbach friction factor ( $f = 8 \cdot u_*^2 / U^2$ ) and compared for the different bed types for similar boundary conditions (relative submergence and shear velocity were kept approximately constant for tests over each bed). Figure 12 shows the variation of  $(8/f)^{0.5}$  with the relative submergence while Figure 13 shows the variation of the friction factor,  $f$  with the Reynolds number,  $Re$ . The lowest values of  $(8/f)^{0.5}$  (i.e. larger friction factors,  $f$ ) were found over the rotated cast-bed for  $h/k < 6$ . For relative submergences  $h/k > 6$ , the difference in  $(8/f)^{0.5}$  between the rotated cast-bed and the cast-bed becomes smaller, which may be attributed to the increasing relative submergence. Figure 13 reveals that the friction factors are higher for rotated cast-bed for all  $Re$  values. However, the friction factor for the rotated cast-bed and the gravel-bed are approximately the same for  $Re \approx 170000$ . The lower value of  $f$  for the rotated cast-bed can be associated with the uncertainty in the water surface slope measurement as this condition (BC6) was characterized by the lowest water surface slope ( $S_w \approx 0.05\%$ ). For all other tests, the higher friction factors  $f$  for the rotated cast-bed mean that the rotated cast-bed exerted larger resistance on the flow than the water-worked gravel-bed or cast-bed (Figure 12 and Figure 13). This confirmed that the grain orientation plays a vital role in the flow resistance. Moreover, the higher flow resistance exerted by the rotated cast revealed that the water working creates a

hydraulically effective bed configuration (e.g. Leopold and Langbein, 1962). In fact, during water working, small grains settled in the less turbulent zones such as lee areas (behind the big stones). For the rotated cast, these small grains in lee areas became exposed to the flow and imposed additional resistance, because they could not be eroded further as they were part of the immobile bed.

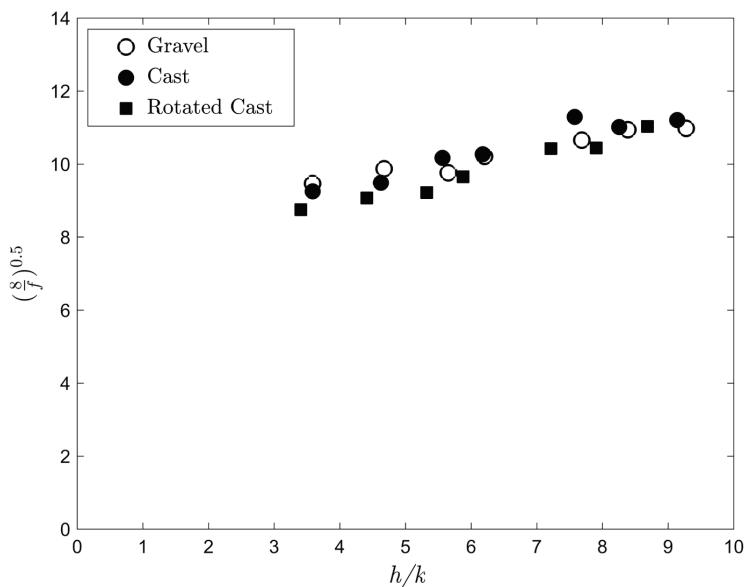


Figure 12:  $(8/f)^{0.5}$  as function of relative submergence ( $h/k$ ).

The comparison of flow resistance over the water-worked gravel-bed and the cast-bed allows for the evaluation of the effect of gravel-bed porosity on the flow resistance. The water-worked gravel-bed showed slightly higher resistance than the cast-bed except for the first two boundary conditions for which the cast-bed exerted higher resistance to the flow (Figure 12 and Figure 13). The lower flow resistance over the water-worked gravel-bed for boundary conditions BC1 & BC2 can partly be explained by the low relative submergence and low discharge. Unlike for the cast-bed, a certain amount of water was conveyed through the subsurface of the water-worked gravel-bed. As shown by Table 1, the difference in discharge between the tests with the water-worked gravel-bed and the cast-bed for BC1 and BC2 was 0 and 0.002 m<sup>3</sup>/s respectively. If a subsurface flow of 0.001 – 0.002 m<sup>3</sup>/s is assumed for the water-worked gravel-bed test and deducted from the measured bulk discharge, the water-worked

gravel-bed would result in higher or approximately equal friction factor for BC1 and BC2 respectively. For  $h/k \geq 5.7$  ( $Re \geq 100,000$ ), the water-worked gravel-bed shows higher friction factors than the cast-bed as the significance of the subsurface flow decreases with increasing discharges (Figure 12 and Figure 13). However, the water-worked gravel-bed and the cast-bed show approximately equal flow resistance for  $Re \approx 170,000$ . As mentioned above, this condition was characterized by the lowest water surface slope ( $\approx 0.05\%$ ), and thus by the highest uncertainties in the slope measurements. Moreover, the higher flow resistance over the permeable gravel-bed validates the results reported in the literature.

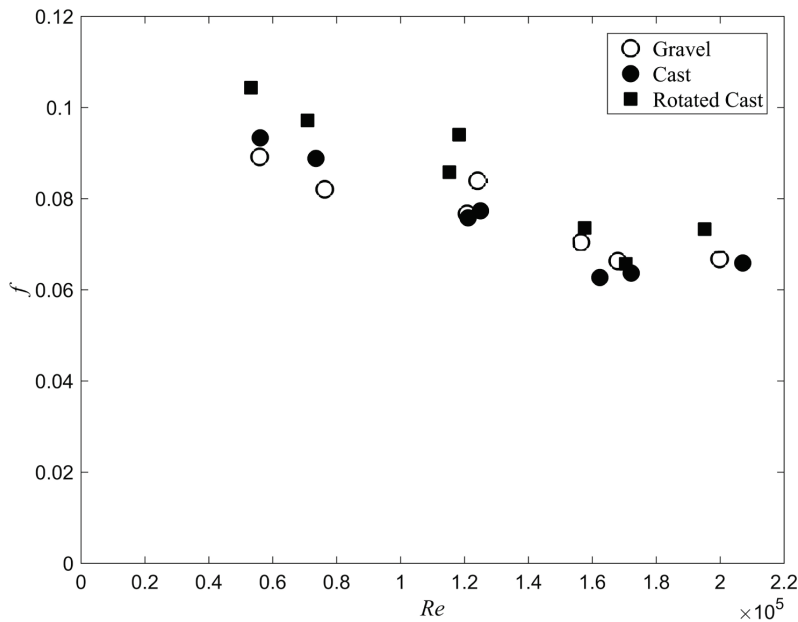


Figure 13: The variation of bulk friction factors with  $Re$  for the tested bed surfaces

Figure 14 shows exemplarily the vertical profile of the double-averaged longitudinal velocities obtained for BC4 (Table 1). The vertical elevation  $z = 0$  was set at the mean bed elevation and double-averaged velocities were normalized with the shear velocity. It should be noted that the local roughness crest (roughness crest within the PIV window) was at  $z = 8$  mm. The double averaged velocities above the crest ( $z > 8$  mm) are smaller over the water-worked gravel-bed than over the cast-bed whereas the velocities over the rotated cast-bed are smaller than over the cast-bed for up to  $z \approx 80$

mm and they are approximately equal above  $z \approx 80$  mm (Figure 14). The smaller velocities over the porous water-worked gravel-bed than over the non-porous cast-bed are additional evidence that the water-worked gravel-bed exerts higher resistance than its impermeable counterpart. It is interesting to note that in the interfacial sublayer ( $z < 8$  mm), flow velocities were slightly larger over the water-worked gravel-bed than over the cast-bed. This can be explained by the ‘no slip’ condition for the impermeable cast-bed and sub-surface flow for the permeable gravel-bed. For different boundary conditions, the double-averaged velocity profiles (normalized with shear velocities) over the cast-bed did not collapse on a single line and slightly deviated from each other (see Figure 10 in Paper IV). In order to cross-check this discrepancy, the velocity profiles were integrated over the depth to calculate the respective discharges which were then compared with the measured discharges. The results showed that the calculated and measured discharges were approximately similar.

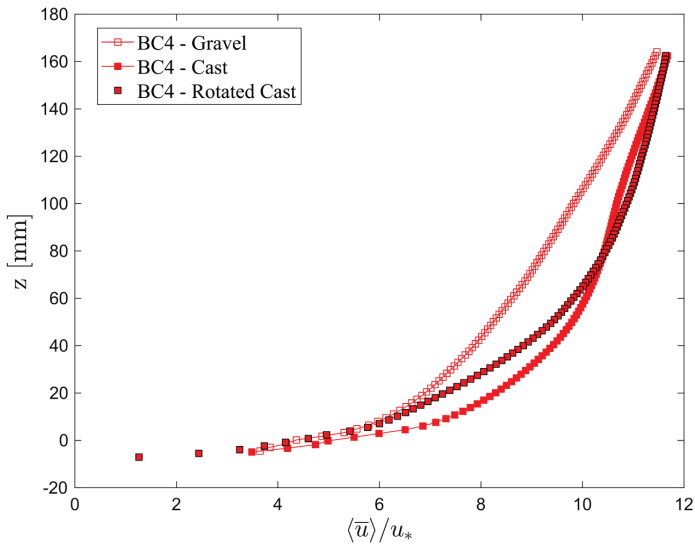


Figure 14: The double-averaged streamwise velocity profiles.

#### 4.4 Turbulence Characteristics

The obtained velocity data were analysed further to study the turbulence characteristics over different bed types. These additional results have not yet been published in the listed papers. Figure 15 (a), (b), and (c) show exemplarily the

normalized streamwise, vertical turbulence intensities as well as the normalized Reynolds shear stress profiles. The vertical distance was normalized with the water depth. It is apparent from the plots that the turbulence intensities and Reynolds stresses over the rotated cast are much different than over the gravel-bed and cast-bed. This is mainly due to the fact that, as mentioned above, the flow is spatially heterogeneous and largely influenced by the roughness elements. In fact, cast tiles were rotated 180 degrees so that the gravel grains in the downstream of the PIV measurement window became located upstream for the rotated cast. Therefore, the upstream area of the velocity measurement was characterized by different roughness elements for the rotated cast-bed than for the gravel-bed or cast-bed. However, the shape of the turbulence intensity and shear stress profiles are validated through the theoretical and experimental evidence, for example, the Reynolds stress linearly increases with the decreasing elevation until it reaches a maximum in the proximity of the bed surface and then decreases towards the bed surface.

While the turbulence characteristics over the rotated cast-bed greatly differ from that over the gravel-bed or the cast-bed, the turbulence characteristics over the water-worked gravel-bed and cast-bed are comparable. Figure 15 shows that the streamwise and vertical turbulence intensities are slightly higher over the cast-bed than over the gravel-bed. On the other hand, the Reynolds shear stresses are slightly higher over the water-worked gravel-bed than over the cast-bed for  $z/h > 0.1$ , and smaller for  $z/h < 0.1$ . The normalized elevation  $z/h \approx 0.1$  corresponded to the global roughness crest (the roughness crest of the whole scanning section, i.e. 4.65 m x 0.66 m). This means that above the global roughness crest, the Reynolds shear stresses are higher over the water-worked gravel-bed than over the cast-bed. This further validates that the water-worked gravel exerted larger resistance on the surface flow than the cast-bed. The flow statistics at the roughness crest for all three beds are summarized in Table 3. The roughness crest was chosen for the flow statistics, because roughness crest is the height where the maximum fluid exchange occurs in the sediment-water interface (Mignot et al., 2009; Cooper et al., 2018). The turbulence correlation coefficient (Figure 15d) was slightly higher (~ 5%) for the water-worked gravel-bed than for the cast-bed. Despite the smaller turbulence intensities found over the water-worked gravel-bed than over the cast-bed, slightly higher turbulence correlation coefficient over the gravel-bed than the cast-bed reveals that higher momentum flux occurs as the turbulent flow is more

coherent in the temporal domain. A similar behaviour was also found by Cooper et al. (2018) and Breugem et al. (2006).

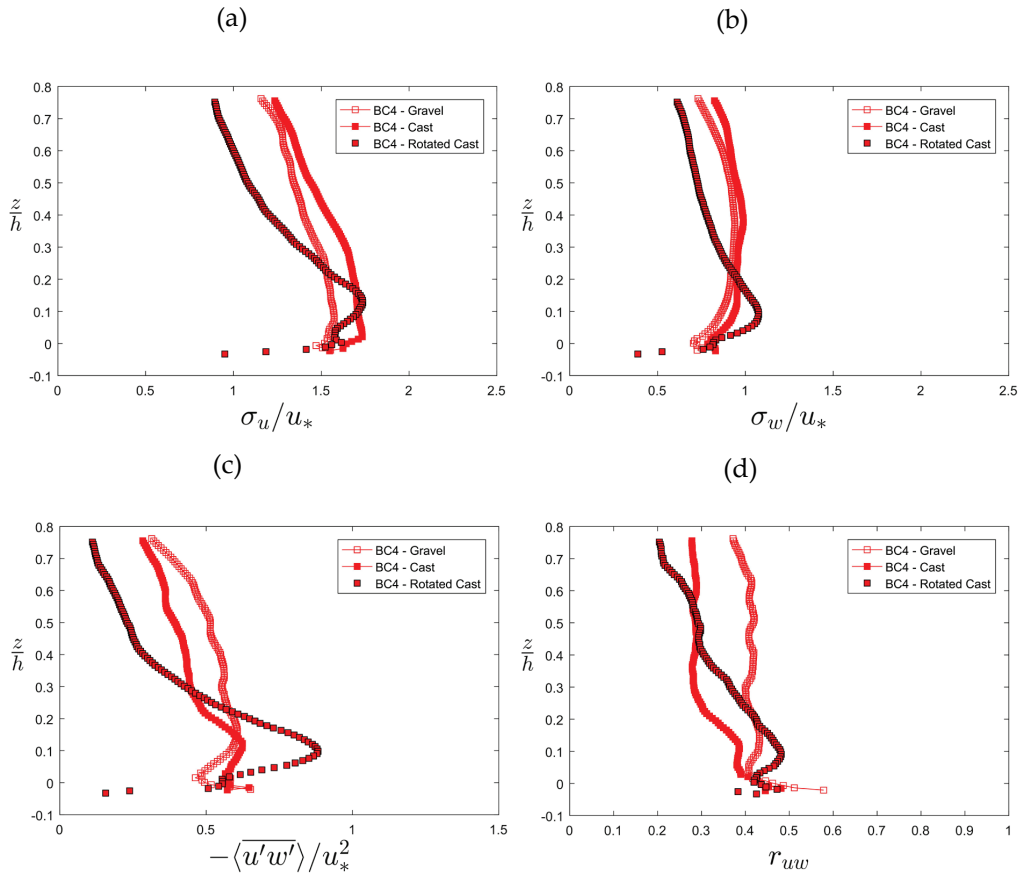


Figure 15: (a) Streamwise turbulent intensity, (b) Vertical turbulent intensity, (c) Reynolds stress distribution, (d) Turbulence coefficient

The vertical profiles of streamwise and vertical form-induced stresses are plotted in Figure 16. The profiles validate the typical form-induced intensity/stress profiles, i.e. the form-induced stresses are negligible from the water surface to the upper boundary of the form-induced sublayer ( $z/h \approx 0.15$  here). They increase to a maximum below the crest and subsequently reduce to a small value within the interfacial region (e.g., Aberle et al., 2008).



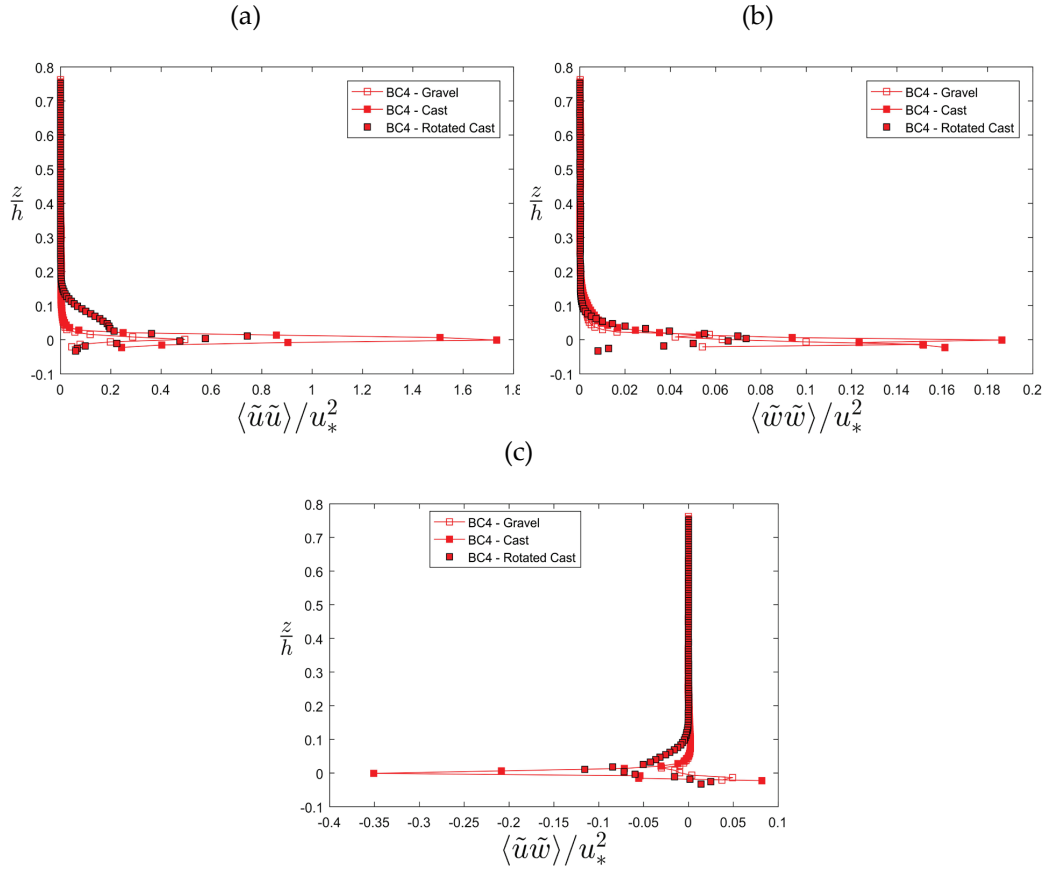


Figure 16: (a) Streamwise form-induced intensity, (b) Vertical form-induced intensity, (c) Form-induced stress

The cast-bed shows higher streamwise and vertical form-induced intensity than the other two beds. At the level of the roughness crest, the streamwise and vertical form-induced intensities are 57% and 50% lower over water-worked gravel-bed than over the cast-bed, respectively. This finding is consistent with the results of Cooper et al. (2018) who found a similar behaviour and the same order of magnitude difference. It is apparent that the impermeable effect for the non-porous cast-bed (or the solid bottom of the cast-bed), prevents the fluid infiltration into the bed, causing a strong recirculation of the fluid within the roughness layer. This strong recirculation is more stable with time and has strong contribution to the spatial heterogeneity in the time-averaged flow in streamwise and vertical direction, thus the non-porous cast-bed produces larger form-induced stress. Moreover, the absolute value of form-induced

stresses was smaller than the Reynolds shear stress over the water-worked gravel-bed. Therefore, form-induced stress contributes only a small amount to the momentum transfer compared to the momentum transfer due to the Reynolds shear stress for the water-worked gravel-bed. The flow statistics at the roughness crest over different bed types are summarized in Table 3. In general, the difference in the flow statistics values are smaller than what was presented in Cooper et al. (2018). This may partly be associated with the difference in experimental set-up /procedure and the range of shear velocity tested in the present study and i.e. shear velocities are smaller than what was used in the study of Cooper et al. (2018).

Table 3: Flow statistics at the roughness crest

| <b>Parameter</b>                               | <b>Gravel-bed</b> | <b>Cast-bed</b> | <b>Rotated-Cast</b> |
|--|-------------------|-----------------|---------------------|
| $\langle \bar{u} \rangle / u_*$                | 5.97              | 7.11            | 6.10                |
| $\sigma_u / u_*$                               | 1.54              | 1.73            | 1.58                |
| $\sigma_w / u_*$                               | 0.77              | 0.84            | 0.95                |
| $-\langle \overline{u'w'} \rangle / u_*^2$     | 0.48              | 0.57            | 0.65                |
| $r_{uw}$                                       | 0.41              | 0.39            | 0.43                |
| $TKE / u_*^2$                                  | 2.44              | 3.14            | 2.84                |
| $\langle \tilde{u}^2 \rangle / u_*^2$          | 0.03              | 0.07            | 0.19                |
| $\langle \tilde{w}^2 \rangle / u_*^2$          | 0.01              | 0.02            | 0.03                |
| $ \langle \tilde{u}\tilde{w} \rangle  / u_*^2$ | 0.005             | 0.011           | 0.042               |



# 5

## Conclusions and Recommendations

This thesis presented the results from five primary papers and two secondary papers (SP) (refer to List of Papers) related to research work specifically designed to study the effect of bed porosity on the flow resistance and the near-bed turbulence. Firstly, the porosity distribution in a water-worked gravel-bed was investigated and it was found that the porosity profiles obtained from the water displacement method were similar to what was reported in the literature (e.g. Aberle, 2007). However, it was shown that the capillary action influenced the results which means that the absolute minimum porosity found at the level of roughness trough was not only associated with the small particle entrainment during the water working, but also due to the capillary action. Similarly, the large porosity values found close to the plastic bottom of the flume originated from the combined effect of poor sorting of the gravel grains at the bottom as well as the effect of capillary action in the water displacement method (Paper II).

Secondly, the accuracy of the casting technique was investigated for small and large scale of cast bed production. The small-scale cast production consisted of small rough surfaces such as fine sand paper and a section bed composed of golf balls. The accuracy was evaluated based on the geometry and hydraulics over the original and cast surfaces. The results showed that the cast duplicated the original surface with high accuracy (Paper III). Moreover, the non-porous counterpart of the water-worked gravel-bed was, for the first time, produced in large-scale using the casting technique. The accuracy of the cast production and placement showed that the cast-bed replicated the water-worked gravel-surface with an accuracy of  $\pm 5$  mm. The accuracy of the cast-bed was also verified through the 2D-second order structure function which confirmed that both porous gravel-bed and its non-porous counterpart (cast-bed) can be characterized by the same characteristic roughness length scale (Paper IV, V).

In order to study the effect of gravel bed porosity on the flow resistance and near-bed turbulence characteristics, hydraulic measurements were performed over the porous water-worked gravel-bed and non-porous cast-bed. In addition, cast tiles were rotated 180 degrees ('rotated cast-bed') and hydraulic measurements were taken for similar hydraulic conditions (the same relative submergence and water surface slope). The experiments with the rotated cast-bed were performed to study the influence of gravel grain orientation on the flow resistance and surface flow characteristics. The results showed that the rotated cast imposed larger flow resistance on the surface flow than the water-worked gravel-bed or cast-bed. This result implies that the bed roughness cannot solely be described by a characteristic grain size and both grain orientation and surface structure play an important role in the determination of flow resistance. Furthermore, for lower discharge and lower relative submergence, the sub-surface flow became significant when determining the flow resistance over the water-worked gravel-bed and the significance of the sub-surface flow decreased with the increasing discharges. Therefore, for higher relative submergences and higher discharges (higher  $Re$ ), the water-worked gravel-bed offered slightly higher resistance than its non-porous counterpart and confirmed the findings in the literature.

Turbulence characteristics over three bed surfaces have been analysed. The results showed that the turbulence characteristics over the rotated cast greatly differed from those over the gravel-bed or cast-bed. These differences were due to the fact that the upstream area of the velocity measurement for the rotated cast-bed was characterized by different roughness elements than for the gravel-bed or cast-bed. Slight differences in turbulence characteristics were found over the water-worked gravel-bed and cast-bed. Slightly larger shear stresses and turbulence correlation coefficients over the water-worked gravel-bed than over the cast-bed revealed that momentum transfer occurred across the sediment-water interface as the turbulence was more coherent in the temporal domain. The form induced stresses were smaller than the Reynolds shear stresses over the water-worked gravel-bed. Therefore, the Reynolds shear stresses contributed more to the total stresses and subsequently to the momentum transfer. The higher form-induced intensity for the cast-bed revealed that a strong recirculation of the fluid due to the non-porous effect causing a larger spatial heterogeneity on the flow. Moreover, the turbulent flow statistics at the roughness crest have been compared with the flow statistics in the study of Cooper et al. (2018). It was found that

the differences in the flow statistics values between the water-worked gravel-bed and the cast-bed were smaller in the present study than in Cooper et al. (2018). This may partly be associated with the small shear velocities used in the present study than in Cooper et al. (2018), and difference in the experimental set-up/procedure between these two studies.

### **Recommendations**

Some recommendations for future work can be formulated based on the experiences and results obtained in the present study.

- Firstly, more detailed analysis of the coherent structure is recommended in order to obtain more knowledge about the spatial flow structure and transport mechanism of momentum.
- Secondly, similar tests to what is reported in the present study can be performed for a wide range of shear velocities or Reynolds number so that the difference in the turbulence characteristics between the porous and non-porous beds would become more distinguishable.
- Thirdly, it would be interesting to measure the subsurface flow to study the exchange process and couple it to the surface flow measurements to get a complete insight into the hyporheic exchange.



## References

- ABERLE, J. (2007). Measurements of armour layer roughness geometry function and porosity. *Acta Geophysica*, 55, 23-32.
- ABERLE, J., KOLL, K. & DITTRICH, A. (2008). Form induced stresses over rough gravel-beds. *Acta Geophysica*, 56, 584-600.
- ADRIAN, R. J. & WESTERWEEL, J. (2011). *Particle Image Velocimetry*, New York, USA, Cambridge.
- BESCHTA, R. L. & RIPPLE, W. J. (2012). The role of large predators in maintaining riparian plant communities and river morphology. *Geomorphology*, 157-158, 88-98.
- BOANO, F., HARVEY, J. W., MARION, A., PACKMAN, A. I., REVELLI, R., RIDOLFI, L. & WÖRMAN, A. (2014). Hyporheic flow and transport processes: Mechanisms, models, and biogeochemical implications. *Reviews of Geophysics*, 52, 603-679.
- BREUGEM, W. P., BOERSMA, B. J. & UITTENBOGAARD, R. E. (2006). The influence of wall permeability on turbulent channel flow. *Journal of Fluid Mechanics*, 562, 35-72.
- BRUNKE, M. (1999). Colmation and Depth Filtration within Streambeds: Retention of Particles in Hyporheic Interstices. *International Review of Hydrobiology*, 84, 99-117.
- CHURCH, M. (2006). Bed material transport and the morphology of alluvial river channels. *Annual Review of Earth and Planetary Sciences*, 34, 325-354.
- COLEMAN, S. E., NIKORA, V. I. & ABERLE, J. (2011). Interpretation of alluvial beds through bed-elevation distribution moments. *Water Resources Research*, 47, W11505.
- COOPER, J. R., ABERLE, J., KOLL, K. & TAIT, S. J. (2013). Influence of relative submergence on spatial variance and form-induced stress of gravel-bed flows. *Water Resources Research*, 49, 5765-5777.
- COOPER, J. R., OCKLEFORD, A., RICE, S. P. & POWELL, D. M. (2018). Does the permeability of gravel river beds affect near-bed hydrodynamics? *Earth Surface Processes and Landforms*, 43, 943-955.
- DEY, S. & DAS, R. (2012). Gravel-Bed Hydrodynamics: Double-Averaging Approach. *Journal of Hydraulic Engineering*, 138, 707-725.
- FANG, H., HAN, X., HE, G. & DEY, S. (2018). Influence of permeable beds on hydraulically macro-rough flow. *Journal of Fluid Mechanics*, 847, 552-590.
- FORSETH, T. & HARBY, A. (2014). Handbook for environmental design in regulated salmon rivers. In: Forseth, T. & Harby, A. (eds.) *NINA Special Report*. Trondheim: NINA.
- FRANCISCO, N. G., PEDRO, M. V. J. & G., K. M. (2016). Porosity and size gradation of saturated gravel with percolated fines. *Sedimentology*, 63, 1209-1232.
- GRAF, W. H. & SONG, T. (1995). Bed-shear stress in non-uniform and unsteady open-channel flows. *Journal of Hydraulic Research*, 33, 699-704.
- HENDRICK, R. R., ELY, L. L. & PAPANICOLAOU, A. N. (2010). The role of hydrologic processes and geomorphology on the morphology and evolution of sediment clusters in gravel-bed rivers. *Geomorphology*, 114, 483-496.



- JIMÉNEZ, J. (2004). Turbulent flows over rough walls. *Annual Review of Fluid Mechanics*, 36, 173-196.
- JIMÉNEZ, J., UHLMANN, M., PINELLI, A. & KAWAHARA, G. (2001). Turbulent shear flow over active and passive porous surfaces. *Journal of Fluid Mechanics*, 442, 89-117.
- KATUL, G., WIBERG, P., ALBERTSON, J. & HORNBERGER, G. (2002). A mixing layer theory for flow resistance in shallow streams. *Water Resources Research*, 38, 32-1-32-8.
- KIRONOTO, B. A., GRAF, W. H. & REYNOLDS (1994). Turbulence Characteristics in Rough Uniform Open-Channel Flow. *Proceedings of the Institution of Civil Engineers - Water Maritime and Energy*, 106, 333-344.
- KOLL, K. (2006). Parameterisation of the vertical velocity profile in the wall region over rough surfaces. In: Ferreira, R. M. L., Alves, E. C. T. L., Leal, J. G. a. B. & Cardoso, A. H. (eds.) *River Flow 2006*. Lisbon, Portugal: CRC Press.
- KUWATA, Y. & SUGA, K. (2017). Direct numerical simulation of turbulence over anisotropic porous media. *Journal of Fluid Mechanics*, 831, 41-71.
- LEOPOLD, L. B. & LANGBEIN, W. B. (1962). The Concept of Entropy in Landscape Evolution *Theoretical Papers in the Hydrologic and Geomorphic Sciences*. United States Government Printing Office, Washington
- MANES, C., POGGI, D. & RIDOLFI, L. (2011a). Turbulent boundary layers over permeable walls: scaling and near-wall structure. *Journal of Fluid Mechanics*, 687, 141-170.
- MANES, C., POKRAJAC, D., MCEWAN, I. & NIKORA, V. (2009). Turbulence structure of open channel flows over permeable and impermeable beds: A comparative study. *Physics of Fluids (1994-present)*, 21, -.
- MANES, C., POKRAJAC, D., NIKORA, V. I., RIDOLFI, L. & POGGI, D. (2011b). Turbulent friction in flows over permeable walls. *Geophysical Research Letters*, 38, L03402.
- MARION, A., NIKORA, V., PUJALON, S., BOUMA, T., KOLL, K., BALLIO, F., TAIT, S., ZARAMELLA, M., SUKHODOLOV, A., O'HARE, M., WHARTON, G., ABERLE, J., TREGNAGHI, M., DAVIES, P., NEPF, H., PARKER, G. & STATZNER, B. (2014). Aquatic interfaces: a hydrodynamic and ecological perspective. *Journal of Hydraulic Research*, 52, 744-758.
- MIGNOT, E., BARTHELEMY, E. & HURTHER, D. (2009). Double-averaging analysis and local flow characterization of near-bed turbulence in gravel-bed channel flows. *Journal of Fluid Mechanics*, 618, 279-303.
- MOHAJERI, S. H., RIGHETTI, M., WHARTON, G. & ROMANO, G. P. (2016). On the structure of turbulent gravel bed flow: Implications for sediment transport. *Advances in Water Resources*, 92, 90-104.
- NEZU, I. & NAKAGAWA, H. (1993). *Turbulence in Open Channel Flows*, Rotterdam, A.A. Balkema.
- NIKORA, V., GORING, D., MCEWAN, I. & GRIFFITHS, G. (2001). Spatially Averaged Open-Channel Flow over Rough Bed. *Journal of Hydraulic Engineering*, 127, 123-133.
- NIKORA, V., KOLL, K., MCEWAN, I., MCLEAN, S. & DITTRICH, A. (2004). Velocity Distribution in the Roughness Layer of Rough-Bed Flows. *Journal of Hydraulic Engineering*, 130, 1036-1042.

- NIKORA, V., MCEWAN, I., MCLEAN, S., COLEMAN, S., POKRAJAC, D. & WALTERS, R. (2007a). Double-Averaging Concept for Rough-Bed Open-Channel and Overland Flows: Theoretical Background. *Journal of Hydraulic Engineering*, 133, 873-883.
- NIKORA, V., MCLEAN, S., COLEMAN, S., POKRAJAC, D., MCEWAN, I., CAMPBELL, L., ABERLE, J., CLUNIE, D. & KOLL, K. (2007b). Double-Averaging Concept for Rough-Bed Open-Channel and Overland Flows: Applications. *Journal of Hydraulic Engineering*, 133, 884-895.
- POKRAJAC, D. & MANES, C. (2009). Velocity Measurements of a Free-Surface Turbulent Flow Penetrating a Porous Medium Composed of Uniform-Size Spheres. *Transport in Porous Media*, 78, 367.
- POTHOS, S., TROOLIN, D., LAI, W. & MENON, R. (2009). V3V – Volumetric Three-Component Velocimetry For 3D Flow Measurements-Main Principle, Theory and Applications. *Termotehnica*, 2, 25-32.
- QIN, J., ABERLE, J., HENRY, P.-Y., WU, T. & ZHONG, D. (2018). Statistical significance of spatial correlation patterns in armoured gravel beds. *Journal of Hydraulic Research*.
- SARKAR, S. & DEY, S. (2010). Double-averaging turbulence characteristics in flows over a gravel bed. *Journal of Hydraulic Research*, 48, 801-809.
- SPILLER, S. & RÜTHER, N. (2012). Artificial reproduction of the surface structure in a gravel bed. *2nd IAHR Europe Conference Munich, Germany*.
- STERNECKER, K., DENIC, M. & GEIST, J. (2014). Timing matters: species-specific interactions between spawning time, substrate quality, and recruitment success in three salmonid species. *Ecology and Evolution*, 4, 2749-2758.
- STEWART, M. T. (2014). *Turbulence structure of rough-bed open-channel flow*. Doctor of Philosophy PhD Thesis, University of Aberdeen.
- TONINA, D. & BUFFINGTON, J. M. (2007). Hyporheic exchange in gravel bed rivers with pool-riffle morphology: Laboratory experiments and three-dimensional modeling. *Water Resources Research*, 43, W01421.
- ZAGNI, A. F. E. & SMITH, K. V. H. (1979). Channel flow over permeable beds of graded spheres. *Journal of the Hydraulic Division* 102, 207.
- ZIPPE, H. J. & GRAF, W. H. (1983). Turbulent boundary layer flow over permeable and non-permeable rough surfaces. *Journal of Hydraulic Research*, 21, 51-65.





**Research Articles**



## **Paper I**

---

### **The effect of bed porosity on near-bed turbulent flow characteristics in gravel-bed rivers**

Christy Ushanth Navaratnam, Jochen Aberle

VANN, 2017, 52 (2)

---



# The effect of bed porosity on near-bed turbulent flow characteristics in gravel-bed rivers

*Av Christy Ushanth Navaratnam and Jochen Aberle*

*Christy Ushanth Navaratnam* is a PhD candidate at the Department of Civil and Environmental Engineering, NTNU and *Jochen Aberle* is a professor at the Department of Civil and Environmental Engineering, NTNU.

## Sammendrag

Denne artikkelen presenterer en litteraturstudie på strømningstyper og -lag over elveleier av grov grus, og hvilken innvirkning bunnens porøsitet har på strømningens karakteristika. Strømningstyper og -lag er definert i henhold til relativ dybde. Viktigheten av utvekslingsprosesser mellom overflatestrøm og strømning i grusen er diskutert. Litteraturstudien viser at effekten av elveleiets porøsitet på strømmingsforholdene nær bunnen enda ikke er fullstendig forstått, og at en porøs bunn viser større strømningsmotstand (friksjon) enn en ikke porøs bunn med identisk ruhet. Videre beskriver artikkelen et pågående forskningsprosjekt ved NTNU som har som mål å kvantifisere effekten av bunnens porøsitet på strømningens karakteristika.

## Summary

This paper provides a brief literature review on flow types and layers over rough gravel beds which is extended towards the effect of bed porosity on surface flow characteristics. Dependent on the relative submergence, different flow layers and types are defined and the significance of exchange processes between surface and sub-surface flows is highlighted. The literature review shows that the effect of bed porosity on near bed

flow hydraulics is not yet completely understood and that porous beds impose higher resistance to flow than non-porous beds with an identical roughness texture. Moreover, the paper briefly describes an ongoing research project at NTNU aiming to quantify the effect of gravel bed porosity on surface flow characteristics.

## Introduction

Gravel bed rivers represent an important stream-type in the fluvial environment and are the dominating river type in mountainous areas. They are characterized by a variable morphology ranging from step-pool-systems through braided channels to static and mobile armor layers (e.g. Church, 2006). The occurrence of morphological features in gravel-bed rivers is directly linked to dynamic fluvial processes which depend on a number of parameters such as hydrology, near-bed hydraulics, sediment size and composition, slope and anthropogenic influences. Moreover, gravel bed rivers play an important role in regard to ecological considerations as they provide habitat for fauna and flora, which in turn dynamically interact with the aforementioned parameters and hence the morphology of gravel-bed rivers (e.g., Beschta and Ripple, 2012, Boano *et al.*, 2014,



Marion *et al.*, 2014, Hauer *et al.*, 2016, Forseth and Harby, 2016). Consequently, gravel bed rivers have been in the focus of research for a long time due to their importance for many engineering and ecological applications.

The present paper focuses on flow features associated with armoured gravel beds by providing a brief overview of the state-of-the-art of rough bed hydrodynamics. Following a brief introduction into the double-averaging methodology for the analysis of spatially variable flows, an overview of different flow types and flow layers over rough gravel beds is given. The review is then extended towards the effect of the porous subsurface on near bed surface flow characteristics in order to discuss exchange processes between the surface and subsurface flows (hyporheic exchange). The paper is concluded by a brief description of an ongoing research project at the Norwegian University of Science and Technology (NTNU) aiming at an experimental quantification of the significance of hyporheic exchange processes on surface flow characteristics over armour layers.

### Double-averaging methodology (DAM)

Although the hydrodynamics of rough bed flows, in general, and of gravel bed rivers, in particular, has been investigated extensively in the past, there are still many problems awaiting clarification. Most of these are associated with the spatial flow heterogeneity in the near bed region due to low relative submergences (ratio between the water depth and roughness height) and the associated complex interaction of the flow with large roughness elements and the bed-surface texture (e.g., Nikora *et al.*, 2007a, b, Cooper *et al.*, 2013). Until today, the flow structure in the near-bed region of rough beds has mainly been investigated based on the Reynolds equations, i.e., time-averaged Navier-Stokes equations. These equations have served for both experimental data interpretation and modelling although the time averaged flow field of rough bed flows is highly three-dimensional which makes the application of the solely time-averaged momentum equations

rather impracticable (Nikora *et al.*, 2001, 2004, 2007a, b, Aberle *et al.*, 2008).

The proper assessment of near bed hydrodynamics requires the consideration of the flow field over a certain spatial scale, and a methodological approach for this purpose is the Double-Averaging Methodology (DAM). The terminology double-averaging is related to the averaging of the Navier-Stokes equations in both the temporal and spatial domain, or in other words by spatially averaging the Reynolds equations. The DAM-approach provides a solid theoretical background for the assessment of the spatial flow variability of the time averaged flow field based on form-induced stresses describing the spatial correlation between time-averaged velocity components within the averaging domain (Nikora *et al.*, 2007a, b). The theoretical background of DAM and various applications can be found in the recent scientific literature (e.g., Nikora *et al.*, 2001, 2004, 2007a, b, 2013, Nikora and Rowinski, 2008, Dey and Das, 2012, Cooper *et al.*, 2013, and references therein) and will not be repeated here.

### Vertical flow field of rough bed flows

The DAM-approach allows for a classification of rough-bed flow types with respect to the flow submergence. Figure 1a shows these flow types and corresponding flow layers as defined by Nikora *et al.* (2007a, b). Before discussing the flow types and layers in more detail below it should be noted that the flow depth is defined as the distance from the free water surface,  $z_{ws}$ , to the roughness trough,  $z_t$ , and the roughness height as the distance from roughness tops,  $z_c$ , to roughness trough,  $z_t$ .

#### Flow layers

The subsurface layer occupies the flow in the substratum (i.e. in the pore space between granular particles) and its upper boundary may be defined as the location where the bed porosity  $\phi$  does not significantly change with depth (i.e.  $d\phi/dz \approx 0$ ). Physically measured vertical porosity-profiles of an armoured gravel bed are shown in Figure 1b.

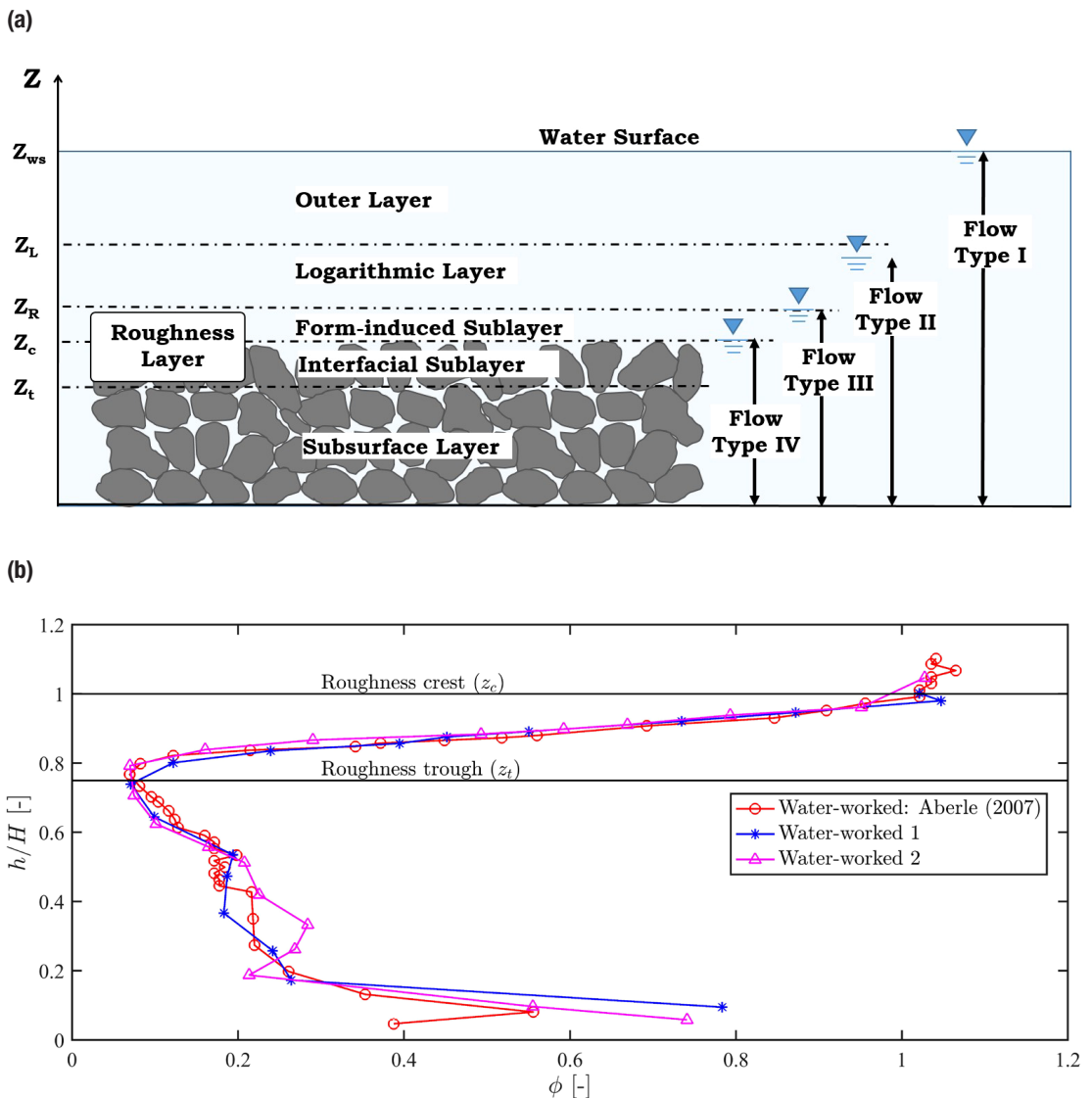


Figure 1. (a) Flow layers and flow type classification over rough permeable beds (adapted from Nikora et.al 2007b). (b) Vertical distribution of porosity  $\phi$ , where  $h$  is distance from the flume bottom and  $H$  is the total bed height (the porosity distributions for water-worked beds 1 and 2 were obtained in the NTNU-experiments presented later; see also Navaratnam et al., 2017).

These profiles were obtained using the so-called water displacement method in a laboratory flume (e.g., Aberle, 2007) and indicate a monotonically decrease of porosity from the roughness tops towards the troughs. Note that the minimum-value of porosity in the region of the roughness trough may partly be caused by an artefact from the measurement technique (capillary action during the measurements; Navaratnam et al.,

2017) or the depth of the active sediment layer during armouring (Aberle, 2007). In general, it may be expected that the porosity will be approximately constant just below the roughness trough within the undisturbed subsurface layer (see the range from  $0.2 < h/H < 0.6$  in Figure 1b). As a rough approximation, the upper boundary of the subsurface layer may therefore be assumed to correspond to the elevation of the roughness

trough  $z_t$ . For completeness, it should be mentioned that the increase of porosity for  $h/H < 0.2$  in Figure 1b can be associated with the solid flume bottom (Aberle, 2007, Navaratnam *et al.*, 2017).

The interfacial sublayer occupies the region between the roughness troughs and crests, i.e. the region from  $z_t$  to  $z_c$  which is occupied by roughness elements. In this layer, the porosity changes from the subsurface-porosity value to  $\phi = 1$  just above the roughness crest  $z_c$  (Figure 1b). The flow in this region is highly three dimensional and affected by form drag of the roughness elements. The so-called form-induced sublayer is found above the roughness crests (extending from  $z_c$  to  $z_r$ ) and is affected by form-induced stresses arising due to flow separation from the roughness elements (e.g., Nikora *et al.*, 2001). The combination of the form-induced and interfacial sublayer is also called the roughness layer. An example of the spatial flow heterogeneity in the roughness layer is shown in Figure 2 presenting 48 velocity profiles measured at different

locations over a rough permeable gravel bed using Laser-Doppler Anemometry. The velocity data were acquired in the study described by Aberle *et al.* (2008) and highlight the large variation of flow velocities around the mean value (indicated by the bold red line). In fact, the variability of flow velocities increases below the roughness crest (interfacial sublayer) and negative values of flow velocities can be observed in wake zones behind larger cobbles. Above the roughness crest (form-induced sublayer), the spatial heterogeneity is not as pronounced but still clearly visible. Note that flow velocities could only be measured up to  $z = 0.15$  m due to experimental peculiarities.

The upper boundary of the roughness layer,  $z_r$ , is the lower boundary of the logarithmic layer, in which the vertical distribution of the flow velocity can be described by the logarithmic formula arising from the law-of-the-wall (e.g., Gersten and Schlichting, 2006). The logarithmic layer occupies the flow region above the form induced sublayer up to  $z_t$ , corresponding to

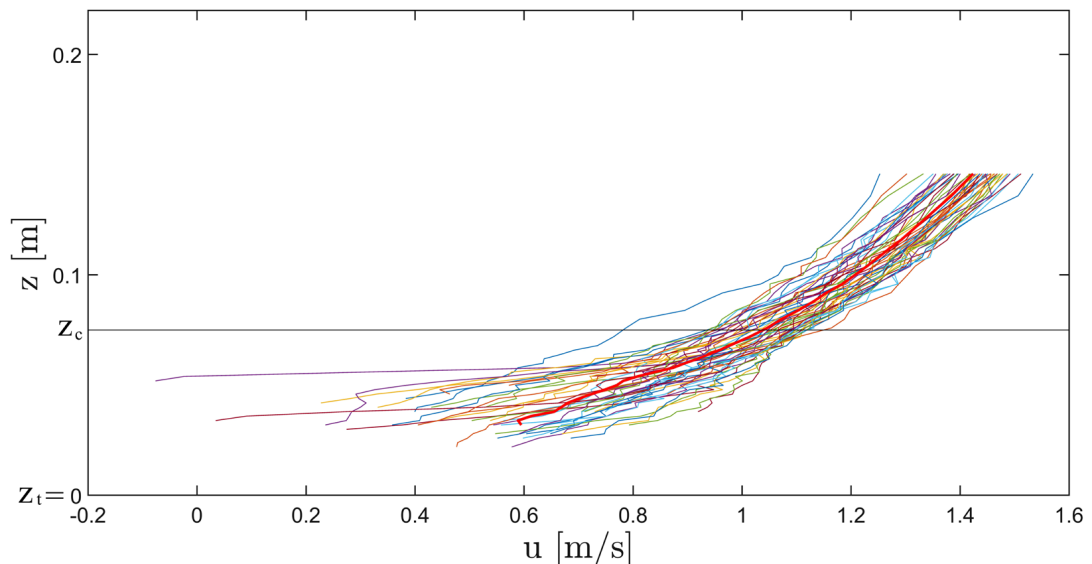


Figure 2. 48 vertical velocity profiles measured at different locations over a rough permeable gravel bed using a Laser-Doppler Anemometer in the study of Aberle *et al.* (2008). The data stem from an experiment carried out in a 0.9 m wide flume with a flow discharge of  $Q = 180$  l/s and a slope of  $S = 1\%$ . The extent of the interfacial sublayer was 0.075 m (from  $z_c$  to  $z_t$ , note that  $z_t$  denotes the origin of the vertical axis) and the mean water surface elevation corresponded to 0.22 m. The horizontal line indicates the elevation of the roughness crest and the bold red line indicates the averaged velocity profile.

approximately 20% of the water depth (Nezu and Nakagawa, 1993, Jiménez 2004). Compared to the roughness layer, the flow in this layer is not affected by form-induced fluxes and the spatial flow heterogeneity becomes therefore negligible. In general, this layer is similar to the logarithmic layer for flows over hydraulically smooth beds. An important prerequisite for the existence of this layer is that the water depth is much larger than the roughness height (large relative submergence).

The outer layer is located above the logarithmic layer and extends to the water surface,  $z_{ws}$ . It is, as the logarithmic layer, not affected by form-induced fluxes. As a consequence, the spatially averaged equations are identical to the time-averaged equations. In general, there are few distinct differences in the hydraulics of the logarithmic and outer layer due to the influence of the free surface (for details see Nikora *et al.*, 2001, Nikora *et al.*, 2007b).

### Flow types

If all the aforementioned flow layers exist in a flow, the water depth will be much larger than the roughness height (Flow type I; Figure 1a). The velocity distribution will have the classical shape with larger velocities in the outer and logarithmic layer and reduced velocities in the near bed region due to roughness effects. Flow type II (Figure 1a) is characterized by an intermediate relative submergence (e.g., below 10) and consists of the subsurface and roughness layer along with an upper flow region which does not necessarily manifest a logarithmic velocity profile, as the relative submergence is not large enough (Nikora *et al.*, 2004). Note that such a case is shown in Figure 2. Nonetheless, the corresponding velocity profile has often been parameterized in the upper flow region of this flow type using the logarithmic function (see also Koll, 2002) or alternatively in analogy to the mixing layer theory (e.g., Katul *et al.*, 2002).

Flow type III corresponds to flows with small relative submergence where the roughness layer extends to the free surface. The shape of the flow velocity distribution for this flow type will be

similar to the distribution for flow type II, i.e. larger velocities above the roughness crests and spatial heterogeneous velocities in the interfacial layer (see Figure 2). Flow type IV describes flow situations over partially inundated beds and the velocity distribution for this flow type depends significantly on roughness characteristics (Nikora *et al.*, 2004). Dependent on the vertical distribution of the roughness, different theoretical velocity profile shapes can be derived within the interfacial sublayer ranging from constant velocity over depth (no vertical variation of roughness characteristics – e.g., cylinder-arrays) through exponential (e.g., well submerged roughness elements with low variability in roughness geometry over depth while the overlying layer is the dominant source of momentum) to linear velocity distributions (monotonically decrease of porosity – e.g. sediment beds), as described in detail in Nikora *et al.* (2004).

The above review focused on surface flow processes, i.e. flows that can be directly seen, but it needs to be extended towards effect of flow processes within the subsurface layer for which relevant information may be found in textbooks (e.g., Bear, 1979) or the scientific literature. The following section focuses on how subsurface-layer characteristics can affect the hydraulics of surface flow. For this purpose, we will briefly highlight exchange processes between the main stream and groundwater flow from a hydraulic point of view.

## Effect of subsurface characteristics on surface flow

### Hyporheic Exchange

The exchange of mass, energy and momentum in the water-sediment interfacial region, i.e. between surface and subsurface flow, is also known as hyporheic exchange. Hyporheic flow itself is controlled by hydrodynamic processes operating across a range of spatial and temporal scales (e.g., Boano *et al.*, 2014, Marion *et al.*, 2014, Tonina and Buffington, 2007). Moreover, in case fine particles are transported by the surface flow, hyporheic exchange can lead to the entrainment of these fine particles into the subsurface layer.

This process can lead to an accumulation of fine sediment around coarse-bed grains which is also known as colmation (Brunke, 1999) or embeddedness (Boano *et al.* 2014), and which can result in the formation of a thin seal disconnecting the surface water from hyporheic water. Such a seal can thus hinder exchange processes and degrade aquatic habitat. An example for the latter is the degradation of spawning areas of lithophilic fish species such as salmon (Sternecker *et al.*, 2014). The reverse process, i.e. the entrainment of fine particles from the subsurface layer into the surface flow, is known as decolmation (Brunke, 1999, Huston and Fox, 2015). This process can be associated with pressure fluctuations in the bed (Detert and Parker, 2010).

**Effect of porosity on surface flow characteristics**

Hyporheic exchange, colmation and decolmation depends on many boundary conditions such as near-bed turbulence characteristics, the interaction of the flow with irregularities of the streambed such as gravel particles or bedforms, subsurface layer characteristics and hydraulic conductivity of the subsurface layer. As indicated in the above review, the hydraulics of gravel bed rivers has mostly been classified in regard to surface flow characteristics. For example, rough-beds have often been simulated by gluing a single layer of rough particles onto an impermeable bottom (e.g., Koll, 2002 and references therein) but there exist also many studies in which turbulent flows over porous beds have been investigated in both laboratory and field conditions (e.g., Mohajeri *et al.* 2016, Stewart, 2014, Pechlivanidis *et al.*, 2012, Aberle *et al.* 2008, Kironoto *et al.*, 1994).

However, only few studies exist in which the influence of bed-porosity on surface flow characteristics has been directly addressed and quantified. These studies revealed significant differences between flows over permeable and non-permeable beds in regard to bulk flow characteristics such as the friction factor, near bed turbulence characteristics and the shape of velocity profile. In fact, numerical simulations

as well as laboratory studies carried out over beds with artificial roughness elements (e.g., spheres) revealed that the friction factors for permeable beds are higher than for impermeable beds with the same roughness texture (Zagni and Smith, 1979, Zippe and Graf, 1983, Jiménez *et al.*, 2001, Prinós *et al.*, 2003, Breugem *et al.* 2006, Manes *et al.* 2009, 2011, Sparrow *et al.* 2012, Keramaris 2016). Moreover, these studies provide evidence that the friction factor for permeable beds depends on the Reynolds number even for the hydraulically rough regime (e.g., Manes *et al.* 2011, Sparrow *et al.* 2012).

The difference in friction factor has been associated with the shear penetration within the permeable bed, i.e. with a more efficient energy dissipation as a consequence of the momentum exchange between the surface and subsurface flow (Zagni and Smith, 1979, Manes *et al.* 2009, 2012). In this context, Keramaris (2016) found for two beds with identical porosity but different subsurface texture a lower surface flow velocity for the bed which was characterized by a larger penetration depth. Further studies have addressed differences in near bed turbulence characteristics and coherent flow structures in much more detail, or investigated the pressure fluctuations in the hyporheic zone and their effect on sediment entrainment (e.g., Vollmer *et al.*, 2002, Smart and Habersack 2007, Detert *et al.* 2010, Keramaris 2016).

Most of the aforementioned studies were based on beds composed of artificial elements and a detailed quantification of the effect of bed porosity on surface flow characteristics in gravel beds is therefore still lacking. To the best of our knowledge, there exists only one study which directly addressed this issue. Ockelford *et al.* (2013) conducted hydraulic measurements over a number of water-worked gravel bed surfaces as well as impermeable facsimiles of the porous beds created using a casting technique. However, the corresponding results have so far only been reported in a conference abstract indicating that the results observed over artificial beds are also valid for gravel beds. Moreover, the study of Ockelford *et al.* (2013) indicates the effect of bed



porosity depends also on surface topography characteristics.

### Current research at NTNU

An ongoing study at the Department of Civil and Environmental Engineering at NTNU aims at the quantification of the effect of bed porosity on the near-bed flow turbulent flow field in gravel bed rivers. In order to study the effect of bed porosity on the near-bed flow turbulence, an armoured gravel bed surface created in a hydraulic flume will be reproduced with high accuracy (Figure 3) using a novel bed casting technique (Spiller and R  ther, 2012, Spiller, 2014, Navaratnam *et al.*, 2016). Hydraulic experiments will be performed over both the initial armoured gravel bed and its

impermeable counterpart by acquiring velocity data for a range of relative submergences by means of 2D - 3C PIV technique (2 Dimension - 3 Component Particle Image Velocimetry). Figure 4 shows exemplarily a time-averaged velocity field of the longitudinal velocity component over an armoured gravel bed which can be captured by this measurement technique. Within the study, the spatially and temporal high-resolution velocity data will be used to determine differences in friction factor, turbulence characteristics and spatial flow heterogeneity in the near bed region between the permeable and impermeable bed based on the DAM-approach. Such a study is also required in regard to further development of experimental techniques as the technological

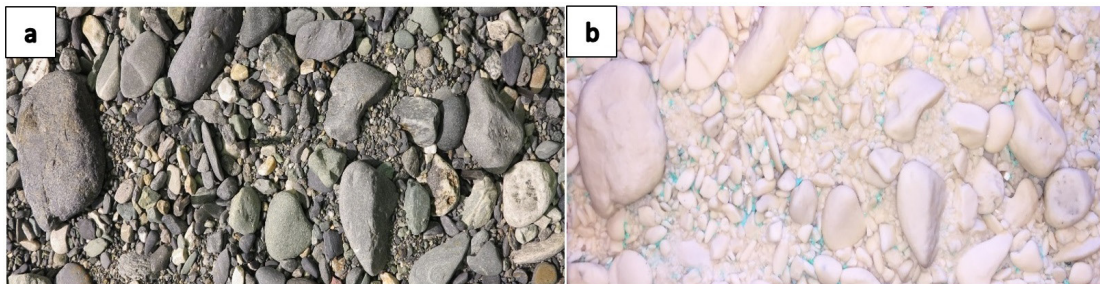


Figure 3. Photographs of a) gravel bed armour layer and b) its artificially reproduced counterpart without porous subsurface.

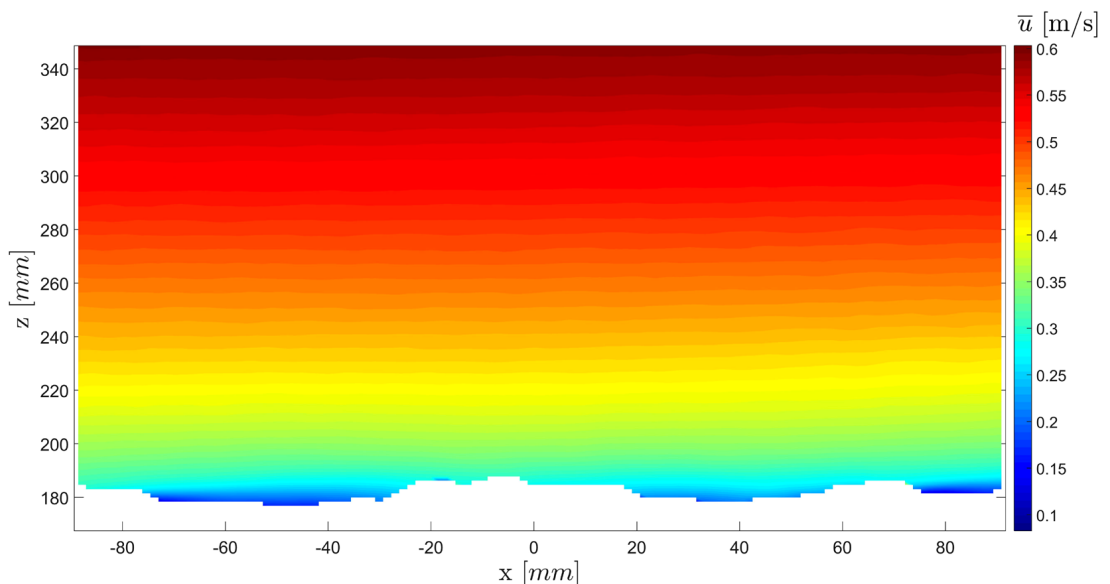


Figure 4. The time-averaged velocity field over an armoured-gravel bed.

development allows nowadays for the printing of 3D surfaces (e.g., Bertin *et al.* 2014) but not yet for the accurate reproduction of subsurface characteristics.

## Conclusions

This paper reviewed flow features over rough gravel bed surfaces and addressed additionally the significance of bed porosity on the hydrodynamics of such flows. Dependent on the relative submergence, different flow layers and flow types have been defined in accordance with recent literature. The literature review revealed also that permeable beds impose higher resistance on the flow than the impermeable beds due to the flow penetration into the porous medium and that the friction factor for permeable beds depends on the Reynolds number. The paper concluded with the brief introduction to an undergoing research project focusing on the quantification of the effect of the gravel bed porosity on the near-bed flow turbulence.

## References

Aberle, J. (2007). Measurements of armour layer roughness geometry function and porosity. *Acta Geophysica*, 55, 23-32.

Aberle, J., K. Koll and A. Ditttrich (2008). Form induced stresses over rough gravel-beds. *Acta Geophysica*, 56(3): 584-600; DOI: 510.2478/s11600-11008-10018-x.

Bear, J. (1979) *Hydraulics of Groundwater*. Dover publications, Mineola, New York.

Bertin, S., H. Friedrich, P. Delmas, E. Chan and G. Gimel'farb (2014). DEM quality assessment with a 3d printed gravel bed applied to stereo photogrammetry. *The Photogrammetric Record* 29(146): 241-264.

Beschta, R. L. and W.J. Ripple, (2012). The role of large predators in maintaining riparian plant communities and river morphology. *Geomorphology* 157-158, 88-98.

Boano, F., J. W. Harvey, A. Marion, A. I. Packman, R. Revelli, L. Ridolfi and A. Wörman (2014). Hyporheic flow and transport processes: Mechanisms, models, and biogeochemical implications. *Reviews of Geophysics*, 52(4), 603-679.

Breugem, W. P., B. J. Boersma and R. E. Uittenbogaard, (2006). The influence of wall permeability on turbulent channel flow. *Journal of Fluid Mechanics*, 562, 35-72.

Brunke, M. (1999). Colmation and Depth Filtration within Streambeds: Retention of Particles in Hyporheic Interstices. *International Review of Hydrobiology*, 84(2): 99-117.

Church, M. (2006). Bed material transport and the morphology of alluvial river channels. *Annual Reviews of Earth and Planetary Sciences*, 34, 325-354.

Cooper, J. R., J. Aberle, K. Koll and S. J. Tait (2013). Influence of relative submergence on spatial variance and form-induced stress of gravel-bed flows. *Water Resources Research*, 49(9): 5765-5777.

Detert, M. and G. Parker (2010). Estimation of the wash-out depth of fine sediments from a granular bed. *Journal of Hydraulic Engineering* 136(10): 790-793.

Detert, M., V. Weitbrecht and G. H. Jirka (2010). Laboratory measurements on turbulent pressure fluctuations in and above gravel beds. *Journal of Hydraulic Engineering* 136(10): 779-789.

Dey, S. and R. Das (2012). Gravel-bed hydrodynamics: Double-averaging approach. *Journal of Hydraulic Engineering* 138(8): 707-725.

Forseth, T. and A. Harby, (eds.) (2014). Handbook for environmental design in regulated salmon rivers. - NINA Special Report 53. 90 pp.

Gersten, K. and H. Schlichting (2006). *Grenzschicht-Theorie*. Berlin, Heidelberg, Springer.

Hauer, F.R., Locke, H., Dreitz, V.J., Hebblewhite, M., Lowe, W.H., Muhlfeld, C.C., Nelson, C.R., Proctor, M.F. and Rood, S.B (2016). Gravel-bed river floodplains are the ecological nexus of glaciated mountain landscapes. *Science Advances*, 2(6), DOI: 10.1126/sciadv.1600026.

Huston, D. L. and J. F. Fox (2015). Clogging of Fine Sediment within Gravel Substrates: Dimensional Analysis and Macroanalysis of Experiments in Hydraulic Flumes. *Journal of Hydraulic Engineering*, 141, 04015015.

Jiménez, J. (2004). Turbulent flows over rough walls. *Annual Review of Fluid Mechanics* 36: 173-196.

Jiménez, J., M.Uhlmann, A. Pinelli and G. Kawahara, (2001). Turbulent shear flow over active and passive porous surfaces. *Journal of Fluid Mechanics*, 442, 89-117. doi:10.1017/S0022112001004888

Katul, G., P. Wiberg, J. Albertson and G. Hornberger (2002). A mixing layer theory for flow resistance in shallow streams. *Water Resources Research*, 38(11): 32-31 - 32-38.

Keramaris, E. (2016). Turbulent structure in uniform inclined open channel flow over different rough porous beds. *International Journal of Sediment Research*.

- Kironoto, B. A., W. H. Graf, and Reynolds (1994). Turbulence Characteristics in Rough Uniform Open-Channel Flow. *Proceedings of the Institution of Civil Engineers - Water Maritime and Energy*, 106, 333-344.
- Koll, K. (2002). Feststofftransport und Geschwindigkeitsverteilung in Raugerinnen, Universität Karlsruhe.
- Manes, C., D. Pokrajac, I. McEwan and V. Nikora (2009). Turbulence structure of open channel flows over permeable and impermeable beds: A comparative study. *Physics of Fluids*, 21: 125109.
- Manes, C., D. Pokrajac, V. I. Nikora, L. Ridolfi and D. Poggi (2011). Turbulent friction in flows over permeable walls. *Geophysical Research Letters* 48(L03402): doi:10.1029/2010GL045695.
- Manes, C., L. Ridolfi and G. Katul (2012). A phenomenological model to describe turbulent friction in permeable-wall flows. *Geophysical Research Letters*, 39(14): L14403.
- Marion, A., V. Nikora, S. Puijalon, T. Bouma, K. Koll, F. Ballio, S. Tait, M. Zaramella, A. Sukhodolov, M. O'Hare, G. Wharton, J. Aberle, M. Tregnaghi, P. Davies, H. Nepf, G. Parker and B. Statzner (2014). Aquatic interfaces: a hydrodynamic and ecological perspective. *Journal of Hydraulic Research*, 52(6): 744-758.
- Mohajeri, S. H., M. Righetti, G. Wharton, and G. P. Romano (2016). On the structure of turbulent gravel bed flow: Implications for sediment transport. *Advances in Water Resources*, 92, 90-104.
- Navaratnam, C. U., J. Aberle and S. M. Spiller (2016). Evaluation of the accuracy of a bed casting technique. River Flow 2016. St. Louis, Missouri, USA. CRC Press, 398-403.
- Navaratnam, C. U., J. Aberle and Daxnerová, J. (2017). An Experimental Investigation on Porosity in Gravel Beds. XXXVI International School of Hydraulics, 2017 Jachranka, Poland. (accepted manuscript)
- Nezu, I. and H. Nakagawa (1993). Turbulence in open-channel flows, IAHR Monograph.
- Nikora, V. I. and P. M. Rowinski (2008). Rough-bed flows in geophysical, environmental, and engineering systems: Double-Averaging Approach and its applications. *Acta Geophysica*, 56(3): 529-533.
- Nikora, V. I., D. G. Goring, I. McEwan and G. A. Griffiths (2001). Spatially averaged open channel-flow over rough bed. *Journal of Hydraulic Engineering*, 127(2): 123-133.
- Nikora, V., K. Koll, I. McEwan, S. McLean and A. Dittrich (2004). Velocity distribution in the roughness layer of rough-bed flows. *Journal of Hydraulic Engineering*, 130(10): 1036-1042.
- Nikora, V., I. McEwan, S. McLean, S. Coleman, D. Pokrajac and R. Walters (2007a). Double-Averaging concept for rough-bed open-channel and overland flows: Theoretical Background. *Journal of Hydraulic Engineering*, 133(8): 873-883.
- Nikora, V., S. McLean, S. Coleman, D. Pokrajac, I. McEwan, L. Campbell, J. Aberle, D. Clunie and K. Koll (2007b). Double-Averaging concept for rough-bed open-channel and overland flows: Applications. *Journal of Hydraulic Engineering*, 133(8): 884-895.
- Nikora, V., F. Ballio, S. Coleman and D. Pokrajac (2013). Spatially Averaged Flows over Mobile Rough Beds: Definitions, Averaging Theorems, and Conservation Equations. *Journal of Hydraulic Engineering*, 139(8): 803-811.
- Ockelford, A., J. Cooper, S. Rice and M. Powel (2013). Effect of Bed Porosity on Momentum Exchange in Gravel-Bed Rivers. *EGU General Assembly 2013*. Vienna, Austria: Geophysical Research Abstracts.
- Pechlivanidis, G. I., E. Keramaris, I. G. Pechlivanidis and G. A. Samaras, (2012). Measuring the turbulent characteristics in an open channel using the PIV method. *Global NEST Journal*, 14, 378-385.
- Prinos, P., D. Sofialidis and E. Keramaris (2003). Turbulent flow over and within a porous bed. *Journal of Hydraulic Engineering*, 129(9): 720-733.
- Smart, G. M. and H. Habersack (2007). Pressure fluctuations and gravel entrainment in rivers. *Journal of Hydraulic Research*, 45(5): 661-673.
- Sparrow, K., D. Pokrajac and D. A. van der A (2012). The Effect of Bed Permeability on Oscillatory Boundary Layer Flow. *Coastal Engineering Proceedings*, 1(33), waves.26. doi: <http://dx.doi.org/10.9753/icce.v33.waves.26>
- Spiller, S. (2014). *Physical effects of load fluctuations in rivers*. PhD Thesis, Norwegian University of Science and Technology.
- Spiller, S. and N. Rüther, (2012). Artificial reproduction of the surface structure in a gravel bed. *2nd IAHR Europe Conference Munich*, Germany.
- Sternecker, K., M. Denic, and J. Geist (2014). Timing matters: species-specific interactions between spawning time, substrate quality, and recruitment success in three salmonid species. *Ecology and Evolution*, 4, 2749-2758.
- Stewart, M. T. (2014). *Turbulence structure of rough-bed open-channel flow*. Doctor of Philosophy PhD Thesis, University of Aberdeen.



Tonina, D. and J. M. Buffington (2007). Hyporheic exchange in gravel bed rivers with pool-riffle morphology: Laboratory experiments and three-dimensional modeling. *Water Resources Research*, 43: W01421, doi:01410.01029/02005WR004328.

Vollmer, S., F. d. l. S. Ramos, H. Daebel and G. Kühn (2002). Micro scale exchange processes between surface and subsurface water. *Journal of Hydrology*, 269(1-2): 3-10.

Zagni and Smith (1979). Channel flow over permeable beds of graded spheres. *Journal of the Hydraulic Division*, 102, 207.

Zippe, H. J. and W. H. Graf (1983). Turbulent boundary layer flow over permeable and non-permeable rough surfaces. *Journal of Hydraulic Research*, 21, 51-65.

**Bergen Vann KF har ansvar for drift og vedlikehold av alle kommunale for vann og avløp i kommunene Bergen og Os. Vårt mål er å være en profesjonell og ledende VA-operatør, og vi er et kompetansesenter innen våre kjerneområder. Vi tilbyr våre tjenester til offentlige og private kunder i Vestlandsregionen.**



bergen vann

### BERGEN VANN KF

Bergen Vann KF utfører drift og vedlikehold av alle offentlige VA anlegg i kommunene Bergen og Os.

#### Vannforsyning

Produksjon og distribusjon av bruksmessig godt og hygienisk trygt drikkevann til 280 000 innbyggere i BERGEN og 18 000 i OS. Oppgaven omfatter drift og vedlikehold av:

- 8 vannbehandlingsanlegg av ulike typer og størrelser
- 1000 km vannledningsnett med ca. 30 høydebasseng, ca. 80 pumpestasjoner m.m.
- Særlig kompetanse innen prosessoptimalisering, aktiv lekkasje-kontroll, vannkvalitetskontroll med mer

#### Avløp og slam

Transportere og rense avløpsvann for å sikre gode miljøkvaliteter for innbyggerne i Bergen og OS. Oppgaven omfatter drift og vedlikehold av:

- 1 kjemisk/mekanisk renseanlegg, 5 kjemisk/biologiske anlegg, 5 større mekaniske anlegg og 12 mindre anlegg, samt 950 km avløpsledninger og 170 avløpspumpestasjoner
- 4 av de store renseanleggene i Bergen bli oppgradert til sekundærrensing i løpet av kommende år. Dessuten vil et sentralrenseanlegg for avløp vil bli satt i drift i OS
- Et biogassanlegg vil bli satt i drift i løpet av kommende år. Anlegget vil produsere gass blant annet til drivstoff i busser basert på slam fra kloakkrenseanleggene.

Bergen Vann ble etablert i 2004 og har nå ca. 150 medarbeidere. Produksjonen er organisert i fire seksjoner; vannbehandling, vann-distribusjon, avløpstransport og avløpsrensing. Dessuten har vi grupper for elektro og automasjon og et eget akkreditert vannlaboratorium. Selskapet er sertifisert etter NS-EN-9001.

[www.bergenvann.com](http://www.bergenvann.com)

## **Paper II**

---

### **An Experimental Investigation on Porosity in Gravel Beds**

Christy Ushanth Navaratnam, Jochen Aberle, Jana Daxnerová

Free Surface Flows and Transport Processes, 2018 (21; pp. 323-334)  
[https://doi.org/10.1007/978-3-319-70914-7\\_21](https://doi.org/10.1007/978-3-319-70914-7_21)

---

Is not included due to copyright  
Available at  
[https://doi.org/10.1007/978-3-319-70914-7\\_21](https://doi.org/10.1007/978-3-319-70914-7_21)

## **Paper III**

---

### **Evaluation of the accuracy of a bed casting technique**

Christy Ushanth Navaratnam, Jochen Aberle, Stephan Spiller

River Flow 2016 – International Conference on Fluvial Hydraulics,  
St. Louis, Missouri, USA (pp. 398-403)

---

Is not included due to copyright  
available at  
<http://doi.org/10.1201/9781315644479-65>

## **Paper IV**

---

### **Influence of Gravel-Bed Porosity and Grain Orientation on Bulk Flow Resistance**

Christy Ushanth Navaratnam, Jochen Aberle, Jie Qin, Pierre-Yves Henry




Water, 2018, 10 (5), 561  
<https://doi.org/10.3390/w10050561>

---



Article

# Influence of Gravel-Bed Porosity and Grain Orientation on Bulk Flow Resistance

Christy Ushanth Navaratnam <sup>1,\*</sup> , Jochen Aberle <sup>1,2</sup>, Jie Qin <sup>3</sup>  and Pierre-Yves Henry <sup>1</sup> 

<sup>1</sup> Department of Civil and Environmental Engineering, Norwegian University of Science and Technology (NTNU), S.P.Andersens veg 5, 7491 Trondheim, Norway; jochen.aberle@tu-braunschweig.de (J.A.); pierre-yves.henry@ntnu.no (P.-Y.H.)

<sup>2</sup> Leichtweiß-Institut für Wasserbau, Technische Universität Braunschweig, 38106 Braunschweig, Germany

<sup>3</sup> College of Harbour, Coastal and Offshore Engineering, Hohai University, Xikang road #1, Nanjing 210098, China; jqin@hhu.edu.cn

\* Correspondence: christy.ushanth.navaratnam@ntnu.no; Tel.: +47-73-595-158

Received: 19 March 2018; Accepted: 20 April 2018; Published: 26 April 2018



**Abstract:** This paper presents results from experiments that were carried out to study the effect of porosity and grain orientation on flow resistance. Experiments were performed over three rough surfaces; a water-worked gravel-bed, its non-porous facsimile (cast-bed) and the rotated cast-bed (cast tiles rotated through 180°). The first two beds were used to isolate the influence of gravel-bed porosity on the bulk flow resistance and the rotated cast was used to study effect of the grain orientation on the flow resistance. The results showed that the rotated cast-bed exerted the highest flow resistance whereas the porous water-worked gravel-bed was, for comparable hydraulic boundary conditions, characterized by slightly higher flow resistance than its non-porous counterpart. The results from the bulk flow analysis were substantiated by a preliminary analysis of flow velocity data.

**Keywords:** flow resistance; roughness; gravel-bed rivers; casting technique

## 1. Introduction

Gravel bed rivers represent an important stream-type in the fluvial environment. Gravel beds are, in general, characterized by a large roughness influencing hydraulic and fluvial processes, which in turn govern the turbulent flow structure, flow resistance, sediment transport, and morphological development. Although these processes have been in the focus of research for a long time, there is still a lack of knowledge with regard to near bed flow structure, flow resistance (e.g., [1–3]) and exchange processes between the main stream and groundwater flow (e.g., [4,5]). This is partly associated with the fact that many studies have focused mainly on the determination of roughness coefficients as a function of characteristic grain-sizes thereby neglecting the structure of gravel beds.

Traditional methods quantify flow resistance through Manning’s roughness coefficient  $n$ , Chézy’s flow resistance factor  $C$  or Darcy-Weisbach’s friction factor  $f$  [6]. These are interrelated and can be written as a function of the bulk velocity  $U$ , water depth  $h$  and energy slope  $S_f$ . As an example, the Darcy-Weisbach friction factor  $f$  is defined as

$$f = 8 \frac{u_*^2}{U^2} \quad (1)$$

where  $u_*$  denotes the shear velocity which, for uniform flow conditions, can be determined according to  $u_* = (ghS_f)^{0.5}$  with  $g$  = gravitational acceleration. Gravel-bed roughness is often described by a characteristic grain size of the bed material (e.g.,  $d_{50}$ ,  $d_{84}$  or  $d_{90}$ ) and is linked to the friction factor via



empirical or semi-empirical relationships (e.g., [6–10]). However, gravel-beds are characterized by a high degree of irregularities (grain shape, orientation, packing pattern, etc.), multiple roughness scales (e.g., small and meso-scale bedforms such as pebble clusters, steps, pools, etc. [11]) and therefore roughness properties may vary independently of grain size [12]. Some studies suggested that the standard deviation of bed-elevations may be used as characteristic vertical roughness scale (e.g., [3,13–15]) and further studies focused on the determination of characteristic horizontal roughness scales through the analysis of longitudinal profiles or digital elevation models, respectively, using spectral analysis, correlation functions and structure functions (e.g., [12,13,16,17]). Despite the application of surface structure analyses, there is still no consensus regarding the interpretation of the results or the most appropriate measure of bed roughness [18,19].

Moreover, it has often been tacitly assumed in flow resistance studies that fluvial beds may be considered as non-porous structures despite the fact that natural gravel-beds are typically composed of a coarse surface layer and a porous subsurface layer. This assumption implies that a porous and non-porous bed with an identical surface structure would be characterized by exactly the same flow resistance. However, the flow over porous beds is characterized by mass and momentum exchange across the sediment water interface due to the pressure gradients driving the flow in and out of the bed [20–22]. The exchange processes, also known as hyporheic exchange, are assumed to have a distinct effect on the near bed flow field and hence flow resistance. In fact, compared to flow resistance studies, only few studies have focused on the influence of bed porosity on flow resistance (e.g., [23–26]). These studies have shown that porous beds impose higher flow resistance than similar non-porous beds.

The present paper investigates this topic further by analyzing experimental data which was acquired over a porous gravel-bed armor layer and its impermeable facsimile. In an additional experimental series, the facsimile was rotated through  $180^\circ$  so that the bulk flow analysis could be extended towards the investigation of the effect of grain-orientation on flow resistance. Within this paper, we focus on the effect of bed porosity on bulk flow characteristics such as the friction factor  $f$ , while more detailed considerations regarding the near bed turbulent flow pattern will be presented in a follow up study. The manuscript is organized as follows: the next Section presents a brief review on the significance of bed porosity for flow resistance; Section 3 describes the experimental setup and methodology, and the results are presented and discussed in Section 4. Conclusions are drawn in Section 5.

## 2. Background

The effect of bed porosity on flow patterns has been investigated in several studies based on data acquired in laboratory and numerical experiments over beds composed of different artificial roughness elements. Most of these studies have revealed that the flow resistance over permeable beds is larger than the flow resistance exerted by their impermeable counterparts (e.g., [23–28]). Moreover, various studies have indicated a dependency of the friction factor with the relative thickness of the permeable layer and the Reynolds-number  $Re = Uh/\nu$ , where  $\nu$  is the kinematic viscosity of the fluid (e.g., [24,26,29]). The increase of flow resistance with  $Re$  has been associated with shear penetration into the porous bed [26–28] and the associated exchange of momentum between the surface flow and the flow in the porous medium which increases the Reynolds shear-stress in the near bed region and hence the flow resistance [25,27,29]. In this context, Breugem et al. [25] found that flow resistance increases with bed permeability or  $Re_K = \sqrt{K}u_*/\nu$ , where  $K$  is the permeability, and Manes et al. [27] showed that the characteristic length scale of the turbulent flow over a permeable wall can be defined by the depth of shear penetration. This penetration depth is related to the zero-plane position which may be determined from the velocity profiles above the bed [27].

Comparing flow patterns over a single layer of gravel grains and multiple grain layers, Manes et al. [28] highlighted the dependency flow resistance considerations from the definition of bulk parameters. Assuming that the effective hydrodynamic roughness is related to the thickness of the interface, i.e., the region where the surface and sub-surface flow interacts, and not to the size

of the grains composing the bed, the friction factors of the non-porous bed were determined using the fixed channel bottom as datum for bulk flow parameters such as flow depth and velocity. On the other hand, for the quantification of the friction factors over the porous beds, Manes et al. [28] used the roughness crest as datum to account for the unknown spatial extent of the interface which depends on flow characteristics. This means that the flow in the interfacial sublayer (the region between the roughness crests and troughs) was intentionally neglected in the bulk analysis presented in the study of Manes et al. [28]. Defining the roughness crest as datum for the determination of water depth will result in larger values for the bulk velocities and smaller water depths compared to the case where the roughness trough is defined as datum. Thus, the use of different datums will be associated with different estimates of the friction factor. Moreover, the subsurface flow-rate is typically difficult to measure in experimental studies and is often not considered separately, i.e., it is often assumed that the discharge used in the experiments represents the surface flow rate, although a small portion of the flow is conveyed through the subsurface layer. For lower discharges, this may hamper the analysis of flow resistance data from bulk analyses.

Most of the aforementioned studies have focused on the analysis of data obtained over beds composed of rather regular roughness elements of similar size, and studies with real gravel-beds remain rare. However, such investigations are needed to account for the non-uniform porosity variation from the crest of the gravel-bed layer to the undisturbed subsurface layer (see [30,31]). The recent study of Cooper et al. [32] used a casting technique to reproduce a non-porous section of 0.4 m length and width of a water-worked gravel surface that was created in a 8.2 m long and 0.6 m wide flume. The flow patterns over the permeable and non-permeable test section were compared based on velocity measurements obtained with Particle Image Velocimetry (PIV). Focusing on the near-bed region, Cooper et al. [32] concluded that the flow resistance imposed by the non-porous surface was higher than that by the porous water-worked gravel-bed, which is contrary to the previous findings. Cooper et al. [32] explained their findings from the analysis of the flow velocity data acquired at the roughness crest. They observed higher double-averaged velocities (velocities averaged in the time and space domain) over the gravel-bed than over the reproduced section and hypothesized that the higher efficiency in the momentum transfer and lower kinetic energy over the porous gravel-bed is a strong indicator that less energy was extracted from the mean flow.

To summarize, all studies related to the effect of bed-porosity revealed that flow resistance is altered by the porosity. More specifically, most studies found that a porous bed offers higher flow resistance than a comparable impermeable bed. This has been associated with the shear penetration and momentum exchange over the porous medium caused by large-scale vortical structures. On the other hand, the study carried out by Cooper et al. [32] over a gravel-bed concluded that flow resistance over a non-porous water-worked gravel-bed is larger than over its permeable counterpart. Some possible explanations for these contradicting results are discussed in Section 4 of this paper, as the experimental methodology of our study is similar to the one used by Cooper et al. [32]. It is worth mentioning that experiments presented in the following section were already ongoing when the study of Cooper et al. [32] was published. Thus, the results of the experiments can be used to shed more light on the influence of bed gravel-bed porosity on flow resistance.

### 3. Experimental Setup and Procedure

#### 3.1. Experimental Facility

Experiments were conducted in a 12.5 m long 1 m wide and 1 m deep closed-circuit tilting flume in the hydraulics laboratory at the Norwegian University of Science and Technology (NTNU), Trondheim, Norway. The flume, schematically shown in Figure 1, has a 12.5 m long glass-sided working section and a 2 m long inlet section consisting of a head tank and flow-conditioning section. In the experiments, the flow was recirculated by two centrifugal pumps and the flow rate was regulated by electronic motor speed controllers and the valves at each pump. The flow rate was measured by Euromag

MUT1000 EL inductive discharge meters (IDM) with an accuracy of 0.1%, installed at the pipes leading from the pumps to the inlet tank. The maximum flow rate of each pump was  $0.225 \text{ m}^3/\text{s}$  resulting in a maximum discharge capacity of  $0.45 \text{ m}^3/\text{s}$ . Polyvinyl chloride (PVC) rods with a diameter of 20 mm were installed in the inlet tank to condition the flow, and the inlet tank was separated from the flume channel by a honeycomb panel which served as flow straightener. The water depth could be adjusted by both a weir installed at the downstream end of the flume and by adding or draining water from the flume using drain valves. Dependent on the experiment, water levels in the flume were determined from pressure measurements using 4 pressure taps located at the flume bottom or from water surface elevation measurements using 8 Microsonic ultrasonic sensors (accuracy of 1%). The distance between the static pressure taps was 1.25 m with the first tap being located 6.875 m from the beginning of the working section. The ultrasonic sensors were installed in the same flume reach where the static pressure tubes were located. The spacing between the acoustic sensors varied from 0.4 m to 0.7 m to avoid acoustic interferences of the signals emitted from adjacent sensors.

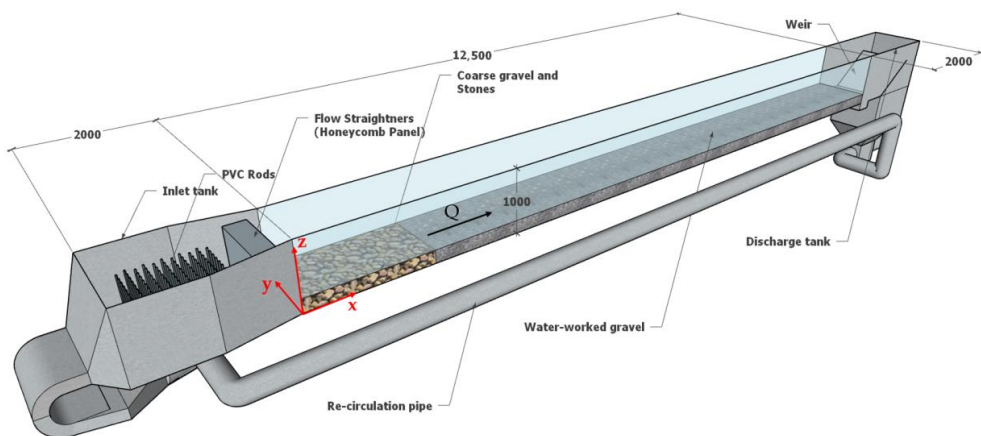


**Figure 1.** Isometric view of the 3D drawing of the recirculating flume (the pumps, which are located below the inlet tank, are not shown). All units are in [mm].

### 3.2. Bed Types

The first series of measurements was carried out over a water worked gravel-bed armor layer with a porous subsurface. For the generation of the armor layer, a 0.20 m high and 10.31 m long gravel layer consisting of a well-mixed sediment mixture ( $0.64 \text{ mm} < d < 64 \text{ mm}$ ; see Figure 2 for the grain-size distribution) was placed in the flume. The sediment mixture was similar to the one used in the study by Aberle and Nikora [16]. The bed was screeded flat and surface compacted to ensure that the bed slope was parallel to the flume slope. The gravel layer was retained by a L-shape perforated sill at its upstream and downstream end to allow for subsurface flow during the experiments. The 2.19 m long flume section between the gravel-bed and the upstream flow straightener was formed by coarse gravel to prevent scouring (Figure 1).

The gravel layer was water-worked with quasi-uniform flow conditions for a discharge of  $Q = 0.2 \text{ m}^3/\text{s}$ , a bed and water surface slope of  $S_b = S_w = 0.0027$ , respectively, and a water depth of  $h = 0.24 \text{ m}$ . The eroded sediment was collected in a basket placed downstream of the gravel layer and the surface was considered to be armored when the sediment transport rate became less than  $2.0 \text{ kg}/\text{h}/\text{m}$ , i.e., the same criterion was used as in Aberle et al. [33]. After the armoring, the bed topography was scanned over a total length of 7 m using an Acuity AR200-100 laser displacement meter attached to a traversing system spanning the flume length. The diameter of the footprint of the laser beam ranged between 55 and 250  $\mu\text{m}$  dependent on the distance of the laser to the bed surface,

and the accuracy of the bed elevation measurements was 30.5  $\mu\text{m}$ . The coordinate system had its origin  $x, y, z = (0, 0, 0)$  at the beginning of working section, the span wise direction  $y = 0$  was at the right glass wall of the flume and the vertical coordinate  $z = 0$  at the plastic channel bottom (see Figure 1). In total, 660 longitudinal profiles were recorded at a span wise step distance of  $\Delta y = 1$  mm. The scanned section did not include the topography near the glass walls (approx. 170 mm on either side) due to the setup of the traversing system. Each longitudinal profile was recorded with a sampling frequency of 100 Hz and a traverse speed of 2000 mm/min resulting in a longitudinal resolution of  $\Delta x = 0.33$  mm. Spikes in the scanned data were removed manually during the post processing and the final data were used to produce digital elevation models (DEM) of the gravel and the cast surfaces, respectively. The scans will be analyzed in Section 4.1.

Porosity measurements were carried out before and after armoring using the water displacement method (WDM) to obtain the vertical distribution of the porosity of both the initial and water-worked gravel-bed (see [31] for details). In addition to the WDM, the porosity distributions were also derived from the laser scans. The corresponding results will be presented in Section 4.1.

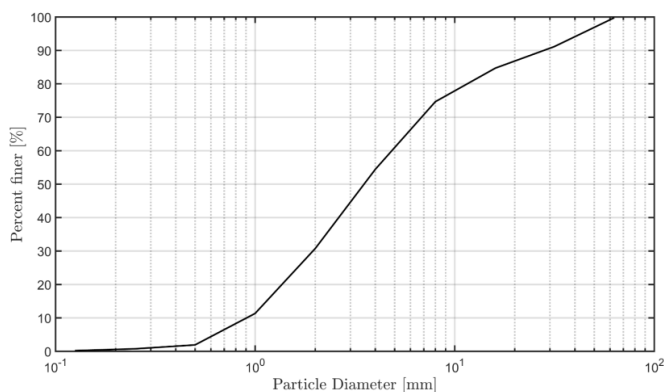


**Figure 2.** Grain size distribution curve of the gravel mixture.

In order to study the effect of the bed subsurface porosity on the flow, a 7 m long section of the armored gravel-bed was reproduced using the casting technique reported in Spiller and R  ther [34], Navaratnam et al. [35] after completion of the hydraulic measurements over the gravel-bed (the latter are described below in Section 3.3). For the preparation of the molds, a thin steel plate was vertically inserted 1 cm into the gravel layer at both ends of the 7 m long section (at  $x = 3250$  mm and 10,250 mm, respectively; see Figure 3) and a bi-component silicon mixture was poured layer-by-layer onto the section. The initial layer was very thin so that the silicon did not alter the grain orientation and did not penetrate the sub-surface. This facilitated the removal of gravel grains from the silicon-mold. It was also ensured that the silicon seeped enough into the interstices in the roughness layer, i.e., into the pore space between the roughness crest and trough. All silicon layers were poured before the initial layer solidified completely to guarantee bonding between the layers. The last silicon layer submerged the highest grain elevation by 2 cm enabling the proper handling of the mold. The final silicon-body was screeded horizontally and allowed to cure for one day. After solidification of the silicon, the two steel plates were removed, and the silicon mat was cut in half and removed from the flume with the help of a crane. The two resulting silicon mats were manually cleaned from sediment particles.

For the preparation of the cast surface, the two silicon mats were further subdivided into two mats of 2.3 m and 1.2 m length, respectively, resulting in a total of 4 molds which originated from Sections 2–5 in Figure 3. Each mold was placed inside a wooden frame and levelled horizontally to avoid the introduction of artificial slopes in the cast. The cast consisted of polyurethane resin mixed with a filling powder (ATH-Aluminum trihydrate) in a volume ratio of 1:2.5 (resin:filler). The filler

powder reduced the heat emission from the exothermal reaction during curing so that the shrinkage of the cast was limited to 1%. The edges of the cast pieces were polished to remove irregularities due to leakage and small irregularities in the wooden frame.

The final cast pieces were placed in the flume so that tiles 2–5 were accurately reproducing the original gravel surface. Copies of the 1.2 m long tiles (tiles 1, 6 and 7 in Figure 3; marked in orange) were cut to the required length and placed at the upstream and downstream end of the bed so that all parts of the bed were completely immobile. Small gaps between the tiles and between the tiles and the glass wall, respectively, were filled with silicon and clay to make it water tight. Both, the upstream and downstream end were sealed to avoid flow development under the cast. After its installation, the cast-bed was scanned using the laser displacement meter.

The third bed configuration was installed following the completion of the hydraulic measurements over the cast-bed to investigate the effect of grain orientation on hydraulic roughness. For this purpose, the cast pieces (except pieces 1, 6 and 7) were rotated through 180 degrees and, after sealing the gaps, the bed was scanned again.

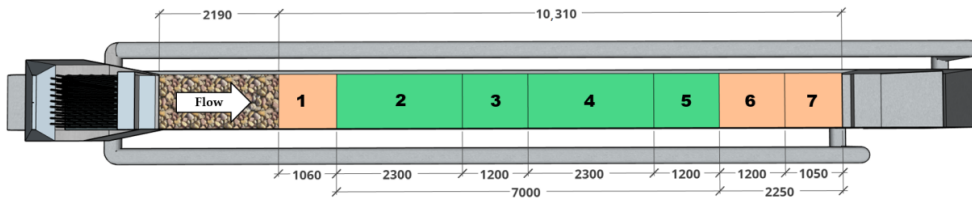


**Figure 3.** Plan view of the flume consisting the working section; colored section and numbers denote the position of the cast tiles placement. All units are in [mm].

### 3.3. Hydraulic Measurements

Hydraulic measurements were carried out over each of the three surfaces for a total of seven different hydraulic boundary conditions. Three different shear velocities were achieved and the range of relative submergence  $h/k$  in the gravel-bed tests varied between 3.6 and 9.3 (see Table 1). The roughness height  $k$  was derived from the laser scan data and corresponded to the difference  $Z_{99} - Z_{01}$ , where,  $Z_{99}$  and  $Z_{01}$  denote the 99th and 1st percentile of the distribution of bed elevations, respectively; the datum for the water depth  $h$  was at the mean bed elevation.

For the gravel-bed tests, the water surface slope was determined using the data from the four pressure taps at the flume bottom. For the cast-bed, the solid bottom prevented the measurements from pressure taps and the water surface slopes were determined using the data from the 8 ultrasonic sensors. Additional tests in which multiple measurements were taken for a particular water surface slope indicated that the results from both measurement systems gave the same mean slope with the same order of magnitude of the deviation from the mean. Although uniform flow conditions were targeted, it was difficult to match the water surface slope exactly with the bed slope due to the mild slopes and the discrete nature of the water surface slope measurements. Both slopes were similar, but still showed some differences so that the St. Venant equation was used to determine the friction velocity [36]:

$$u_* = [ghS_b - gh(S_b - S_w)(1 - Fr^2)]^{1/2} \tag{2}$$

where  $h$  denotes the water depth and  $Fr$  the Froude number which is defined as  $Fr = U/(gh)^{0.5}$ . Equation (2) represents a simplified version of the St. Venant equation which is obtained by assuming that the slopes are very small. In the tests over the impermeable facsimiles (cast), the discharge was adjusted to ensure the same water surface slope and water depth as in the testes over the permeable bed.

**Table 1.** Hydraulic boundary conditions applied for the measurements over the water-worked gravel-bed. The bulk flow velocity was determined from the equation of continuity  $U = Q/A$  where  $A = hb$  denotes the cross-sectional area with  $b =$  flume width (1 m).

| Test | $S_b$  | $S_w$   | $h$<br>[m] | $h/k$<br>[-] | $Q$<br>[m <sup>3</sup> /s] | $U$<br>[m/s] | $Fr$ | $Re$    | $u^*$<br>[m/s] |
|------|--------|---------|------------|--------------|----------------------------|--------------|------|---------|----------------|
| BC1  | 0.0018 | 0.00134 | 0.137      | 3.6          | 0.056                      | 0.41         | 0.35 | 55 890  | 0.043          |
| BC2  | 0.0015 | 0.00103 | 0.178      | 4.7          | 0.076                      | 0.43         | 0.32 | 76 270  | 0.043          |
| BC3  | 0.0015 | 0.00103 | 0.236      | 6.2          | 0.121                      | 0.51         | 0.34 | 120 787 | 0.050          |
| BC4  | 0.0020 | 0.00159 | 0.215      | 5.7          | 0.124                      | 0.58         | 0.40 | 124 107 | 0.059          |
| BC5  | 0.0013 | 0.00083 | 0.293      | 7.7          | 0.156                      | 0.53         | 0.31 | 156 412 | 0.050          |
| BC6  | 0.0010 | 0.00051 | 0.353      | 9.3          | 0.168                      | 0.48         | 0.25 | 167 987 | 0.043          |
| BC7  | 0.0015 | 0.00098 | 0.319      | 8.4          | 0.200                      | 0.63         | 0.35 | 199 883 | 0.057          |

Velocity measurements were taken using the TSI stereoscopic particle image velocity system (SPIV; 2-dimensional 3-component velocimetry). The PIV measurements were carried out at  $x \approx 8000$  mm and  $y \approx 500$  mm, i.e., in the centerline of tile number 4 (see Figure 3). The laser sheet was formed by a Nd:YAG (neodymium-doped yttrium aluminum garnet) double-pulsed laser and was aligned normal to the bed surfaces and parallel to the flume walls. The flow was seeded with polyamide particles of 55  $\mu\text{m}$  diameter. Two high speed 4 Mega Pixel CCD (Charge-coupled device) cameras captured the particle images at a frequency of 20 Hz for a period of 150 s, producing 3000 image pairs per camera i.e., 12,000 images in total. The images were post-processed and analyzed using the TSI Insight 4G software. An interrogation area of  $32 \times 32$  pixels with 50% overlapping was set to increase the probability that the seeding particles close to the edges of the interrogation area correlated well. The resulting grid size of the vector field was  $16 \times 16$  pixels which corresponded to a spatial resolution of  $1.56 \text{ mm} \times 1.56 \text{ mm}$  in streamwise and vertical direction respectively.

## 4. Results and Discussions

### 4.1. Comparability of the Surfaces

The vertical distributions of the porosity for initial gravel (surface-compacted), water-worked gravel, cast and the rotated cast are presented in Figure 4. For the water-worked gravel-bed, the porosity obtained from the WDM measurements decreased from  $\phi = 1$  at the roughness top to an absolute minimum just above the roughness trough before reaching an approximately constant value in the sub-surface. The increase in porosity close to the plastic bottom of the flume was associated with the combined effect of capillary action and poor sorting of gravel at the bottom [31]. The bulk porosity of the water-worked gravel-bed was  $\phi = 0.31$  whereas the bulk porosity of the surface compacted gravel was  $\phi = 0.26$ ; this difference was due to the larger height of the interfacial sublayer of the water-worked bed compared to the surface compacted bed. Note that the porosity values  $\phi > 1$  for the WDM measurements in Figure 4 are associated with the large spatial scale of the measurements (spanning the whole gravel-bed) and the accuracy of the measurements (see also [30]). The porosity distribution of the water-worked gravel-bed obtained by the WDM measurement matched the porosity distribution derived from the laser scans gravel-bed from the roughness crest ( $z/H = 1$ ) to  $z/H \approx 0.85$ , where  $H$  denotes the height of the bed measured from the flume bottom. Below  $z/H \approx 0.85$ , the results from the two methods deviate since the laser scan could not capture the pore space in the subsurface layer, i.e., the measurement range of the laser scan was restricted to the distance from the roughness crest to the roughness trough so that  $\phi = 0$  at the roughness trough for these measurements.

For the cast-beds, the porosity varied from  $\phi = 1$  at the roughness top to  $\phi = 0$  at the roughness trough. These distributions were solely obtained from the analysis of the laser scan data as the non-porous structure of the bed prevented the use of the WDM. The comparison of the porosity distributions derived from the laser scan measurements nearly collapse on a single line which is a first indicator of the accurate reproduction of the bed surface. However, a difference can be observed for



the rotated cast just above the roughness trough and  $\phi < 0.2$ . This is associated with the placement of the tile and is described below in some more detail.

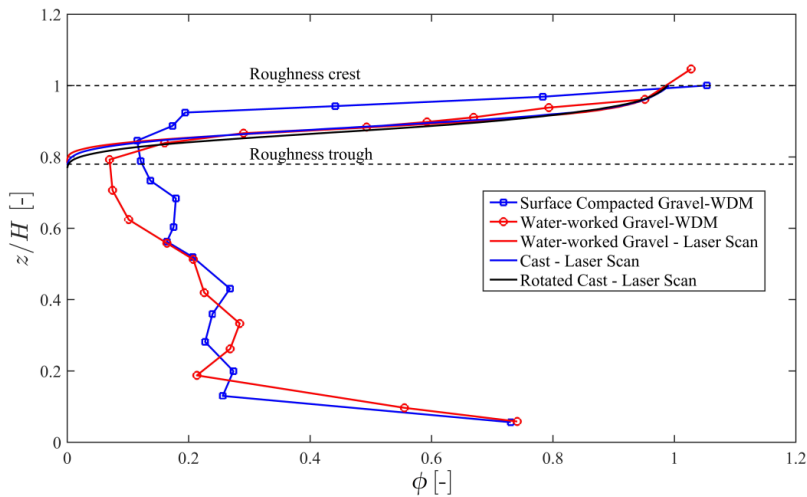


**Figure 4.** The vertical distribution of the porosity for all surfaces,  $z$  is the distance from the flume bottom and  $H$ , the total height of the bed.

The digital elevation models of the surfaces obtained from the laser scan, shown in Figure 5, were used to compare the geometrical properties of the three bed configurations and to ensure accurate placement of the cast pieces. The following analysis focuses on the 4.65 m long section over which the water surface slope was measured (tiles 3 to 5 in Figure 3) and which contained the PIV-measurement area. For the analysis, the DEMs were detrended and the origin of the vertical coordinate corresponds to the mean bed level.

The visual comparison of the permeable gravel-bed (Figure 5a) with its impermeable counterpart (cast; Figure 5b) indicates a good agreement between the two surfaces. The only visible difference is at the transitions between the tiles in Figure 5b at  $x = 6750$  mm and  $9050$  mm. The match of the cast-bed with the water worked gravel-bed can be analyzed by comparing the distributions of the bed elevations (Figure 6a) as well as the histogram of the observed differences in vertical elevations at each DEM grid point between the gravel and cast-bed (Figure 6b). The histograms shown in Figure 6a reveal a good agreement between the gravel and cast-bed, and the histogram of bed elevation differences (Figure 6b) indicates that most of the values characterizing the deviation of the two surfaces are within the range of  $\pm 5$  mm. It is worth noting that the histogram in Figure 6b includes, besides the effects of shrinkage and the joints between the tiles, the tile-alignment as it was based on the subtraction of the two DEMs. The good match of the gravel-bed with the cast-bed can further be substantiated by the statistical moments of the surfaces which are presented in Table 2. The standard deviation of bed elevations  $\sigma$ , skewness and kurtosis are directly comparable and fall into the typical range for armored gravel-bed surfaces as defined by Coleman et al. [3].

The distribution of bed elevations for the rotated cast differs slightly from the distribution of the cast. Strictly speaking, both surfaces should be characterized by identical histograms, however, the observed differences in Figure 6a can be associated with very small transverse slopes induced when replacing the cast sections and due to discontinuities between the tiles. The latter were more pronounced for the rotated cast than for the cast and led to an increased number of measurement errors with the laser displacement meter due to its measurement principle. Despite these differences, Table 2 indicates still a good agreement of the statistical moments of the rotated bed with the ones for the original and cast-bed.

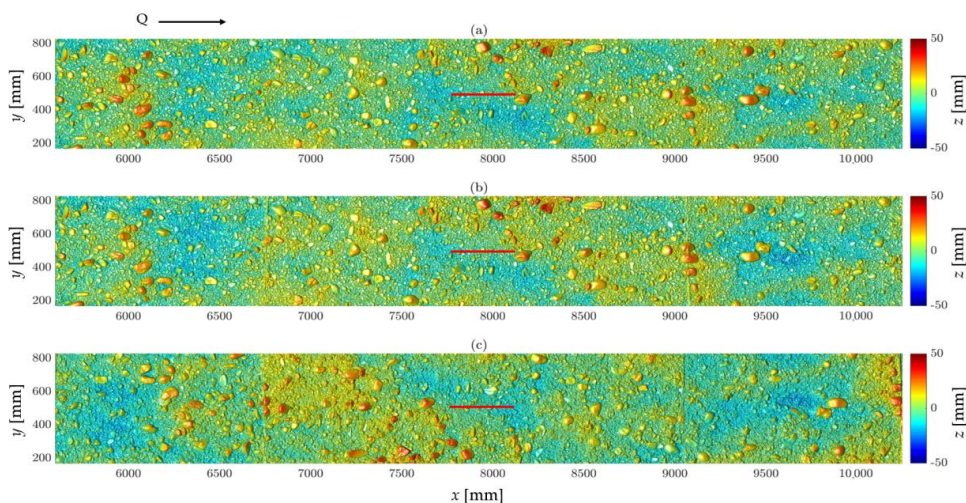


**Figure 5.** Digital elevation models (DEMs) of (a) gravel, (b) cast and (c) rotated cast surface respectively, thick horizontal red line indicates the position of the laser sheet (flow direction is from left to right).

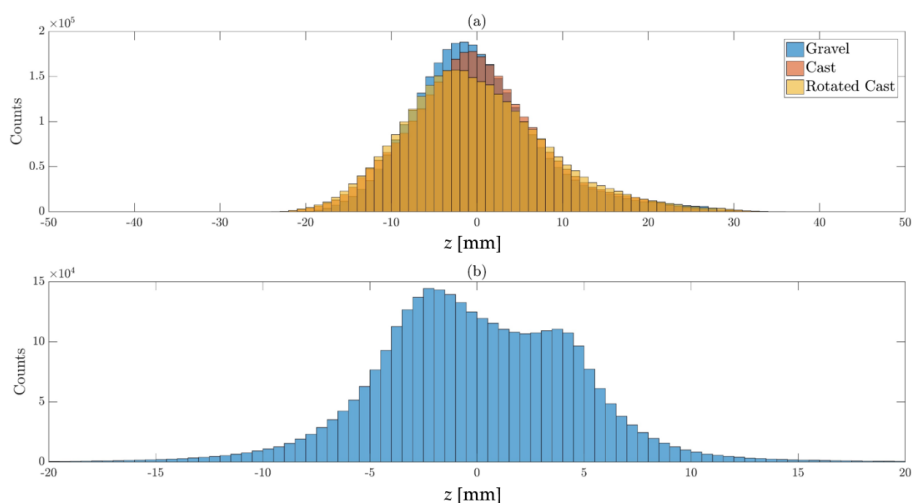


**Figure 6.** (a) Histograms of the vertical elevation of all three surfaces; (b) histograms of the difference in the vertical elevations between gravel and cast surface.

**Table 2.** Statistical moments for the three surfaces.

| Bed Surface  | Roughness Height, $k$<br>[mm] | Standard Deviation $\sigma$<br>[mm] | Skewness<br>[-] | Kurtosis<br>[-] |
|--------------|-------------------------------|-------------------------------------|-----------------|-----------------|
| Gravel       | 38.1                          | 7.57                                | 0.76            | 1.03            |
| Cast         | 38.6                          | 7.96                                | 0.50            | 0.66            |
| Rotated Cast | 40.6                          | 8.52                                | 0.56            | 0.49            |

The beds were also compared on the basis of normalized 2D-second order structure functions (2DSSF). For this purpose, the filtered normalized 2DSSF were determined according to the



method described in detail in Qin et al. [17]. In brief, filtered 2DSSFs show only values in areas which are characterized by statistical significant correlations. The latter are determined by subdividing the surface in small tiles of a certain length scale and reshuffling them to create new surfaces. For these new surfaces, 2DSSF are calculated and used for statistical significance testing. The method is based on Monte Carlo simulations (see [17] for details) and for the present analysis, the reshuffled quadratic sub-areas were characterized by a side length of  $d_{84}$  of the original gravel-bed. The statistical significance testing carried out here was based on a significance level 5% and 100 Monte-Carlo simulations.

Figure 7 shows the filtered 2DSSFs for the three surfaces and the sub-plots reveal areas of high spatial correlation at small spatial lags (the minimum value of 0 indicates perfect spatial correlation and a value of 1 a lack of spatial correlation). The area of high correlation for small spatial lags are characterized by a central ellipse, and the spatial extent of the main axes of the central ellipses can be interpreted as characteristic length scales in the horizontal plane [19]. The benefit of the filtered 2DSSF is that these length scales can be clearly defined and the resulting values of 100 mm (96 mm for the rotated bed) for the long and 40 mm for the short axis (for all three beds) substantiates the high accuracy that was achieved when reproducing the bed.

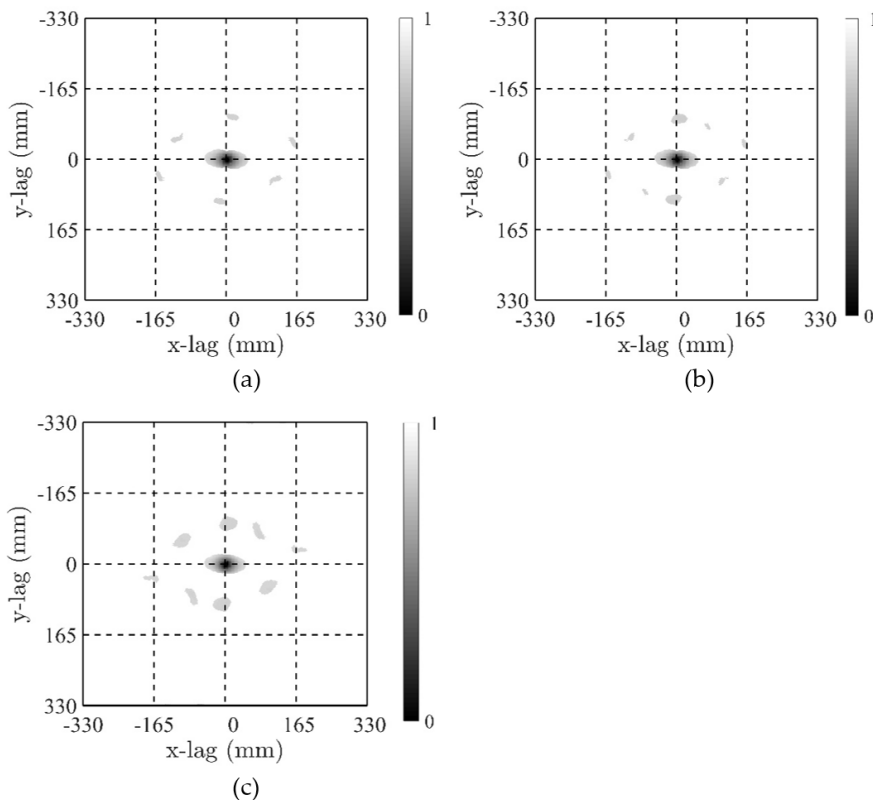


**Figure 7.** The 2D second-order structure function of the surfaces filtered by the upper 5% confidence limit, values lower than the upper 5% confidence limit are preserved. The greyscale corresponds to the values of the normalized structure function which ranges from 0 to 1, where the value of 0 defines perfect spatial correlation. Sub-figures (a–c) correspond to gravel, cast and rotated cast surfaces respectively.

The 2DSSFs can also be used to investigate the mean alignment of larger particles on the bed. For the present case, the orientation of the long axis of the ellipses deviates 5 degrees from the flow direction indicating that most of the larger particles are nearly aligned with their long axis in flow direction. This is in agreement with previous studies investigating the surface structure of stable armour layers [16]. Note that the patterns at larger spatial lags in Figure 7 reflect grain structures larger than individual grains. However, despite the fact that they are statistically significant, their value indicates only a low spatial correlation so that these patterns should not be interpreted [17].

#### 4.2. Flow Resistance

The good agreement between the geometry of the original bed with its counterparts is a prerequisite for the detailed analysis of differences in hydraulic resistance. Figure 8 shows  $(8/f)^{0.5}$  as a function of relative submergence ( $h/k$ ) for the three surfaces. The lowest values of  $(8/f)^{0.5}$ , i.e., a higher Darcy-Weisbach friction factor  $f$ , was observed for the tests over the rotated bed for relative submergences  $h/k < 6$ . For relative submergences  $h/k > 6$ , the difference in  $(8/f)^{0.5}$  between the rotated bed and the cast became smaller which may be due to the increasing submergence. Moreover, the uncertainty associated with the water surface slope measurements increased for the highest submergence for which  $S_w$  was rather small ( $\sim 0.05\%$ ). On the other hand, in all tests with the rotated cast-bed it was necessary to decrease the discharge to obtain the same water levels as in the tests with the cast-bed (discharge reductions of up to 6% were required; the average was 4%). The higher flow resistance exerted by the rotated cast-bed shows that the orientation of the grains on the surface has a significant influence on flow resistance, i.e., the water working results in a more hydraulically efficient bed configuration (e.g., [37]). For example, rotating the fixed cast-bed means that the lee-areas of grains, where small grains typically settle during armoring, become exposed to the flow. Rotating the cast-bed, these particles are directly exposed to the flow but cannot be eroded as they are part of the cast. As a consequence these areas are characterized by a less hydrodynamic shape than comparable frontal areas of real water-worked beds as the associated drag coefficient changes with the shape and orientation [38]. Consequently, the rotated cast-bed imposes a higher resistance on the flow than the cast-bed. This result thus implies that bed roughness cannot solely be described by a characteristic grain size and that both surface structure and grain orientation play a vital role for the determination of flow resistance [14,18,19].

Figure 8 further reveals small differences in flow resistance between the porous gravel-bed and its impermeable counterpart. For the two lowest submergences ( $h/k = 3.6$  and  $4.7$ ),  $(8/f)^{0.5}$  is larger for the porous gravel-bed than for the impermeable cast-bed while for the larger relative submergences this trend is reversed. This means that, for the two lowest submergences, larger friction factors were obtained for the cast-bed than for the porous gravel-bed. These two experiments were carried out with discharges of  $Q = 0.056 \text{ m}^3/\text{s}$  and  $0.076 \text{ m}^3/\text{s}$ , respectively, for the gravel-bed and  $Q = 0.056 \text{ m}^3/\text{s}$  and  $0.074 \text{ m}^3/\text{s}$  respectively, for the cast-bed to obtain identical water depths  $h$ . Noting that a certain amount of the flow is conveyed through the subsurface in the porous-bed tests, the discharge used for the calculations of the bulk values in Table 1 should, strictly speaking, be reduced to account for subsurface flow. The experimental setup did not allow for the measurement of the subsurface flow rate but assuming a flow rate of approx.  $0.001\text{--}0.002 \text{ m}^3/\text{s}$ , computations indicated that for these two cases the flow resistance of the porous gravel-bed would be slightly larger than for the cast-bed ( $h/k = 3.7$ ) or approximately equal ( $h/k = 4.7$ ). The significance of subsurface flow rate gradually decreases with increasing discharge (and hence increasing relative submergence) so that the results for the experiments carried out with  $h/k \geq 5.7$  (discharges  $Q \geq 0.121 \text{ m}^3/\text{s}$ ; Table 1) are less affected, i.e., in these tests the flow resistance of the porous bed was larger than for the cast-bed.

The literature review revealed that flow resistance over porous beds depends on  $Re$  (e.g., [24]), and therefore  $f$  is plotted as a function of  $Re$  in Figure 9. Regarding the comparison of  $f$  obtained for the experiments over the cast-bed and the rotated cast-bed, Figure 9 yields the same conclusions as before; the rotated bed is characterized by higher flow resistance for all boundary conditions except

for  $Re \approx 170,000$  corresponding to the test which was carried out with the lowest water surface slope ( $\sim 0.05\%$ ). For  $Re > 100,000$  ( $h/k \geq 5.7$ ), Figure 9 reveals again that the porous gravel bed showed a higher resistance to the flow than its non-porous counterpart. In fact, for the experiments over the cast-bed the discharge had to be increased for  $h/k \geq 5.7$  to obtain the same water depth and shear velocity as in the porous-bed experiments, which confirms the observed trend. The deviation of the friction factors for the tests carried out for the lowest  $Re$  values would be mitigated if subsurface flow would be accounted for (see above).

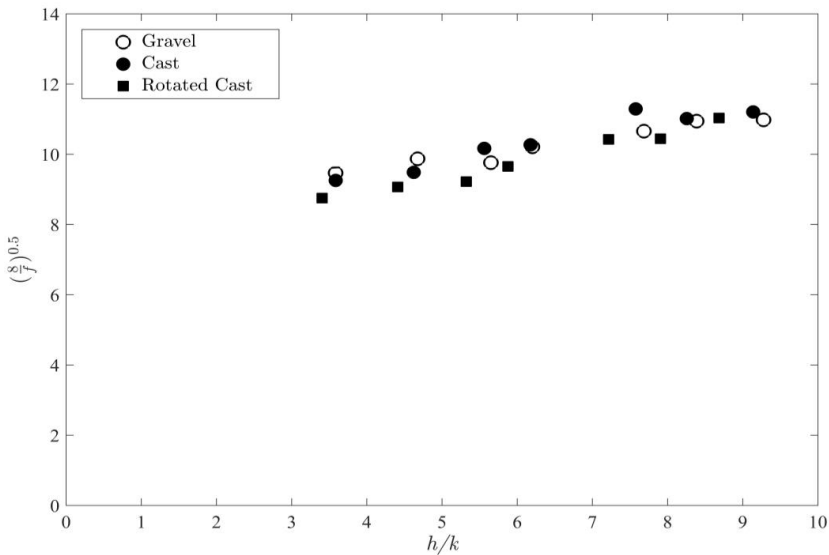


Figure 8.  $(8/f)^{0.5}$  as function of relative submergence ( $h/k$ ).

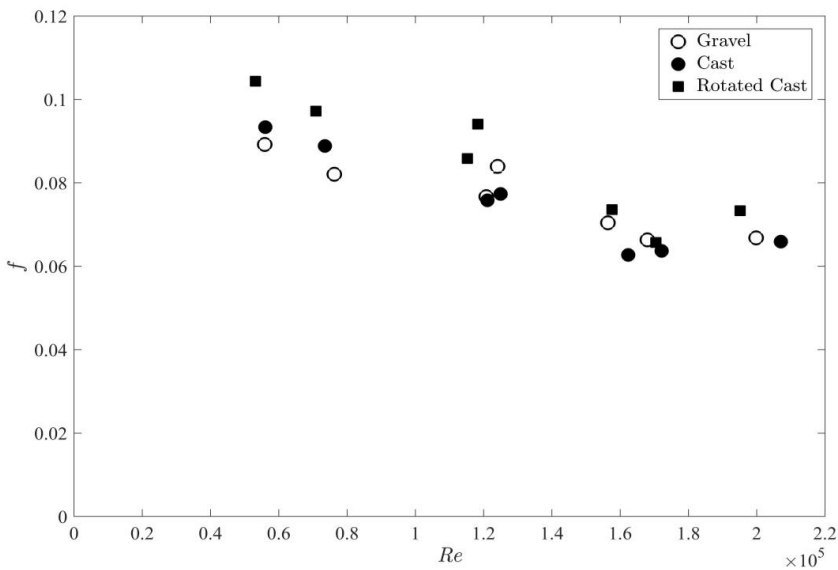
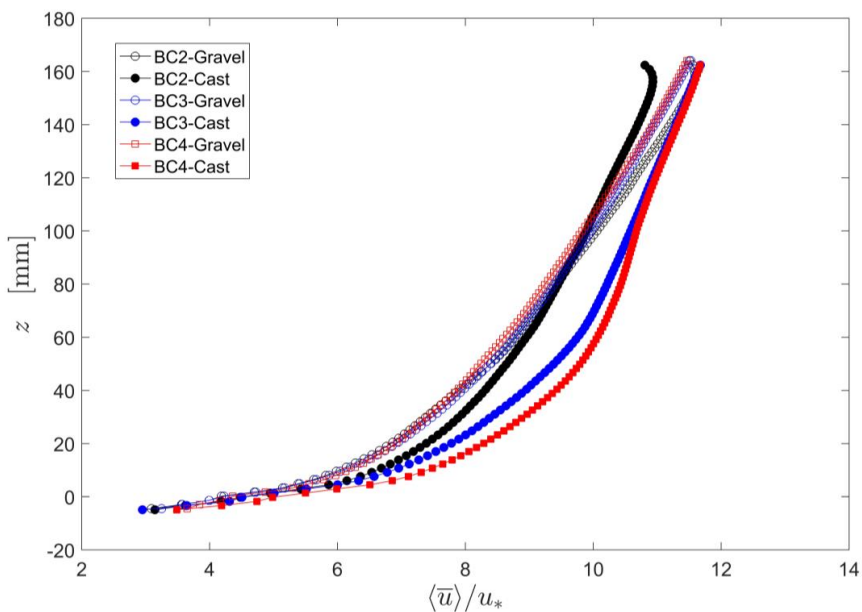


Figure 9. The variation of bulk friction factors with  $Re$  for the tested bed surfaces.

The above discussion regarding the differences in friction factors needs to be extended regarding the surface properties. For example, the cast-bed was characterized by slightly larger  $k$ -values and standard deviations  $\sigma$  than the porous bed (Table 2). These values indicate that the cast-bed may be slightly ‘rougher’ in geometrical terms than the gravel-bed, and this may contribute to the observed trend at lower submergences (and hence low  $Re$ ). Similarly, the rotated cast-bed was characterized by larger  $k$ - and  $\sigma$ -values than the cast-bed, which in turn means that the rotated cast-bed was already rougher due to its placement. However, the differences in  $k$  and  $\sigma$  are rather small (less than 2 mm for  $k$  and 0.56 mm for  $\sigma$ ) so that it can be hypothesized that this effect is negligible.

The comparison of the porous and non-porous bed can be further investigated by a preliminary and qualitative analysis of the double averaged longitudinal velocity distributions (i.e., time-averaged PIV-velocities, which were then spatially averaged in planes parallel to the mean bed elevation). Figure 10 shows exemplarily the velocity distributions, normalized with the shear velocities obtained by Equation (2), for three different boundary conditions (BC2, BC3 and BC4) corresponding to the three different shear velocities (Table 1). The origin of the vertical axis ( $z = 0$ ) in Figure 10 corresponds to the mean bed elevation. The global roughness crest (i.e., the roughness crest of the scanned section) was 23 mm above the mean bed elevation whereas the local roughness crest (i.e., the roughness crest of the shorter PIV section) was only 8 mm above the mean bed level.

The three normalized velocity profiles over the gravel-bed tests (open symbols in Figure 10) nearly collapse on a single line and show the expected logarithmic shape above the roughness crest. The three profiles over the cast-beds (solid symbols) deviate slightly, especially the profile for BC2. Note that the dip in the velocity profile for BC2 at  $z \approx 160$  mm is due to a plastic glass which was placed at the water surface to avoid the refraction of laser sheet caused by surface waves. In order to cross-check the data, the velocity profiles were integrated to estimate the discharge and for all presented profiles, the calculated discharge was similar to the discharge used in the experiments.



**Figure 10.** The double-averaged longitudinal velocities normalized with the shear velocities. Open and filled symbols denote water worked gravel-bed and cast-bed respectively while the colors represent different boundary conditions.

The comparison of the profiles over the gravel-bed with the ones over the cast-bed shows that, for the same boundary condition, the velocities above the crest in the near-bed region ( $8 \text{ mm} < z < 80 \text{ mm}$ ) are larger over the cast-bed than over the porous bed. While the aforementioned cast-bed profile for BC2 shows larger velocities than the gravel-bed profile up to  $z \approx 80 \text{ mm}$ , the velocity profiles for BC3 and BC4 show higher values for the cast-bed up to  $z \approx 140 \text{ mm}$  before nearly matching the velocities over the gravel-bed.

The smaller velocities over the crest of the water-worked gravel-bed in the near-bed region are additional evidence that a porous water-worked gravel-bed imposes higher flow resistance. It is interesting to note that in the interfacial sublayer (i.e.,  $z < 8 \text{ mm}$ ), the flow velocities are partly larger over the water-worked gravel-bed than over the cast, especially below the mean bed elevation ( $z < 0$ ). This can be explained by the ‘no slip’ condition for the non-porous cast-bed while, due to the porosity of the subsurface layer, such a condition does only exist at the gravel-particle surfaces over the gravel-bed. Note that due to the limitations of the PIV-setup, the velocity profiles could not be measured to the roughness trough. Nonetheless, these preliminary results of the PIV data further confirm the results from the bulk-flow analysis that the flow resistance over the porous gravel-bed is larger than over the cast-bed.

The presented results together with the results of the qualitative analysis of the double-averaged velocity profiles can be used to discuss the different results regarding the influence of porosity reported by Cooper et al. [32]. The present study is based on experiments carried out over a casted surface which covered nearly the entire flume area. On the other hand, the length and width of the cast-bed in [32] was limited, corresponding roughly to about 5% of the total water-worked area, and the control of the sub-surface flow was not clearly stated by Cooper et al. [32]. Moreover, the cast tile was placed in the middle of the water-worked gravel and hence the transition from the gravel-bed to the cast-bed could affect the flow patterns; however, here we can only speculate about this effect. On the other hand, it is interesting to note that the range of relative submergence ( $h/k$ ) in Cooper et al. [32] varied between 3.1 and 4.6 with  $Re$  ranging between 64,000 and 84,000. The results presented in Figures 8 and 9 indicate that for comparable relative submergences and  $Re$ -values the cast-bed is ‘rougher’ which coincides with the findings of Manes et al. [28], Cooper et al. [32] although the behavior of the velocity profiles deviates from the one reported by Cooper et al. [32].

## 5. Summary and Conclusions

The present study presents results from an experimental program aiming at the investigation of the effect of gravel-bed porosity and grain orientation on bulk flow resistance. Experiments were carried out over three different surfaces; a water-worked gravel-bed, its non-porous counterpart (cast-bed), and the rotated cast-bed. The quality of the reproduced beds was shown and discussed based on laser-scan data and statistical parameters. Focusing on the analysis of bulk-flow parameters, the results showed that the rotated cast exerted the highest flow resistance which yielded to the conclusion that not only the surface structure but also its alignment regarding the flow direction (i.e., grain orientation) has a major influence on flow resistance. The results also confirmed the findings from studies carried out over artificial beds that a porous gravel-bed imposes higher flow resistance than its non-porous counterpart for comparable relative submergences. In the analysis of the data, the importance of subsurface flow-rates was briefly highlighted, especially for low relative submergences and hence slightly reduced surface flow rates. The subsurface flow rate has often been neglected in flume studies dealing with the determination of flow resistance, and this can hamper the comparability of results from experiments which were carried out over impermeable beds. The results of the present study have practical implications. For example, colmation processes, i.e., the settling of fine particles in the hyporheic zone, can change the porosity of the sub-surface, and hence the flow resistance (or vice versa). Having analyzed bulk flow characteristics in this paper, we will use the PIV-data for the detailed analysis of flow patterns over the three beds to investigate the effect of porosity on the near bed turbulent flow field and turbulence characteristics in our upcoming analyses.

**Author Contributions:** Christy Ushanth Navaratnam and Jochen Aberle conceived and designed the experiments. Christy Ushanth Navaratnam performed the experiments and analyzed the data with support from Jie Qin, Pierre-Yves Henry and Jochen Aberle. All authors contributed to write the manuscript.

**Funding:** This research received no external funding.

**Acknowledgments:** Authors are thankful to C. Manes for providing the data from his study which helped to compare results between these studies.

**Conflicts of Interest:** The authors declare no conflict of interest.

## References

- Nikora, V.; Koll, K.; McEwan, I.; McLean, S.; Dittrich, A. Velocity Distribution in the Roughness Layer of Rough-Bed Flows. *J. Hydraul. Eng.* **2004**, *130*, 1036–1042. [[CrossRef](#)]
- Aberle, J.; Koll, K.; Dittrich, A. Form induced stresses over rough gravel-beds. *Acta Geophys.* **2008**, *56*, 584–600. [[CrossRef](#)]
- Coleman, S.E.; Nikora, V.I.; Aberle, J. Interpretation of alluvial beds through bed-elevation distribution moments. *Water Resour. Res.* **2011**, *47*, W11505. [[CrossRef](#)]
- Vollmer, S. *Einfluß der Oberflächenströmung auf die Permeable Gewässersohle*; Universität Karlsruhe (TH): Karlsruhe, Germany, 2005.
- Detert, M. Hydrodynamic Processes at the Water-Sediment Interface of Sreambeds. Doctoral Thesis, Universität Karlsruhe (TH), Karlsruhe, Germany, 2008.
- Chow, V.T. *Open-Channel Hydraulics*; McGraw-Hill, Inc.: Singapore, 1959.
- Keulegan, G.H. Laws of Turbulent Flow in Open Channels. *J. Res. Natl. Bureau Standards* **1938**, *21*, 707–741. [[CrossRef](#)]
- Hey, R.D. Flow Resistance in Gravel-Bed Rivers. *J. Hydraul. Div.* **1979**, *105*, 365–379.
- Bathurst, J.C. Flow Resistance Estimation in Mountain Rivers. *J. Hydraul. Eng.* **1985**, *111*, 625–643. [[CrossRef](#)]
- Ferguson, R. Flow resistance equations for gravel- and boulder-bed streams. *Water Resour. Res.* **2007**, *43*, W05427. [[CrossRef](#)]
- Hendrick, R.R.; Ely, L.L.; Papanicolaou, A.N. The role of hydrologic processes and geomorphology on the morphology and evolution of sediment clusters in gravel-bed rivers. *Geomorphology* **2010**, *114*, 483–496. [[CrossRef](#)]
- Nikora, V.I.; Goring, D.G.; Biggs, B.J.F. On gravel-bed roughness characterization. *Water Resour. Res.* **1998**, *34*, 517–527. [[CrossRef](#)]
- Smart, G.M.; Duncan, M.J.; Walsh, J.M. Relatively Rough Flow Resistance Equations. *J. Hydraul. Eng.* **2002**, *128*, 568–578. [[CrossRef](#)]
- Aberle, J.; Smart, G.M. The influence of roughness structure on flow resistance on steep slopes. *J. Hydraul. Res.* **2003**, *41*, 259–269. [[CrossRef](#)]
- Yochum, S.E.; Bledsoe, B.P.; David, G.C.L.; Wohl, E. Velocity prediction in high-gradient channels. *J. Hydrol.* **2012**, *424–425*, 84–98. [[CrossRef](#)]
- Aberle, J.; Nikora, V. Statistical properties of armored gravel bed surfaces. *Water Resour. Res.* **2006**, *42*, W11414. [[CrossRef](#)]
- Qin, J.; Aberle, J.; Henry, P.-Y.; Wu, T.; Zhong, D. Statistical significance of spatial correlation patterns in armoured gravel beds. *J. Hydraul. Res.* **2018**, in press.
- Powell, D.M. Flow resistance in gravel-bed rivers: Progress in research. *Earth-Sci. Rev.* **2014**, *136*, 301–338. [[CrossRef](#)]
- Flack, K.A.; Schultz, M.P. Review of Hydraulic Roughness Scales in the Fully Rough Regime. *J. Fluids Eng.* **2010**, *132*, 041203. [[CrossRef](#)]
- Tonina, D.; Buffington, J.M. Hyporheic exchange in gravel bed rivers with pool-riffle morphology: Laboratory experiments and three-dimensional modeling. *Water Resour. Res.* **2007**, *43*, W01421. [[CrossRef](#)]
- Boano, F.; Harvey, J.W.; Marion, A.; Packman, A.I.; Revelli, R.; Ridolfi, L.; Wörman, A. Hyporheic flow and transport processes: Mechanisms, models, and biogeochemical implications. *Rev. Geophys.* **2014**, *52*, 603–679. [[CrossRef](#)]

22. Marion, A.; Nikora, V.; Puijalon, S.; Bouma, T.; Koll, K.; Ballio, F.; Tait, S.; Zaramella, M.; Sukhodolov, A.; O'Hare, M.; et al. Aquatic interfaces: A hydrodynamic and ecological perspective. *J. Hydraul. Res.* **2014**, *52*, 744–758. [[CrossRef](#)]
23. Zagni, A.F.E.; Smith, K.V.H. Channel flow over permeable beds of graded spheres. *J. Hydraul. Div.* **1979**, *102*, 207.
24. Zippe, H.J.; Graf, W.H. Turbulent boundary layer flow over permeable and non-permeable rough surfaces. *J. Hydraul. Res.* **1983**, *21*, 51–65. [[CrossRef](#)]
25. Breugem, W.P.; Boersma, B.J.; Uittenbogaard, R.E. The influence of wall permeability on turbulent channel flow. *J. Fluid Mech.* **2006**, *562*, 35–72. [[CrossRef](#)]
26. Manes, C.; Pokrajac, D.; McEwan, I.; Nikora, V. Turbulence structure of open channel flows over permeable and impermeable beds: A comparative study. *Phys. Fluids* **2009**, *21*, 125109. [[CrossRef](#)]
27. Manes, C.; Poggi, D.; Ridolfi, L. Turbulent boundary layers over permeable walls: Scaling and near-wall structure. *J. Fluid Mech.* **2011**, *687*, 141–170. [[CrossRef](#)]
28. Manes, C.; Pokrajac, D.; Nikora, V.I.; Ridolfi, L.; Poggi, D. Turbulent friction in flows over permeable walls. *Geophys. Res. Lett.* **2011**, *38*, L03402. [[CrossRef](#)]
29. Kuwata, Y.; Suga, K. Direct numerical simulation of turbulence over anisotropic porous media. *J. Fluid Mech.* **2017**, *831*, 41–71. [[CrossRef](#)]
30. Aberle, J. Measurements of armour layer roughness geometry function and porosity. *Acta Geophys.* **2007**, *55*, 23–32. [[CrossRef](#)]
31. Navaratnam, C.U.; Aberle, J.; Daxnerová, J. An Experimental Investigation on Porosity in Gravel Beds. In *Free Surface Flows and Transport Processes*; Springer International Publishing: Cham, Germany, 2018; pp. 323–334.
32. Cooper, J.R.; Ockleford, A.; Rice, S.P.; Powell, D.M. Does the permeability of gravel river beds affect near-bed hydrodynamics? *Earth Surf. Process. Landf.* **2018**, *43*, 943–955. [[CrossRef](#)]
33. Aberle, J.; Dittrich, A.; Koll, K.; Schoneboom, T. Sohlnahes turbulentes Strömungsfeld. In *BAW-Workshop: Boden- und Sohl-Stabilität—Betrachtungen an der Schnittstelle zwischen Geotechnik und Wasserbau*; Bundesanstalt für Wasserbau: Karlsruhe, Germany, 2004.
34. Spiller, S.; Rütger, N. Artificial reproduction of the surface structure in a gravel bed. In *2nd IAHR Europe Conference*; TU Munich: Munich, Germany, 2012.
35. Navaratnam, C.U.; Aberle, J.; Spiller, S.M. Evaluation of the accuracy of a bed casting technique. In *River Flow 2016*; CRC Press: St. Louis, MO, USA, 2016; pp. 398–403.
36. Graf, W.H.; Song, T. Bed-shear stress in non-uniform and unsteady open-channel flows. *J. Hydraul. Res.* **1995**, *33*, 699–704. [[CrossRef](#)]
37. Leopold, L.B.; Langbein, W.B. The Concept of Entropy in Landscape Evolution. In *Theoretical Papers in the Hydrologic and Geomorphic Sciences*; United States Government Printing Office: Washington, DC, USA, 1962; pp. A1–A20.
38. Cassan, L.; Roux, H.; Garambois, P.-A. A Semi-Analytical Model for the Hydraulic Resistance Due to Macro-Roughnesses of Varying Shapes and Densities. *Water* **2017**, *9*, 637. [[CrossRef](#)]



## **Paper V**

---

### **An experimental investigation on the flow resistance over a porous gravel bed surface and its non-porous counterpart**

Christy Ushanth Navaratnam, Jochen Aberle, Jie Qin, Pierre-Yves Henry

River Flow 2018 - International Conference on Fluvial Hydraulics, Lyon, France

<https://doi.org/10.1051/e3sconf/20184005073>

---





# An experimental investigation on the flow resistance over a porous gravel-bed surface and its non-porous counterpart

Christy Ushanth Navaratnam<sup>1,\*</sup>, Jochen Aberle<sup>1,2</sup>, Jie Qin<sup>3</sup> and Pierre-Yves Henry<sup>1</sup>

<sup>1</sup>Department of Civil and Environmental Engineering, Norwegian University of Science and Technology (NTNU), S.P.Andersens veg 5, 7491, Trondheim, Norway.

<sup>2</sup>Leichtweiß-Institut für Wasserbau, Technische Universität Braunschweig, 38106, Braunschweig, Germany.

<sup>3</sup>College of Harbour, Coastal and Offshore Engineering, Hohai University, Xikang road #1, 210098, Nanjing, China.

**Abstract.** This paper presents preliminary results from laboratory experiments which were specifically designed to determine the flow resistance over a water-worked gravel-bed and its impermeable counterpart (cast-bed). The technique used to create the cast-bed is introduced, followed by the description of the experimental setup and the procedure to quantify flow resistance over both the water-worked and cast-bed. The influence of the grain orientation on flow resistance was investigated in an additional set of experiments by rotating the cast-bed through 180° in the flume. The main focus of the paper is on the comparison of the bulk flow characteristics for the three different cases for which the beds are characterized not only by the same characteristic grain-diameter but also by an identical surface structure. The obtained results show that the porous, non-porous bed and rotated bed result in different flow resistance and that both bed porosity and grain-orientation have a significant effect on flow resistance.

## 1. Introduction

The quantification of flow resistance of rivers and stream rivers is of fundamental importance for fluvial geomorphology, river hydraulics, and ecology since it determines flow properties such as mean flow velocity, turbulence, and sediment transport as well as habitat conditions. Traditionally, the roughness of gravel-bed rivers has been associated with a characteristic grain size of the bed material (e.g.,  $d_{50}$ ,  $d_{84}$ , or  $d_{90}$ ) and flow resistance is parametrized by 'roughness coefficients' or 'friction factors' such as Manning's  $n$ , Chezy's  $C$  and Darcy-Weisbach's  $f$  [e.g., 1-5]. All existing approaches have in common that the structure of the subsurface layer is not specifically taken into account; in fact, it is often tacitly assumed that porous and non-porous beds are characterized by the same flow resistance given that their surface geometry is identical. However, river beds with a porous sub-surface are characterized by mass and momentum exchange occurring across the sediment-water interface due to the pressure gradients that drive the flow into and out of the bed [6-8]; this

---

\* Corresponding author: [christy.ushanth.navaratnam@ntnu.no](mailto:christy.ushanth.navaratnam@ntnu.no)

exchange may affect the hydraulic resistance. Some studies showed that porous beds impose higher flow resistance than their non-porous counterpart for the same flow conditions [e.g., 9-12] and that the friction factors depend on the Reynolds number for a given relative submergence [13]. These studies were mainly based on investigations with artificial beds composed of, for example, single and multiple layers of spheres to mimic a non-porous and porous bed, respectively. On the other hand, a recent study [14] was using a casting technique to reproduce the non-porous counterpart of a gravel-bed surface and indicated that the non-porous cast imposed higher flow resistance than its porous counterpart.

To further explore these aforementioned issues, this paper presents preliminary results from experiments that were specifically designed to study the influence of the sub-surface porosity on flow resistance in gravel-bed rivers. Section 2 describes the preparation of the permeable and non-permeable test surfaces and the experimental program. The results of the measurements are presented and discussed in Section 3. The paper is concluded with a summary of the main findings and an outlook to future research in this field.

## 2. Methodology

### 2.1. Preparation of gravel and cast surfaces

Experiments were carried out in a 12.5 m long, 1 m wide and 1 m deep tilting flume at the hydraulics laboratory at the Norwegian University of Science and Technology (NTNU) Trondheim, Norway. In a first step, a 0.2 m high layer consisting of well-mixed gravel mixture, with the grain size distribution as shown in Figure 1, was screeded at a length of 10.61 m. In the next step, a stable armor layer was produced by water-working the bed with a steady discharge of 0.2 m<sup>3</sup>/s and quasi-uniform flow conditions (the water surface slope equaled the bed slope of  $S = 0.0027$ ). Following the creation of the static armor layer, porosity measurements were performed using the water displacement method [see 15,16 for details] to determine the vertical distribution of the porosity of the gravel-bed, which was in average  $\phi = 0.31$ .

Following the hydraulic measurements, which are described in detail in the next section, an impermeable facsimile of a 7 m long section of the water-worked gravel was produced using the bed casting technique described in [17, 18]. The bed reproduction technique consisted of two steps; silicon moulding and casting of the non-porous surface using a synthetic resin. Since it was not possible to cast the 7 m long section in one piece, four smaller sized casts had to be produced (lengths of 1.2 and 2.3 m, two pieces each). Due to their weight, the cast pieces were placed in the flume with the help of a crane. We note that the upstream section of the 10.61 m long gravel-bed which was not reproduced was replaced by a copy of the cast forming the middle section of the flume surface. Both the gravel and cast-beds were scanned using an Acuity AR200-100 laser measurement sensor to obtain digital elevation models (DEMs) of the surfaces. The resolution of the scanned data was 0.3 mm x 1 mm (longitudinal x transverse directions). The DEMs were used to assess the accuracy of the casting technique and to verify how accurate the cast tiles were placed with respect to the original gravel surface (see below).

The use of the casts also allowed for an additional investigation regarding the effect of grain orientation on the flow resistance. For this purpose, each cast tile was rotated through 180 degrees after the measurements over the initially placed cast surface. Thus, hydraulic measurements were carried out over three different surfaces types: i) water-worked gravel-bed, ii) impermeable cast-bed and iii) impermeable rotated cast-bed. Figure 2 shows photos of the water-worked gravel surface and its non-porous cast surface and Table 1 presents the geometrical properties of the three surfaces in terms of the mean bed elevation (from the

flume bottom), the standard deviation of the bed elevations as well as skewness and kurtosis. The presented values, especially the mean value and the standard deviation, show that the water worked bed could be well reproduced by the cast. The observed minor differences in the statistical parameters for the different bed-types can be associated with the placing of the cast-tiles and the reproduction technique.

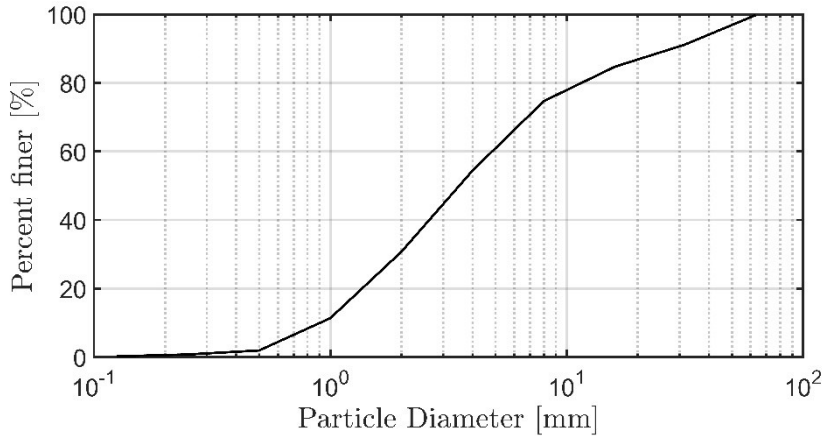


**Fig. 1.** Grain size distribution of the gravel-mixture



**Fig. 2.** *Left:* Water-worked gravel surface, *Right:* Non-porous counterpart of gravel (cast)

**Table 1.** Statistical details of the bed surfaces

| Bed Surface            | Mean (from flume bottom) [mm] | Standard Deviation [mm] | Skewness | Kurtosis |
|------------------------|-------------------------------|-------------------------|----------|----------|
| Gravel                 | 182.0                         | 7.6                     | 0.76     | 1.03     |
| Cast                   | 182.1                         | 8.0                     | 0.50     | 0.66     |
| Cast180 (Rotated Cast) | 180.5                         | 8.5                     | 0.56     | 0.49     |

## 2.2. Hydraulic Measurements

Hydraulic measurements over the three bed types were carried out for seven different hydraulic boundary conditions (BCs) which are summarised in Table 2. The discharge was measured using inductive flow meters mounted on the recirculation pipes in the flume. In the experiments with the gravel-bed, water surface slopes and water depths were determined with

four static pressure tubes located at the flume bottom. For the cast measurements, the pressure tubes could not be used as the subsurface was sealed off. Instead, 8 ultrasonic sensors were used to measure the water surface elevations and water surface slope. From these measurements, the mean water depth was determined using the mean bed elevation as datum. Additional tests carried out with the two measurement systems (not shown here) showed that both gave the same water depth and water surface slope so that the results from the experiments carried out over the different surfaces are directly comparable. Although care was taken to carry out the measurements with uniform flow conditions, it was difficult to exactly match the bed slope with the water surface slope. To account for the differences between the bed and water surface slope, the St. Venant equation for non-uniform flow was used to determine the friction velocity [19]:

$$u_* = \left[ ghS_b + \left( -gh \frac{\partial h}{\partial x} \right) (1 - Fr^2) \right]^{1/2} \tag{1}$$

where,  $u_*$  is the friction velocity,  $g$  is the gravitational acceleration,  $h$ , the water depth,  $S_b$  is the bed slope,  $\partial h/\partial x$  is the water depth variation in longitudinal direction and  $Fr$  is the Froude number. Equation 1 can be simplified for small slopes as in the present experiments:

$$u_* = [ghS_b - gh(S_b - S_w)(1 - Fr^2)]^{1/2} \tag{2}$$

where,  $S_b$  is the bed slope and  $S_w$  is the water surface slope. The bulk friction factors were determined using the Darcy-Weisbach friction factor

$$f = 8 \cdot \frac{u_*^2}{U^2} \tag{3}$$

where the  $U$  is the cross-sectionally averaged flow velocity. It should be noted that the relative submergence was kept as constant as possible for each boundary condition and that the discharge was adjusted to achieve the required water surface slope to have comparable conditions.

**Table 2.** Hydraulic boundary conditions for gravel-bed surface,  $k$  is defined as roughness height ( $z_{99} - z_{01}$ ), where  $z_{99}$  and  $z_{01}$  are 99<sup>th</sup> and 1<sup>st</sup> percentile of vertical elevation of the bed surface respectively.

| Test | Bed slope ( $S_b$ ) | Water Surface Slope ( $S_w$ ) | Water level from flume bottom [mm] | Water depth, $h$ [m] | $h/k$ | $Q$ (m <sup>3</sup> /s) | $U$ [m/s] | $Fr$ | $Re$   | $u_*$ [m/s] |
|------|---------------------|-------------------------------|------------------------------------|----------------------|-------|-------------------------|-----------|------|--------|-------------|
| BC1  | 0.0018              | 0.00134                       | 318.4                              | 0.137                | 3.6   | 0.056                   | 0.41      | 0.35 | 55890  | 0.043       |
| BC2  | 0.0015              | 0.00103                       | 359.9                              | 0.178                | 4.7   | 0.076                   | 0.43      | 0.32 | 76270  | 0.043       |
| BC3  | 0.0015              | 0.00103                       | 418.2                              | 0.236                | 6.2   | 0.121                   | 0.51      | 0.34 | 120787 | 0.050       |
| BC4  | 0.0020              | 0.00159                       | 397.1                              | 0.215                | 5.7   | 0.124                   | 0.58      | 0.40 | 124107 | 0.059       |
| BC5  | 0.0013              | 0.00083                       | 474.6                              | 0.293                | 7.7   | 0.156                   | 0.53      | 0.31 | 156412 | 0.050       |
| BC6  | 0.0010              | 0.00051                       | 535.2                              | 0.353                | 9.3   | 0.168                   | 0.48      | 0.25 | 167987 | 0.043       |
| BC7  | 0.0015              | 0.00098                       | 501.3                              | 0.319                | 8.4   | 0.200                   | 0.63      | 0.35 | 199823 | 0.057       |

### 3. Results and Discussion

Figure 3 shows the variations of the bulk friction factor  $f$  with the Reynolds-number  $Re = Uh/\nu$  for the three bed-types ( $\nu$  denotes the kinematic viscosity). The figure reveals that the rotated cast exerted higher resistance to the flow than the other two bed surfaces for all boundary conditions except for  $Re \approx 170,000$ , for which the friction factor of the rotated cast was slightly lower than that of the gravel-bed. This may partly be associated with the uncertainties in the water surface slope measurements for this boundary condition which was characterized by the lowest water surface slope (approx. 0.05%). The higher flow resistance exerted by the rotated bed shows that the grain orientation has significant influence on the flow resistance and indicates the effectivity of the flow to create a bed imposing less hydraulic roughness (e.g., [20]); the grains for the rotated cast are oriented in the opposite direction compared to the other two surfaces. This result is hence also a strong indicator that the bed roughness cannot be solely described by a characteristic grain diameter and that the surface structure and the orientation of the grains to the flow direction play an important role [4, 5, 21].

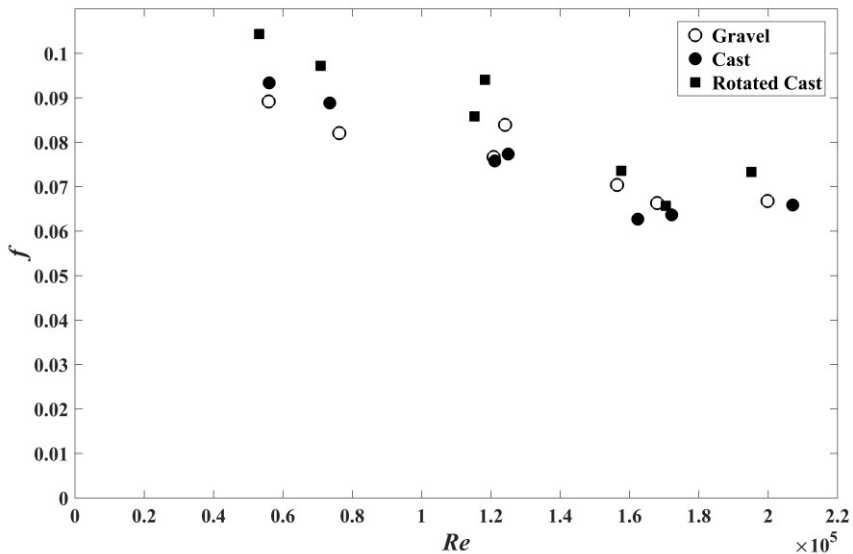


**Fig. 3.** The variation of bulk friction factors with  $Re$ , for different surfaces

The water-worked gravel surface exhibited higher flow resistance than the cast surface for  $Re > 100,000$ . However, for the two runs with  $Re < 100,000$  (i.e. for the lowest discharges used), a lower friction factor was obtained for the water-worked gravel-bed than for the cast-bed (discussed below). The higher friction over the water-worked gravel-bed can be associated with the momentum transfer in the porous gravel-bed, as the solid bottom of the cast prevents momentum transfer. The effective hydraulic roughness over a porous surface is generally related to the thickness of the interface region [13], i.e. the region of the flow where the surface flow interacts with the porous medium. The interface region is larger for the porous gravel-bed than for the non-porous cast for which it is restricted from the roughness crest to the roughness trough, i.e. in this case it does not include parts of the subsurface layer. Defining the relative submergence as the ratio of water depth to the height of the interface region, the relative submergence will be, for a given water depth, lower for the water-worked gravel-bed than for the cast. This implies a higher friction factor for the flow over the gravel surface compared to the flow over the cast. It should be noted that the

depth of momentum penetration is limited by the thickness of the porous layer. If the depth of momentum penetration occupies the whole porous layer, the flow resistance can be assumed to be independent of relative submergence.

In order to elaborate this issue further, data from [13] are plotted in Figure 4. The shown friction factors were obtained in experiments over a porous gravel-bed ( $f_l$ ) and a non-porous gravel-bed ( $f$ ) (a single layer of gravel grains) for a range of relative submergences. However, the friction factors for the porous and non-porous surfaces were determined in slightly different ways. For the non-porous surface, the datum for the analysis was the flume bottom whereas for porous bed, the datum was located at the roughness top. Thus, the friction factor over the porous bed was slightly underestimated as the relative submergence would be higher compared to the non-porous bed. The level of underestimation is increasing with increasing  $Re$  as the depth of momentum penetration is also increasing; as Figure 4 shows, the porous bed imposes higher resistance to the flow than the non-porous bed for a given ratio of water depth to particle diameter  $d$ . In fact, [13] concluded that the flow resistance in porous beds increases with increasing  $Re$  for a given relative submergence. In our study, the relative submergence was kept approximately constant for a given boundary condition enabling the comparison of friction factors between the three-different surfaces, and the higher friction over the water-worked gravel-bed confirms basically the results of [13]. The observed lower friction over the water-worked gravel-bed for the first two boundary conditions may be explained could be associated with the placement of the cast surfaces, because the standard deviation of the bed elevation is slightly higher for the cast than for the gravel which in turn may affect hydraulic roughness, especially for the lowest discharges. On the other hand, the differences in  $f$  may also be related to the fact that the subsurface flow rate for the porous-bed test was not explicitly measured; i.e. it was not accounted for in the calculation of the bulk-parameters. Preliminary test-computations showed that, considering a subsurface flow rate of 2 l/s, larger  $f$ -values would be obtained for the porous bed than for the cast-bed.

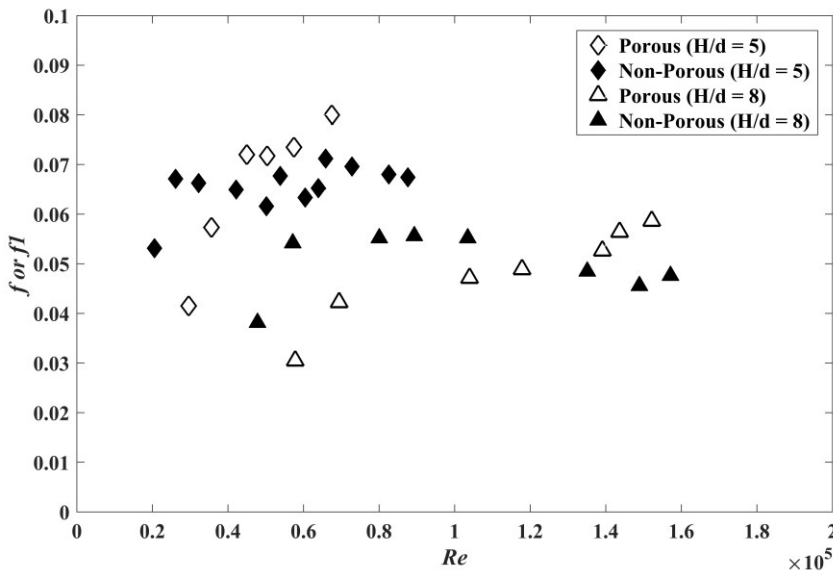


Fig. 4. The variation of friction factors with  $Re$ , obtained from [13]

The results of the presented experiments were also compared to the results of the recent study of [14], which was based on a similar experimental method. In this study, it was found



that the bulk flow resistance exerted by a non-porous cast section was higher than the flow resistance exerted by the porous gravel-bed which is not in agreement with the finding of this study (except for two BCs) as well as the aforementioned studies. A possible explanation for this deviation may be that only a small gravel-bed surface section was reproduced in the study of [14] which corresponded to about 5% of the total water-worked gravel-bed area. In other words, a small section of a cast tile was placed in the middle of a long porous gravel-bed section. As far as the bulk flow resistance is concerned, a larger section of porous gravel-bed ( $\approx 95\%$ ) interacts thus with the flow. In contrast to the experiments carried out by [14], the experiments presented in this paper were carried out over a complete non-porous cast-bed and ensured that there was no flow under the cast by sealing off the gaps and joints of the cast tiles. Moreover, about 70% of the water-worked gravel-bed surface was reproduced in this study and accuracy was verified as reported in the previous section.

## 4. Conclusion

This paper presented preliminary results from an investigation focusing on the bulk flow resistance of three different surfaces; porous water-worked gravel, non-porous facsimiles of gravel (cast) and rotated cast (each cast piece was rotated through 180 degrees). It was shown that the porous gravel-bed exerts higher flow resistance on the flow than its non-porous facsimiles. This was due to the momentum penetration in the porous bed which is dependent on  $Re$  for a given relative submergence. A practical implication of this result is that the colmatation process (the settling of fine particles in the hyporheic zone), may change the porosity of the sub-surface, and hence flow resistance, or vice versa. The results also revealed that the rotated cast imposed higher friction on the flow than the other two surfaces which demonstrates that grain orientation has significant influence on flow resistance. Thus, it can be concluded that a complete description of gravel-bed roughness requires not only information on the surface structure and on the grain-size distribution of the surface layer, but also information on the sub-surface layer. This issue will be in the focus of our subsequent analyses using flow velocity data acquired with Particle Image Velocimetry over the different beds.

The authors thank Dr. Costantino Manes for providing the data from his study which helped to discuss the findings in this paper.

## References

1. R. D. Hey, *J. Hydr. Div.*, **105**, 365-379, (1979)
2. J.C. Bathurst, *J. Hydr. Eng.*, **111**, 625-643, (1985)
3. V.I. Nikora, D.G. Goring, B.J.F. Biggs, *Wat. Res. Res.*, **34**, 517-527, (1998)
4. J. Aberle, G.M. Smart, *J. Hydr. Res.*, **41**, 259-269, (2003)
5. D.M. Powell, *Eart. Scie. Rev.*, **136**, 301-338, (2014)
6. D. Tonina, J.M. Buffington, *Wat. Res. Res.*, **43**, W01421 (2007)
7. F. Boano, J.W. Harvey, A. Marion, A.I. Packman, R. Revelli, L. Ridolfi, A. Wörman, *Revi. of Geop.*, **52**, 603-679, (2014)
8. A. Marion, V. Nikora, S. Puijalón, T. Bouma, K. Koll, F. Ballio, S. Tait, M. Zaramella, A. Sukhodolov, M. O'Hare, G. Wharton, J. Aberle, M. Tregnaghi, P. Davies, H. Nepf, G. Parker, B. Statzner, *J. Hydr. Res.*, **52**, 744-758, (2014)
9. A.F.E. Zagni, K.V.H. Smith, *J. Hydr. Div.*, **102**, 207, (1976)



10. H.J.Zippe, W.H.Graf, J. Hydr. Res., **21**, 51-65, (1983)
11. W.P. Breugem, B. J. Boersma, R.E. Uittenbogaard, J. Flui. Mech., **562**, 35-72, (2006)
12. C. Manes, D. Pokrajac, I. McEwan, V.I. Nikora, Phys. of Flui., **21**, 125109 (2009)
13. C. Manes, D. Pokrajac, V.I. Nikora, L. Ridolfi, D. Poggi, Geop. Res. Let, **38**, L03402, (2011)
14. J.R. Cooper, A. Ockleford, S.P. Rice, D.M. Powell, Eart. Surf. Proc. Land., (In press)
15. J. Aberle, Acta Geop. **55**, 23-32, (2007)
16. C.U. Navaratnam, J. Aberle, J. Daxnerová, in: *Free Surface Flows and Transport Processes* (Springer, 2018)
17. S. Spiller, N. Rütger, *2nd IAHR Europe Conference* (Munich, Germany, 2012)
18. C.U. Navaratnam, J. Aberle, S.M. Spiller, in : *River Flow 2016* (CRC Press, Taylor & Francis Group, 2016)
19. W.H. Graf, T. Song, J. Hydr. Res., **33**, 699-704, (1995)
20. L.B. Leopold, W.B. Langbein, in: *Theoretical papers in the hydrologic and geomorphic sciences*, (U.S. Govt. Print. Off, 1962)
21. K.A. Flack, M.P. Schultz, J. of Fluids Eng., **132**, 041203-041203-10, (2010)

# B

## Secondary Papers



## Experimental hydraulics on fish-friendly trash-racks: an ecological approach

Marcell Szabo-Meszaros, Christy Ushanth Navaratnam, Jochen Aberle, Ana T. Silva, Torbjørn Forseth, Olle Calles, Hans-Petter Fjeldstad, Knut Alfredsen

*Ecological Engineering*, 2018, 113

**Abstract:** The obstruction of fish migratory routes by hydroelectric facilities is worldwide one of the major threats to freshwater fishes. During downstream migration, fish may be injured or killed on the trash-racks or in the hydropower turbines. Fish-friendly trash-racks that combine both ecological and technical requirements are a solution to mitigate fish mortality at a low operational cost. This study presents results from an experimental investigation of head-losses and the hydrodynamic performance of six angled trash-rack types with 15mm bar spacing, varying bar-setup (vertical-streamwise, vertical-angled and horizontal bars) and bar profiles (rectangular and drop shape) under steady flow conditions. The trash-racks were positioned at 30° to the wall of the flume and combined with a bypass at their downstream end. The impact of the different trash-rack types on the upstream flow field was characterized using Image based Volumetric 3-component Velocimetry (V3V) and at the bypass-entrance using an Acoustic Doppler Velocimeter (ADV). The results show that trash-racks with vertical-streamwise and horizontal oriented bars with drop-shape profiles have similar head-losses (13% difference), while trash-racks with vertical-angled bars provide 3–8 times larger head-losses compared to the remaining configurations. The velocity measurements showed that the highest flow velocities occurred for configurations with vertical-angled bars ( $0.67\text{ms}^{-1}$  and  $0.81\text{ms}^{-1}$  on average, respectively). Turbulence related parameters (e.g. Reynolds shear stresses and Turbulent kinetic energy) were also investigated to evaluate the performance of the alternative trash-racks from both, engineering and ecological perspectives.

## **Geometric and hydraulic assessment of the accuracy of a bed moulding technique**

Christy Ushanth Navaratnam, Jochen Aberle, Stephan Spiller

*IAHR World Congress 2015, The Hague, The Netherlands.*

**Abstract:** This paper presents preliminary results from an experimental study aiming at the investigation of the significance of bed porosity on surface flow characteristics in gravel beds. In order to quantify this influence, hydraulic measurements need to be conducted over permeable beds and their impermeable counterparts having the identical surface structure. Recent developments in experimental techniques have resulted in innovative casting methods which can be used to reproduce such surfaces with high accuracy. In the present study, we used a liquid two-component silicone rubber to manufacture a negative imprint of granular and artificial beds. The corresponding surfaces were subsequently reproduced from the silicon form using a two-component pouring resin. The accuracy of the applied moulding technique is evaluated based on a geometrical analysis of the surface structures of the prototype surfaces and their moulded counterparts. Moreover, preliminary results from hydraulic measurements using a 2D-Particle Image Velocimetry (PIV) system are presented for a surface consisting of a layer of original and duplicate golf balls. The corresponding measurements were, using identical hydraulic boundary conditions, carried out for two water depths. The obtained data are analyzed using the double averaging methodology and are used to investigate the accuracy of the moulding technique in hydraulic terms by comparing the near bed flow structure and turbulence characteristics over the original and artificially reproduced surface, respectively.

C

**Statements from co-authors**





STATEMENT FROM CO-AUTHOR

(cf. section 10.1 in the PhD regulations)

Christy Ushanth Navaratnam applies to have the following thesis assessed:
Name of candidate

The effect of bed porosity on the turbulent flow in gravel-bed rivers
title

\*) The statement is to describe the work process and the sharing of work and approve that the article may be used in the thesis.

\*) Statement from co-author on article: The effect of bed porosity on near-bed turbulent flow characteristics in gravel-bed rivers VANN 2017, 52 (2)
I hereby declare that I am aware that the article mentioned above, of which I am co-author, will form part of the PhD thesis by the PhD candidate Christy Ushanth Navaratnam who made a major contribution to the work in the experiment, data analysis and writing phase.
Braunschweig 14/18/17
Signature co-author

\*) Statement from co-author on article: An Experimental Investigation on Porosity in Gravel Beds Free Surface Flows and Transport Processes, 2018
I hereby declare that I am aware that the article mentioned above, of which I am co-author, will form part of the PhD thesis by the PhD candidate Christy Ushanth Navaratnam who made a major contribution to the work in the experiment, data analysis and writing phase.
Braunschweig 14/18/17
Signature co-author



\*)

Statement from co-author on article: .....

**Evaluation of the accuracy of a bed casting technique** .....

River Flow 2016, St. Louis, Missouri, USA

I hereby declare that I am aware that the article mentioned above, of which I am co-author, will form part of the PhD thesis by the PhD candidate Christy Ushanth Navaratnam who made a major contribution to the work in the experiment, data analysis and writing phase.

Braunschweig 14/11/11

Place, date

.....  
Signature co-author

\*)

Statement from co-author on article: .....

**Influence of Gravel-Bed Porosity and Grain Orientation on Bulk Flow Resistance** .....

Water, 2018, 10, 561

I hereby declare that I am aware that the article mentioned above, of which I am co-author, will form part of the PhD thesis by the PhD candidate Christy Ushanth Navaratnam who made a major contribution to the work in the experiment, data analysis and writing phase.

Braunschweig 14/11/11

Place, date

.....  
Signature co-author

\*)

Statement from co-author on article: .....

**An experimental investigation on the flow resistance over a porous gravel bed surface and its non-porous counterpart** .....

River Flow 2018, Lyon, France

I hereby declare that I am aware that the article mentioned above, of which I am co-author, will form part of the PhD thesis by the PhD candidate Christy Ushanth Navaratnam who made a major contribution to the work in the experiment, data analysis and writing phase.

Braunschweig 14/11/11

Place, date

.....  
Signature co-author



NTNU

Encl. to application for assessment of PhD thesis

### STATEMENT FROM CO-AUTHOR

(cf. section 10.1 in the PhD regulations)

Christy Ushanth Navaratnam

.....applies to have the following thesis assessed:  
Name of candidate

The effect of bed porosity on turbulent flow in gravel-bed rivers  
title

\*) The statement is to describe the work process and the sharing of work and approve that the article may be used in the thesis.

\*)  
Statement from co-author on article: .....  
**Influence of Gravel-Bed Porosity and Grain Orientation on Bulk Flow Resistance** .....  
Water, 2018, 10, 561

I hereby declare that I am aware that the article mentioned above, of which I am co-author, will form part of the PhD thesis by the PhD candidate Christy Ushanth Navaratnam who made a major contribution to the work in the experiment, data analysis and writing phase.

*Trondheim*  
.....  
Place, date 19/08/2018

*[Signature]*  
.....  
Signature co-author

\*)  
Statement from co-author on article: .....  
.....

.....  
Place, date

.....  
Signature co-author



### STATEMENT FROM CO-AUTHOR

(cf. section 10.1 in the PhD regulations)

Christy Ushanth Navaratnam .....applies to have the following thesis assessed:  
Name of candidate

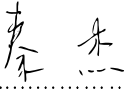
The effect of bed porosity on turbulent flow in gravel-bed rivers .....  
title

\*) The statement is to describe the work process and the sharing of work and approve that the article may be used in the thesis.

\*)  
Statement from co-author on article: .....  
**Influence of Gravel-Bed Porosity and Grain Orientation on Bulk Flow Resistance** .....  
Water, 2018, 10, 561

I hereby declare that I am aware that the article mentioned above, of which I am co-author, will form part of the PhD thesis by the PhD candidate Christy Ushanth Navaratnam who made a major contribution to the work in the experiment, data analysis and writing phase.

Wang Aug 15 2018 .....  
Place, date

 .....  
Signature co-author

\*)  
Statement from co-author on article: .....  
.....

.....  
Place, date

.....  
Signature co-author



### STATEMENT FROM CO-AUTHOR

(cf. section 10.1 in the PhD regulations)

Christy Ushanth Navaratnam .....applies to have the following thesis assessed:  
Name of candidate

The effect of bed porosity on turbulent flow in gravel-bed rivers .....  
title

\*) The statement is to describe the work process and the sharing of work and approve that the article may be used in the thesis.

\*)  
Statement from co-author on article: .....  
**Evaluation of the accuracy of a bed casting technique** .....  
River Flow 2016, St. Louis, Missouri, USA

I hereby declare that I am aware that the article mentioned above, of which I am co-author, will form part of the PhD thesis by the PhD candidate Christy Ushanth Navaratnam who made a major contribution to the work in the experiment, data analysis and writing phase.

*Papenburg, 14.08.2018*  
.....  
Place, date

*Stephan Spil*  
.....  
Signature co-author

\*)  
Statement from co-author on article: .....  
.....

.....  
Place, date

.....  
Signature co-author



NTNU

Encl. to application for assessment of PhD thesis

### STATEMENT FROM CO-AUTHOR

(cf. section 10.1 in the PhD regulations)

Christy Ushanth Navaratnam .....applies to have the following thesis assessed:  
Name of candidate

The effect of bed porosity on turbulent flow in gravel-bed rivers .....  
title

\*) The statement is to describe the work process and the sharing of work and approve that the article may be used in the thesis.

\*)  
Statement from co-author on article: .....  
**An Experimental Investigation on Porosity in Gravel Beds** .....  
Free Surface Flows and Transport Processes, 2018

I hereby declare that I am aware that the article mentioned above, of which I am co-author, will form part of the PhD thesis by the PhD candidate Christy Ushanth Navaratnam who made a major contribution to the work in the experiment, data analysis and writing phase.

Trondheim, 14. 8. 2018 .....  
Place, date

*Christy Ushanth Navaratnam* .....  
Signature co-author

\*)  
Statement from co-author on article: .....  
.....

.....  
Place, date

.....  
Signature co-author